ERDC/CERL SR-01-19

Construction Engineering Research Laboratory

US Army Corps of Engineers
Engineer Research and Development Center

# Seismic Response of Low-Rise Masonry Buildings With Flexible Roof Diaphragms

Gregory L. Cohen, Richard E. Klingner, John R. Hayes, Jr., and Steven C. Sweeney

August 2001

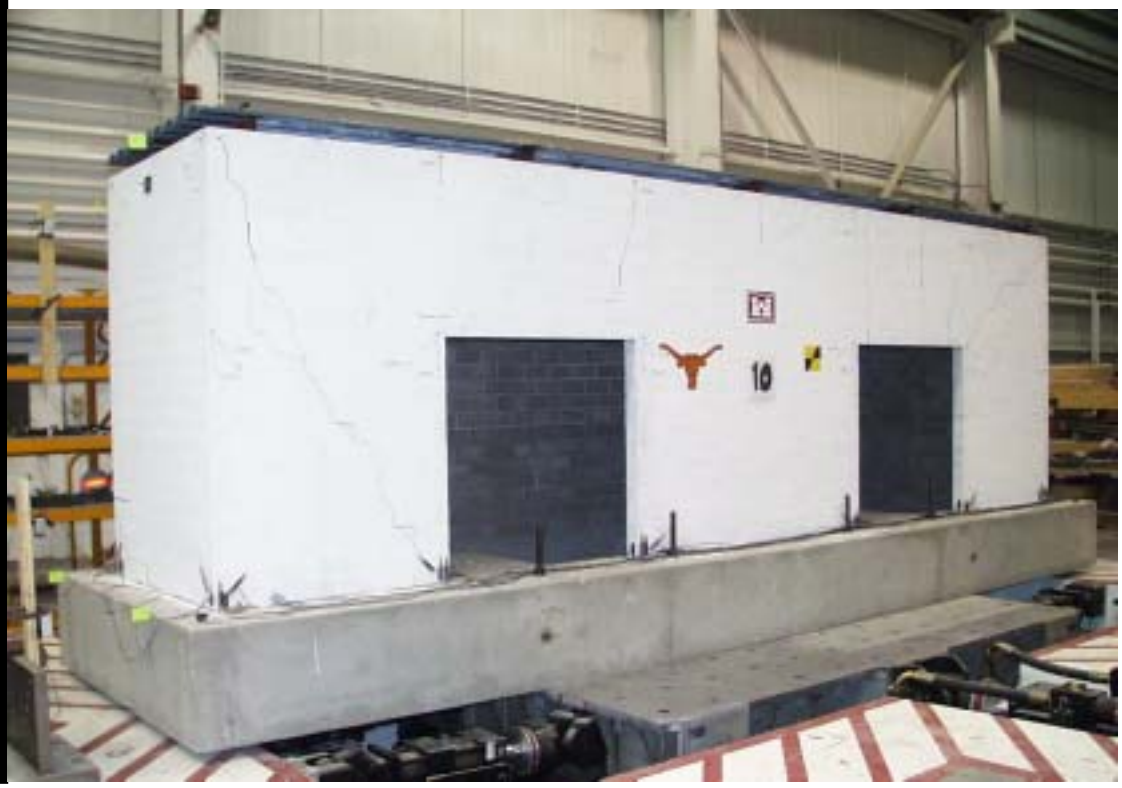

# Foreword

This study was conducted for the U.S. Army Corps of Engineers (USACE) under the Seismic Evaluation and Rehabilitation Program led by Dr. John R. Hayes, Jr. of the Materials and Structures Branch, U.S. Army Engineer Research and Development Center (ERDC), Construction Engineering Research Laboratory (CERL). The work was performed jointly at the Phil M. Ferguson Structural Engineering Laboratory in Austin, Texas and CERL in Champaign, Illinois.

This manuscript was submitted in partial fulfillment of the requirements for the degree of Master of Science in Civil Engineering in the Graduate College of the University of Texas at Austin. Dr. Richard E. Klingner supervised this research project. His constant enthusiasm and excellent teaching skills and personable nature made for an enjoyable and motivating learning environment. His expertise in the fields of earthquake engineering and masonry engineering provided the technical basis necessary for success of this project.

Also thanked is the structural engineering faculty at the University of Texas. In particular, thanks go to Dr. Dan Wheat and Dr. Sharon Wood for their aid in development of parts of this report.

Vulcraft Steel Joist and Deck Company generously donated the corrugated metal decking used in this project. Larry Herm and Mark Johanningsmeier, both of Vulcraft, provided valuable expertise regarding metal deck construction and detailing.

Dr. Hayes and Steven C. Sweeney, both of CERL, are owed a debt of gratitude for their professional attitudes and valuable opinions throughout the project. CERL electronics specialist James B. Gambill is thanked for the terrific job he did running the shaking table and collecting and reducing the test data. CERL laboratory technician William J. Gordon is thanked for his help in the laboratory and for setting up and testing of the specimens. The associated Technical Director at CERL was Paul Howdyshell. The Director of CERL is Dr. Alan W. Moore.

CERL is an element of ERDC, U.S. Army Corps of Engineers. The Commander and Executive Director of ERDC is COL John W. Morris III, EN and the Director of ERDC is Dr. James R. Houston.

# Contents

# List of Figures and Tables

**Figures**

**Tables**

# 1 Introduction

Downsizing of the US military, combined with recent destructive earthquakes in the United States and around the world, such as the 1989 Loma Prieta earthquake and the 2001 Seattle earthquake, has made the US Department of Defense aware of how critical the military's remaining facilities are (http://www.cecer.army.mil). To assess and eventually mitigate the seismic vulnerability of the military's facilities, the US Army allocated funding for research on the seismic reliability of structures designed and built before 1960 in the central United States.

## 1.1 Objectives of Research Program

The primary goal of the overall research program is to gather data regarding the behavior of low-rise masonry buildings with flexible roof diaphragms and highly rectangular footprints. Structures of this type are common in the US Army building inventory. Of particular interest are the in-plane behavior of the roof diaphragm and the associated out-of-plane behavior of the longitudinal walls. This type of behavior has not been extensively studied, and current design procedures may not address it adequately. Ultimately, recommendations for the inclusion of roof diaphragm flexibility in the design and analysis of low-rise masonry buildings are desired.

## 1.2 Scope of Thesis

This report summarizes the research work performed jointly at the University of Texas at Austin and the US Army Engineer Research and Development Center (ERDC) Construction Engineering Research Laboratory (CERL), between September 1999 and March 2001. That research is a coordinated study involving shaking-table testing, analytical confirmation, and the development of improved design approaches for low-rise masonry buildings with flexible roof diaphragms.

First, an experimental program is developed and executed. Prototypical structures are identified and evaluated for characteristic structural features. Two half-scale

specimens are developed, designed, and constructed based on the identified prototypical configurations. The half-scale specimens are tested on the US Army's shaking-table at the CERL facility, and seismic responses are measured using a carefully developed instrumentation scheme. The data are examined for their internal consistency, the dynamic characteristics of the half-scale specimens, and the response behaviors of the half-scale specimens.

To corroborate the observed responses, analytical models representing the half-scale test specimens are created and analyzed using an existing finite element program. The models are first created by assigning typical design values to input parameters, and then adjusting those values as they are required to calibrate the calculated and measured responses. Predictions from those analytical models are compared with measured responses, and the sensitivities of the analytical results are assessed using parametric studies.

Next, observations and conclusions from physical testing and analytical modeling are synthesized into a simplified two-degree-of-freedom design tool. The tool is developed for the general case and then verified using the two, half-scale specimens. Responses calculated using this tool are compared with measured responses of the half-scale specimens, and with the responses calculated by the finite element modeling. Sensitivity of the tool's results is also assessed using parametric studies.

Finally, to arrive at meaningful conclusions and recommendations relevant to the analysis and design of low-rise masonry buildings with flexible roof diaphragms, the implications of geometric scaling are examined. This provides a bridge between the observed responses of the half-scale specimens and the expected behavior of the full-scale prototype.

Ultimately, this report proposes tentative recommendations for including roof-diaphragm flexibility in the design and analysis of low-rise masonry buildings.

## 1.3 Units of Weight and Measure

U.S. standard units of measure are used throughout this report. A table of conversion factors for Standard International (SI) units is provided below.

| SI conversion factors | | |
|---|---|---|
| 1 in. | = | 2.54 cm |

# 2 Background

## 2.1 Theory, Practice, and Gaps in Current Knowledge

Until the 1970s, low-rise masonry buildings were usually designed as single-degree-of-freedom systems using the applicable equivalent lateral force design provisions*. These structures typically have relatively low roof mass and large plan areas of masonry, resulting in low stresses in the masonry walls under lateral design loads. Design of these structures is often governed by prescriptive requirements for reinforcement and detailing.

Such buildings typically have flexible roof diaphragms of wood, metal deck, or precast concrete planks. During seismic response, the in-plane flexibility of the diaphragm tends to uncouple the mass of the roof system from that of the masonry shear walls. The diaphragm, responding in its own plane, excites the connecting masonry walls out-of-plane. These effects become especially pronounced when the building has a high plan aspect ratio (for example 4:1). In effect, the flexibility of the diaphragm introduces additional (or at least, different) degrees of freedom related to the in-plane response of the diaphragm.

* Klingner, R.E. (1999), from the proposal for this research project.

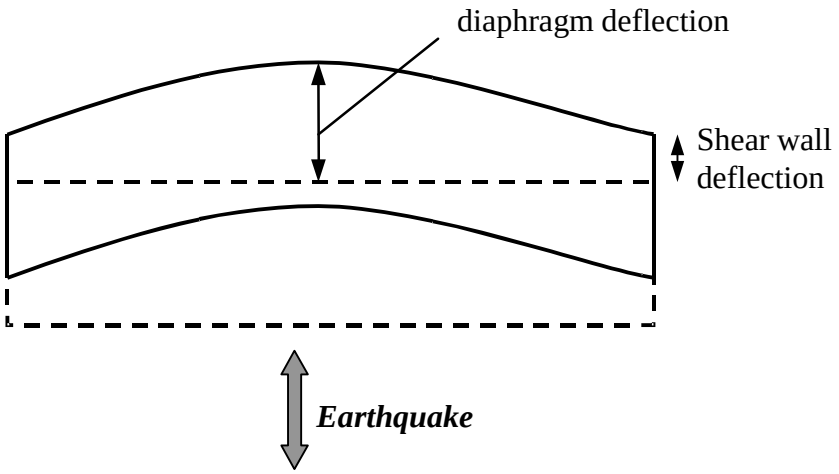


**Figure 2.1. Effect of in-plane flexibility on deformed shape of roof diaphragm during transverse response.**

The effects of the diaphragm flexibility on the response of such structures have not been extensively studied. Expected effects are:

- increase in fundamental period of vibration;
- decrease in mass coupled to the transverse shear walls;
- increase in mass coupled to the in-plane response of the diaphragm and thus an increase in the seismic actions in the diaphragm; and
- increase in magnitude of the out-of-plane response of the longitudinal masonry walls.

Current design practice dictates that these types of buildings be designed as single-degree-of-freedom systems, using the degree of freedom associated with the in-plane response of the shear walls parallel to the direction of excitation. Little guidance is available to the designer regarding more rigorous dynamic analysis considering roof diaphragm flexibility. The in-plane response of flexible diaphragms and the associated out-of-plane response of the connecting masonry walls need to be integrated into design practice.

## 2.2 Literature Review

There is some existing research work involving the testing, design, and analysis of masonry buildings with flexible diaphragms. Some of that research is now

summarized and briefly discussed. Parts of the literature survey were adapted from this research project's original proposal.

### 2.2.1 Previous Research on the Effects of Diaphragm Flexibility on Building Response

The consequence of roof and floor diaphragm flexibility on the seismic response of structures has been documented by several research efforts. Agbabian, Barnes, and Kariotis (ABK 1981a,b,c) present the results of a series of investigations examining the in-plane strength and stiffness of plywood roof diaphragms and their role in the response of low-rise buildings.

Sudhir and Jennings (1984) develop rigorous mathematical descriptions for the response of low-rise buildings with flexible diaphragms. That work, however, formulated the results considering only flexural deformations of the diaphragm. Results of the study are a series of transcendental formulae that are intended to provide for the dynamic response of the system.

The Technical Coordinating Committee for Masonry Research (TCCMAR) directed development of the ABK Lumped Parameter Model, LPM / I (Kariotis *et al*. 1988a). Application of the model for the non-linear dynamic analysis of low-rise shear-wall buildings with lumber and panel diaphragms is discussed in a companion study (Kariotis *et al*. 1988b). The results of a 6-year research program involving large-scale dynamic testing of wood diaphragms and masonry walls are presented by Kariotis (1995).

Tena-Colunga and Abrams (1995, 1996) compare measured responses of a low-rise masonry firehouse during the 1989 Loma Prieta earthquake to the responses calculated from a series of lumped parameter model studies. The studies conclude that the in-plane flexibility of the diaphragms could play an important role in the response of masonry structures.

Tremblay and Steimer (1995) discuss the results of an analytical study of low-rise, frame buildings with flexible metal deck diaphragms. The study found that existing design guidelines could not adequately calculated the fundamental period of the structure, the maximum drifts, the forces and deformations in the roof diaphragm, or the ductility demand on the bracing elements.

Fonseca *et al*. (1996) discusses the strength and deformation capacity of tilt-up structures with plywood roof diaphragms and Porter *et al*. (1990) discusses the strength and stiffness of concrete plank flexible diaphragms.

### 2.2.2 Previous Research on Wood Diaphragms

A significant amount of work has been published on the performance, analysis, and design of wood diaphragms. Peterson (1982) provides a comprehensive bibliography of that work. The Applied Technology Council published document ATC-7, *Guidelines for the design of horizontal wood diaphragms*, in 1981. ATC-7 provides a basis for the lateral design of horizontal wood diaphragms. The document also notes gaps in the, then current, state-of-the-art and subsequently proposes a series of research needs. Some of the noted research needs are to:

- develop simplified analytical models for the prediction diaphragm deflections;
- develop analytical models for various types of wall construction;
- perform dynamic diaphragm tests; and
- correlate observed responses with analytical studies.

This report is intended to address some of those research needs.

Bracci and Peralta* are currently investigating various retrofit techniques for horizontal, unchorded wood diaphragms. That research involves the quasi-static testing of lumber and plywood sheathed diaphragms.

### 2.2.3 Previous Research on Corrugated-Metal Deck Diaphragms

Most information involving metal deck diaphragms involves either racking tests of individual shear panels (for example Easley 1977), or the development of finite element methods for the analysis of orthotropic metal decks (for example Nilson and Anmar 1974). Kinh *et al.* (1979) presents a simplified method for the analysis of metal deck diaphragms and corroborates that work with finite element modeling and physical testing.

* Texas A&M University, current research, 2001

### 2.2.4 Previous Research on the Seismic Performance of Masonry Buildings and Assemblies

Bruneau (1994) provides a comprehensive state-of-the-art report discussing the seismic performance of unreinforced masonry buildings.

The TCCMAR effort dealt with the performance of masonry assemblies. Hamid *et al.* (1989) and Blondet *et al.* (1991) studied masonry walls loaded out-of-plane and Leiva *et al.* (1994) and Seible (1994) studied masonry walls loaded in-plane. Button and Mayes (1992) corroborate some of the work by developing analytical models representing walls loaded out-of-plane and comparing the results of that modeling with the observed TCCMAR results.

A number of experimental studies involving reduced-scale and full-scale plain and reinforced masonry structures have been performed. Abrams and Paulson (1991) and Tomazevic and Weiss (1992) emphasize:

- evaluation of mechanical properties of reduced-scale masonry materials;
- energy dissipation capacity of reinforced masonry assemblies; and
- seismic performance of plain and reinforced masonry buildings.

Seible *et al.* (1994) pseudo-dynamically tested a full-scale, five-story masonry structure to verify new design guidelines, developed by TCCMAR, for reinforced masonry buildings in seismic zones. All three studies noted that reinforced masonry assemblies can exhibit significant ductility with proper detailing.

### 2.2.5 Information on Shaking Tables

Clark (1992) provides a comprehensive discussion of the dynamic characteristics of large, multi-degree-of-freedom shaking tables.

### 2.2.6 Previous Shaking-Table Testing

A number of research programs involved the shaking-table testing of reduced-scale masonry structures:

- a single-story, reduced-scale masonry house (Manos *et al.* 1984);
- a four-story, reduced-scale building (Tomazevic and Zarnic);

- 24 simple two-story, reduced-scale, plain masonry buildings (Benedetti *et al.* 1998);

- two three-story, reduced-scale, reinforced masonry buildings (Abrams and Paulson 1991)

- two three-story, reduced-scale, plain and reinforced masonry buildings (Tomazevic and Weiss 1992); and

- a reduced-scale brick masonry building (Costley and Abrams 1996a,b).

### 2.2.7 Other Available Resources

The National Earthquake Hazard Reduction Program (NEHRP) in conjunction with the Federal Emergency Management Agency (FEMA) produced a series of documents, FEMA 273, *NEHRP Guidelines for the Seismic Rehabilitation of Buildings*, and FEMA 274, *NEHRP Commentary on the Guidelines for the Seismic Rehabilitation of Buildings* (1997a,b). Those documents provide code-type procedures for the assessment, evaluation, analysis, and rehabilitation of existing building structures. Another document, FEMA 306 (1999), *Evaluation of Earthquake Damaged Concrete and Masonry Buildings*, does not explicitly consider the out-of-plane dynamic response of reinforced masonry bearing walls or the associated in-plane response of the connecting diaphragms. That document does, however, note the possible consequence of a diaphragm with inadequate strength, stiffness or both. The text, *Earthquake Resistant Design of Masonry Buildings* (Tomazevic 1999), provides the *European Macroseismic Scale* of earthquake damage evaluation. This report uses that text and the FEMA 306 document to evaluate half-scale test specimen damage.

# 3 Development of Half-Scale Test Specimens

## 3.1 Overall Design of Prototypical Building

Because this research was directed at the seismic vulnerability of US Army structures designed and built before 1960 in the central US, the prototype masonry structure was designed to be typical of that time period. The structure was intended to represent a warehouse or storage facility, markedly rectangular in plan with openings on one long side. These types of structures typically have flexible roof diaphragms of lumber sheathing, corrugated metal decking, or precast concrete planks. The prototype building is shown in Figure 3.1.

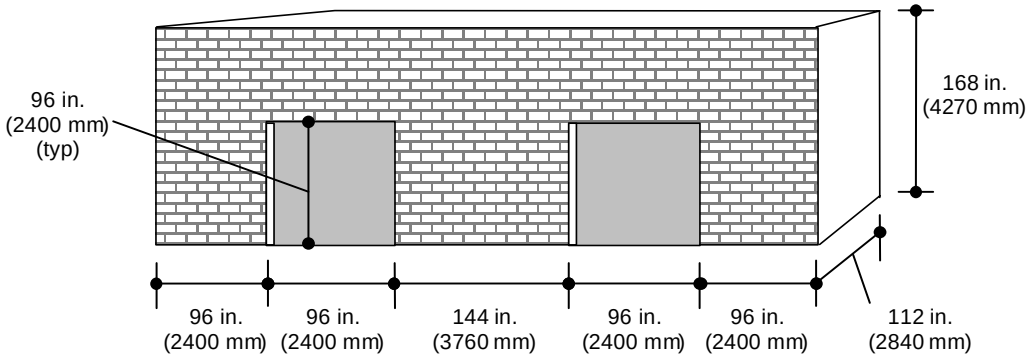


**Figure 3.1. Schematic of full-scale prototype building.**

## 3.2 Initial Remarks on Scaling

The performance capabilities of the US Army Tri-axial Earthquake and Shock Simulator (TESS) limit the size and mass of test specimens. As a result, this test program used half-scale specimens. Scaling offered some advantages over full-scale specimens:

- scaling allowed the testing of structures with large plan aspect ratios (4:1). Full-scale specimens would have been too long for the CERL shaking table; and

- scaling allowed researchers to subject the specimens to well over 1.0g of acceleration (Sections 7 and 8). Full-scale specimens would have had much more mass, decreasing the maximum possible acceleration available from the table actuators.

In this research study, no supplementary mass was affixed to the half-scale specimens. Consistent geometric scaling of the prototype structure permitted the development of literal relationships between response of the half-scale specimens and that of the full-scale prototype structures (Section 11). Supplementary mass affixed to the specimens would invalidate those relationships because:

1. The mass, if unsupported vertically, would generate vertical gravity stresses in the specimens' supporting elements.

2. The additional mass would most likely be distributed differently than the actual distribution of mass in the half-scale specimens, and would thus apply inconsistent inertial forces to the specimens.

3. Unlike framed structures, which are often treated as lumped-parameter shear-beam systems, the half-scale masonry specimens have distributed mass and stiffness. Attachment devices for the supplementary mass would probably restrain deformations in the specimens to some extent, unfavorably altering the specimens' response.

Attaching the supplementary mass in a manner that would permit complete, unrestrained, compatible response between the specimens and masses was judged to be difficult, time-consuming, and probably not cost effective.

Fortunately, it was also unnecessary. As mentioned, the performance capabilities of TESS allowed researchers to subject the half-scale specimens to large accelerations. This allowed the specimens to sustain levels of damage comparable to what they might sustain under the larger inertial forces resulting from supplementary masses.

## 3.3 Masonry Walls

The pre-1960 design procedure for low-rise masonry walls is essentially the same as those used today. Allowable stresses and some prescriptive requirements have changed to some extent. Typical design loads for the prototype structure

are low, however, and design is generally controlled by minimum prescriptive requirements for reinforcement. Prototype design required:

- Eight-inch CMU walls grouted vertically at 48 in. with one #4 reinforcing bar per grouted cell; and

- Walls grouted horizontally at bond beams with two #4 reinforcing bars per bond beam. Bond beams are located above openings and in top courses of the walls.

**Figure 3.2. Half-scale masonry wall under construction.**

After scaling by one-half, the specimen design required the reinforcement shown in Figure 3.3:

- Four-inch, specimen CMU walls grouted vertically at 24 in. with one #3 reinforcing bar per grouted cell (Figure 3.2); and

- Walls grouted horizontally at bond beams with two #3 reinforcing bars per bond beam. Bond beams are located at the top of openings and in the top course of the wall.

Appendix A contains as-built drawings of the masonry walls. Measured-mechanical properties of the masonry used in half-scale Specimen #1 and half-scale Specimen #2 are given in Section 9.1 of this report.

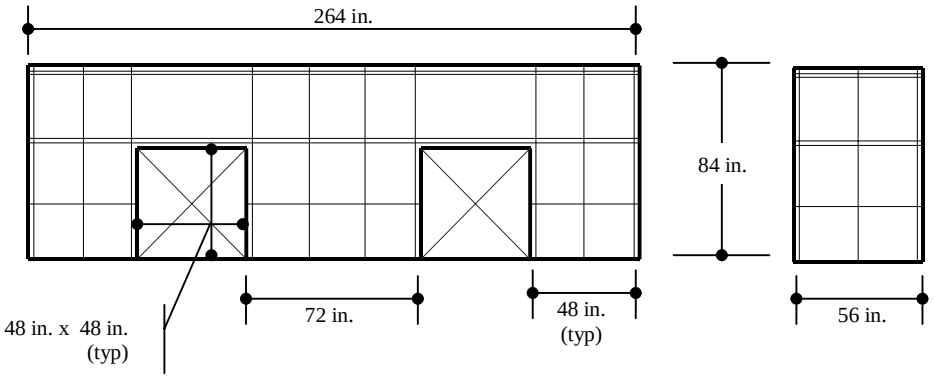


**Figure 3.3. Schematic of half-scale specimen reinforcement for longitudinal and transverse walls.**

## 3.4 Remarks on Half-Scale Specimens

For the purposes of this study, two specimens were developed for testing. The two specimens had identical plan layouts of masonry and also had identical openings in one long wall. The first specimen, called Specimen #1, had a roof diaphragm consisting of a single layer of diagonal-lumber sheathing. The second specimen, called Specimen #2, had a roof diaphragm consisting of untopped, corrugated-metal deck on open-web steel joists.

## 3.5 Half-Scale Specimen #1

### 3.5.1 Preliminary Design of Diagonally Sheathed Lumber Roof Diaphragm

A historical survey performed by CERL personnel provided typical construction details of several US Army masonry buildings designed and constructed before 1960. Based on that survey, the preliminary design of the specimen was refined:

- Typical wall ledgers and toe nailing replaced modern joist hangers.
- Diagonal lumber sheathing replaced the modern use of plywood or oriented strand board.
- Bridging was not included, because code requirements were more lenient prior to 1960.

Prototypical diaphragm design may have required 2x12 in. nominal spruce-pine-fur (SPF) rafters at 24 in. on center with 1x6 in. nominal SPF diagonal lumber sheathing in controlled-random layout. Scaling the dimensional lumber to half-scale specimen size translated to 5-1/2 in. x 3/4 in. SPF roof rafters at 12 in. on center, and 3/8 in. x 2-3/4 in. SPF diagonal sheathing (Figure 3.4, Figure 3.5, and Figure 3.6). Table 3-1 summarizes the roof design of half-scale Specimen #1.

**Table 3-1. Roof design of half-scale Specimen #1**

| Prototype Element | Half-Scale Element |
|---|---|
| SPF 1-1/2 in. x 11-1/2 in. roof rafters | SPF 3/4 in. x 5-1/2 in. roof rafters |
| SPF 3/4 in. x 5-1/2 in. lumber sheathing | SPF 3/8 in. x 3-1/4 in. lumber sheathing |
| 8d or 10d nailing | 4d nailing |

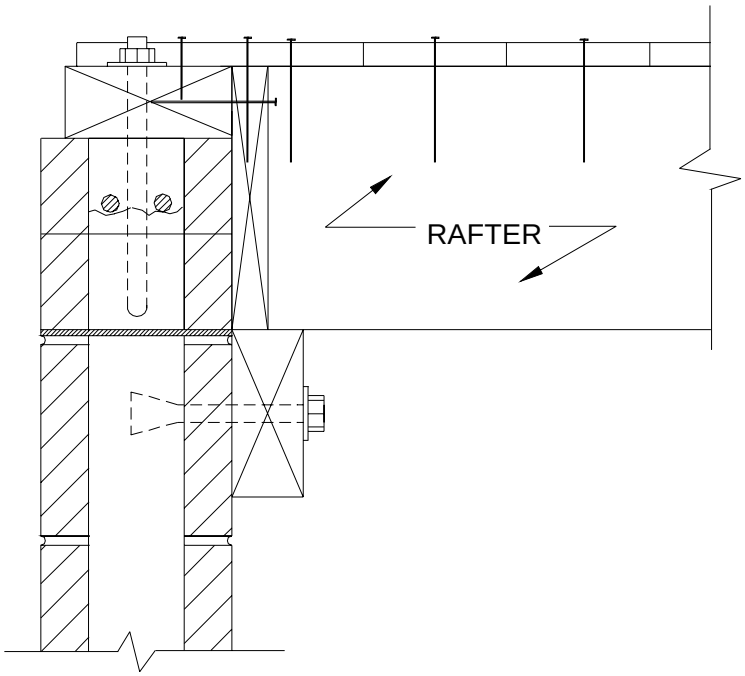


**Figure 3.4. Typical detail of rafter-to-wall connection (Specimen #1).**

**Figure 3.5. Underside of diaphragm as built (Specimen #1).**

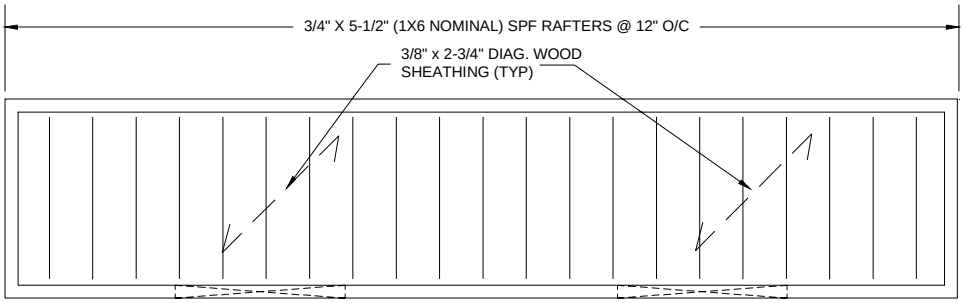


**Figure 3.6. Plan of lumber roof diaphragm (Specimen #1).**

### 3.5.2 Construction of Lumber Diaphragm

Private contractors selected by CERL constructed the masonry walls and lumber diaphragm. Interaction among those contractors, CERL personnel, and University of Texas researchers resulted in several changes to the design:

- nail sizes were changed;
- member sizes were changed slightly based on local availability of lumber, and dimensions were clarified;

- layout of lumber sheathing was clarified; and

- ledger and rafter blocking designs were changed, and nailing patterns were clarified.

The member sizes and nailing requirements resulting from these changes are summarized in Table 3-1. Figure 3.7 and Figure 3.8 show Specimen #1 as built. Appendix B contains as-built drawings of half-scale Specimen #1.


**Figure 3.7. Overall photo of Specimen #1.**

**Figure 3.8. Roof diaphragm in "controlled-random" layout (Specimen #1).**

## 3.6 Half-Scale Specimen #2

### 3.6.1 Preliminary Design of Corrugated Metal Roof Diaphragm

Prototypical diaphragm design would have required open-web steel joists (OWJs) with light-gauge, wide-rib, metal deck spanning between the joists. To facilitate practical and economical scaling, the half-scale specimen used commercially available full-scale, 8-inch deep 8K1 open-web joists with full-scale, 22-gauge, wide-rib metal decking. The equivalent of a 36 / 3 puddle weld pattern (three welds for every 36 inches of deck cross-section) fastened the decking to the joists. A single row of horizontal bridging was provided for lateral stability of joists and load sharing among them.

Prior testing of a similar structure with a lumber roof diaphragm (Specimen #1), effectively segmented the diaphragm into four instrumented panels (Figure 7.1). To remain consistent with this, the half-scale design of Specimen #2 re-created the same four-panel configuration with the spacing of the OWJs (Figure 3.9, Figure 3.10, and Figure 3.11).

Based on the same historical survey described in Section 3.4 of this report, it was determined that this preliminary prototype metal diaphragm design was typical of the pre-1960 time period. Table 3-2 summarizes the roof design of half-scale Specimen #2.

**Table 3-2. Roof design of half-scale Specimen #2.**

| Prototype Element | Half-Scale Element |
|---|---|
| 12 to 24 in. deep OWJ | Vulcraft-8K1, 8 in. deep OWJ |
| 18 to 20 gauge, wide-rib decking | Vulcraft-22 gauge, wide rib, Type B |
| 36 / 3 or 36 / 4 puddle welding | 36 / 3 or 36 / 4 puddle welding |

**Figure 3.9. Typical joist-to-wall connection as designed (Specimen #2).**

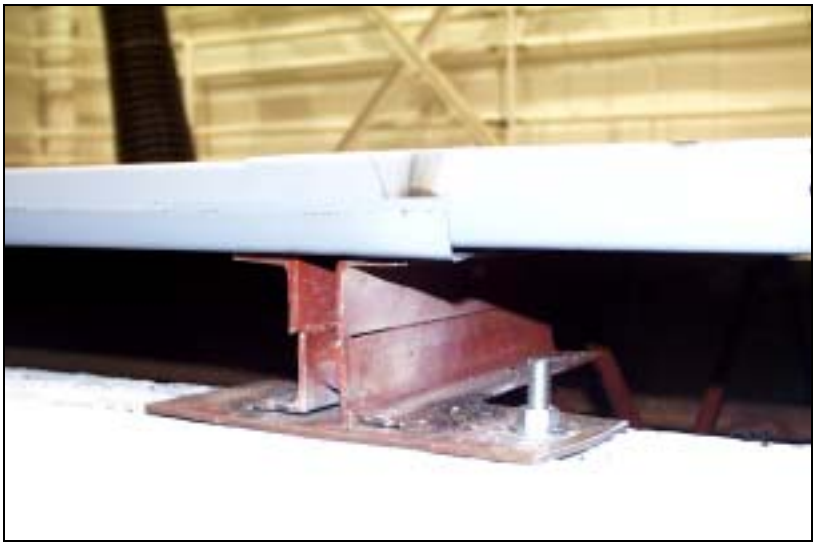

**Figure 3.10. Typical joist-to-wall connection as built (Specimen #2).**

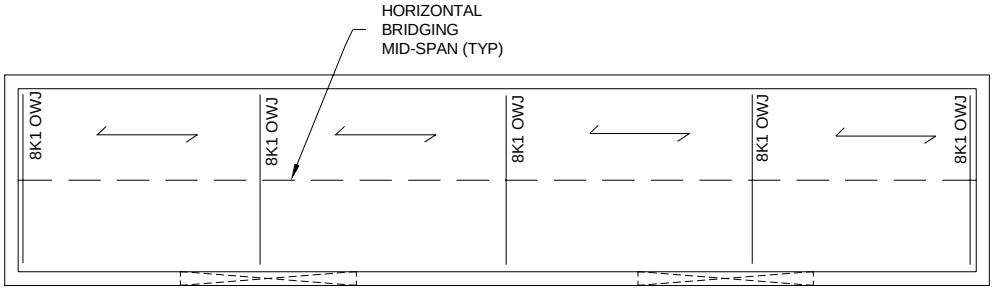


**Figure 3.11. Plan of metal deck diaphragm (Specimen #2).**

### 3.6.2 Construction of Metal Deck Diaphragm

Private contractors, selected by CERL, constructed the masonry walls and the roof diaphragm. Interaction among those contractors, CERL personnel, and University of Texas researchers resulted in several changes to the design:

- layout of individual metal deck sheets was clarified (Figure 3.12);
- to maintain longitudinal symmetry between decking sheets, the 36 / 4 weld pattern was effectively changed to 36 / 3 (Figure 3.13);
- the locations of end-lap puddle welds and side-lap screws were clarified; and
- the angle-to-wall connection of the horizontal bridging was modified to meet the as-built conditions of the wall and diaphragm (Figure 3.14).

Figure 3.15 and Figure 3.16 show the specimen as built. Appendix C contains as-built drawings of half-scale Specimen #2.

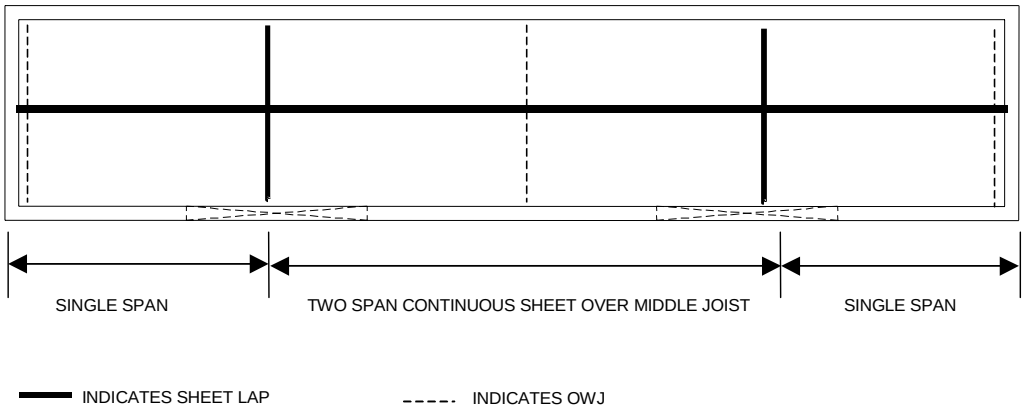


**Figure 3.12. Layout of corrugated metal decking as built (Specimen #2).**

**Figure 3.13. Effective 36 / 3 puddle-weld pattern (Specimen #2).**

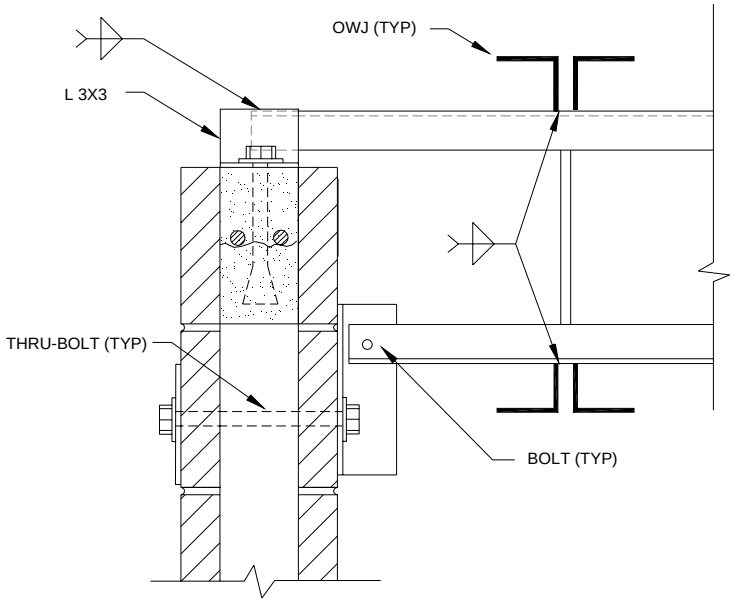


**Figure 3.14. Horizontal bridging-to-wall connection as built (Specimen #2).**

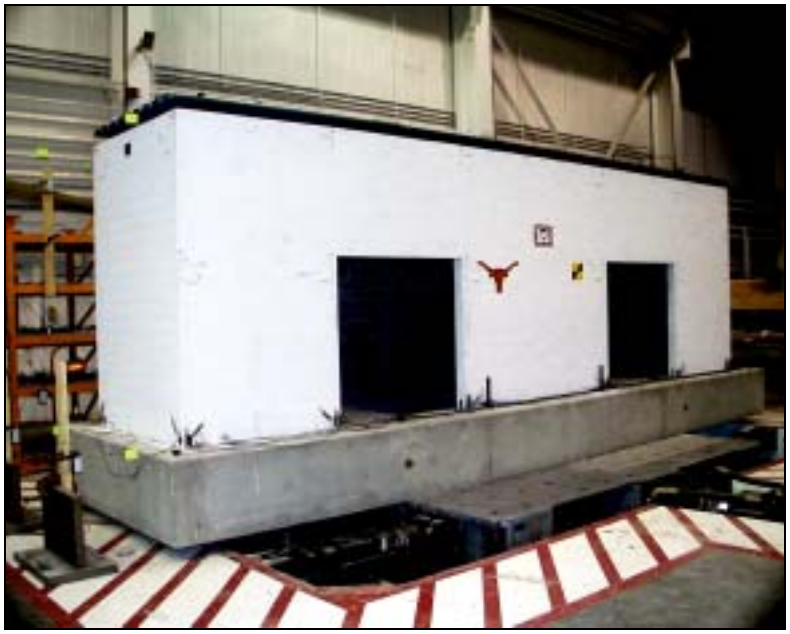

**Figure 3.15. Overall view of Specimen #2 as built.**

**Figure 3.16. Underside of metal-deck roof diaphragm as built (Specimen #2).**

# 4 Specimen Instrumentation and Data Acquisition

## 4.1 Objectives of Specimen Instrumentation

The instrumentation scheme developed for this project was intended to capture both the dynamic response (accelerations) and the deformations (shear, flexure, and rocking) of the half-scale specimens. Specifically, the instrumentation scheme measured:

Deformations

- the approximate in-plane deformed shape of the roof diaphragm;
- the relative contributions of shear and flexure to the in-plane deformation of the roof diaphragm;
- the relative contributions of shear and flexure to the in-plane deformation of the transverse shear walls and the three piers in the perforated longitudinal wall;

Displacements

- wall and pier rocking;
- the global displacement response of the structure at the roof diaphragm;

Accelerations

- the in-plane acceleration response of the diaphragm; and
- the out-of-plane acceleration response of the diaphragm and two of the masonry walls.

The instrumentation of the specimens was designed to capture the response of the specimens and obtain the necessary data for the research effort.

## 4.2 Data-Acquisition System

Seismic test data were recorded with a Pacific Instruments Model 600 Modular Conditioning and Data Acquisition System*, consisting of a mainframe unit with modular plug-in cards for each channel. Each plug-in card was configured specifically for its channel and the associated type of instrument. Each channel provided transducer excitation, balancing, and calibration data. The system included anti-aliasing filters to remove high-frequency noise and to reduce any aliasing effects in the recorded data. The entire data-acquisition system was controlled by personal computer. Software in the personal computer provided for the setup, calibration and transcription of the recorded and digitized data to the computer's hard disk, while also providing real-time display and analysis functions.

Three different types of instruments were used during testing:

- Accelerometers (Endevco Model 7290-10 and Microtron Model 7290-30);
- Displacement Transducers (ETI Inc. Model LCP12A-25-10K and ETI Inc. Model LCP12A-50-10K linear potentiometers); and
- Global Displacement Transducers (Celesco Model PT101-20 variable-resistance, precision rotary displacement transducers.)

Figure 4.1 shows the layout of the data-acquisition system. Section 7.1 and Section 8.1 of this report provide the instrumentation schemes used for each half-scale test specimen.

* Information in this section was provided by James Gambill of the U.S. Army Engineer Research and Development Center's Construction Engineering Research Laboratory (ERDC/CERL), Champaign, IL.

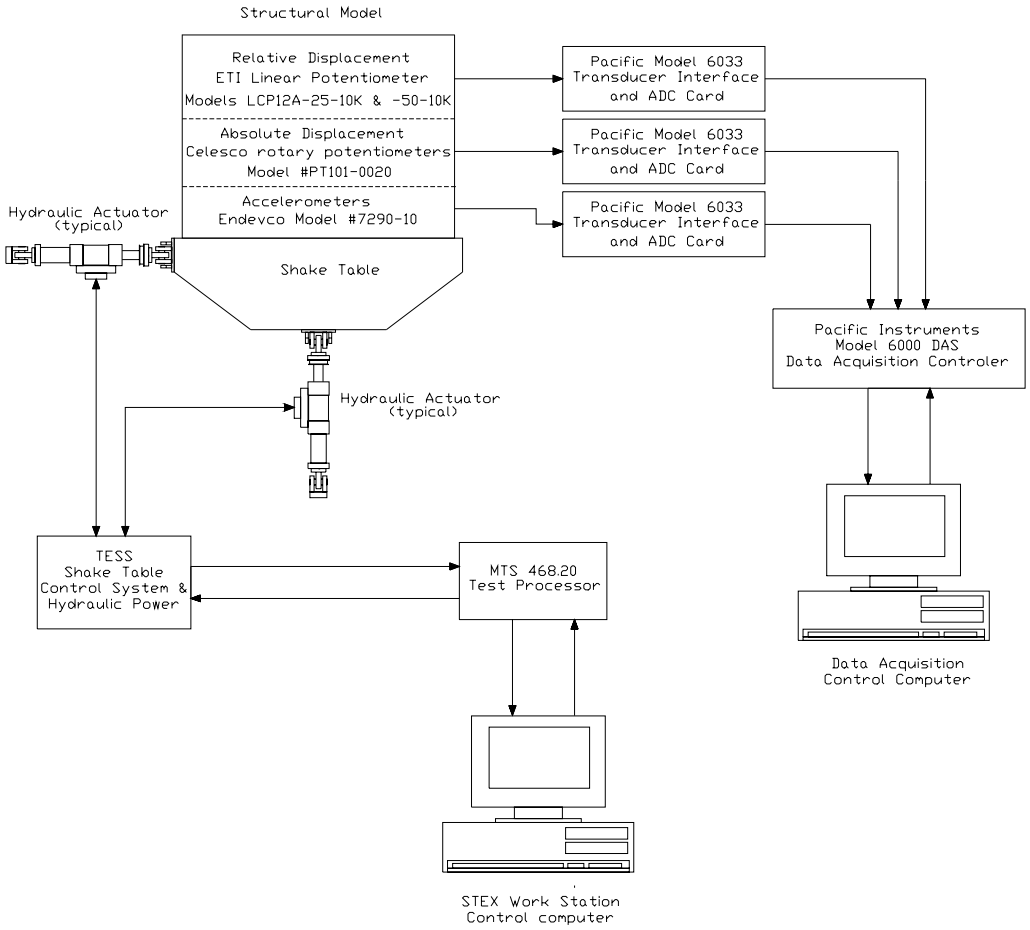


**Figure 4.1. Schematic of data-acquisition system.**

# 5 Selection of Seismic Ground Motions

Projects RR-1 and RR-2 of the Mid-America Earthquake Center (MAE) involved the development of artificial ground motions for three major Mid-American cities: Carbondale, IL; St. Louis, MO; and Memphis, TN (Wen and Wu 1999). Those projects also produced corresponding Uniform Hazard Response Spectra (UHRS) at 10% and 2% levels of expected exceedence in 50 years. The ground motions used in this research were taken from that study.

## 5.1 Estimation of Natural Periods of Prototypes

The preliminary analytical study discussed in detail in Section 10.2 of this report was used to calculate the fundamental periods of the full-scale prototype buildings. Those fundamental periods were about 0.08 second for both prototype buildings (lumber diaphragm and metal deck diaphragm). Ground motions containing high excitation energy at the probable prototype fundamental periods were then identified.

## 5.2 Selected Prototype Ground Motions

After reviewing the hypothetical 2% UHRS for Carbondale, Memphis, and St. Louis, it was determined that motions from the Carbondale suite contained the most excitation energy in the probable range of prototype periods identified by the preliminary analytical study. Time, financial, and practical constraints required the selection of at most two ground motions from that suite. Using a computer program that calculates response spectra, records were identified from the Carbondale suite that contained significant energy in the anticipated periods in both the transverse and the longitudinal direction. Based on that criterion, Motions 09s and 03s from the Carbondale suite (C02_09s and C02_03s) were selected for the transverse and longitudinal directions, respectively. The transverse ground motion has a peak ground acceleration (PGA) of 0.67g and the longitudinal ground motion has a PGA of 0.55g. Figure 5.1 and Figure 5.2 show the response spectra for ground motions C02_09s and C02_03s.

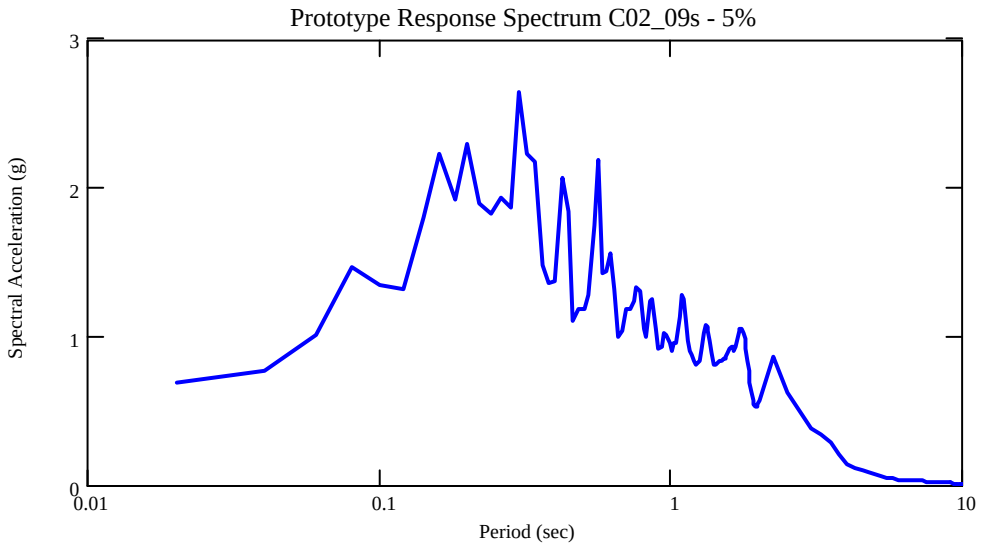


**Figure 5.1. Prototype response spectrum for Carbondale C02_09s ground motion used in transverse direction.**

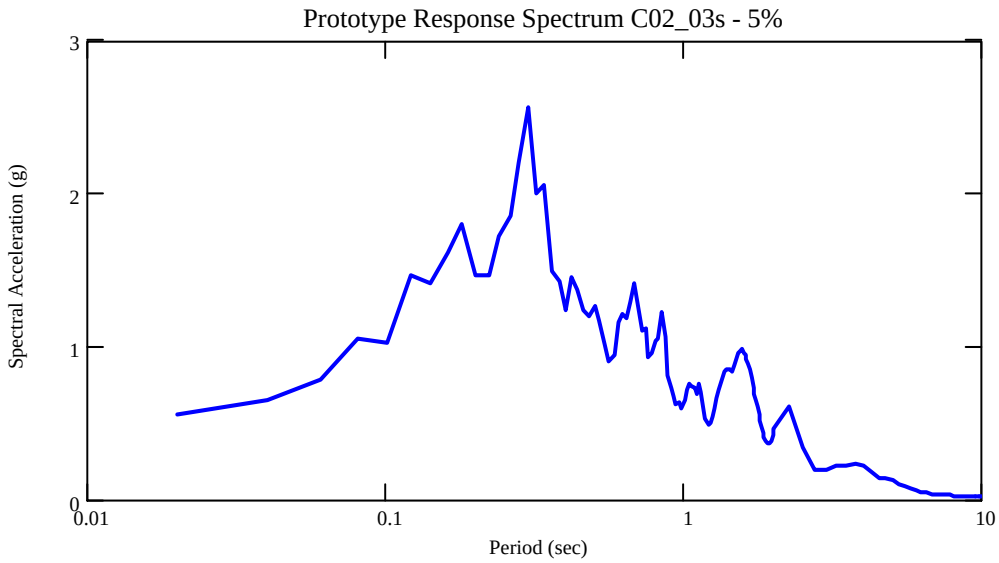


**Figure 5.2. Prototype response spectrum for Carbondale C02_03s ground motion used in longitudinal direction.**

## 5.3 Modification of Selected Input Motions

To avoid very large experimental data files, input records lasting between 30 and 40 seconds were preferred. C02_09s lasted 40 seconds and C02_03s lasted 60 seconds. To truncate them smoothly, they were multiplied in the time range between 30 and 40 seconds by an exponential decay function, so that the value at

30 seconds was 100% of the corresponding original value, and the modified value at 40 seconds was 1% of the corresponding original value. That portion of the record following the exponential decay at 40 seconds was essentially zero, and was therefore discarded. In addition, a segment was cropped from the beginning of each record. The cropped portion contained little or no significant motion and thus had negligible effect on response.

At each step in this modification process, the record was input to a single-degree-of-freedom response program to test for possible changes in response. Maximum responses consistently occurred at identical times and with identical values. It was therefore concluded that the half-scale specimens would respond to the modified ground motions essentially as they would have responded to the original motions.

The half-scale specimens would respond differently from the corresponding full-scale prototypes to a given ground motion, however, because of geometric scaling effects. As discussed shortly, compressing the time scale by a factor of two maintained dynamic similitude between the half-scale specimens and the full-scale prototypes. This preserved the relationship between the natural frequencies of the half-scale specimens and the spectral peaks of the input motion. The natural periods of the half-scale buildings are one half those of the full-scale prototype structures, as shown in Equation 5-3. Thus, the prototype input time step of 0.01 second was changed to a scaled input time step of 0.005 second. This can be justified by dimensional analysis of the natural circular frequency, $\omega_n$, as now explained.

The relationship between the circular frequency of the half-scale specimen and that of the prototype is:

$$\frac{\omega_{model}}{\omega_{prototype}} \propto \frac{\sqrt{\frac{K_m}{M_m}}}{\sqrt{\frac{K_p}{M_p}}} \qquad \textbf{(5-1)}$$

If the stiffness of the half-scale specimen depends primarily on the in-plane shearing stiffness of the transverse shear walls, then

$$\frac{\omega_{model}}{\omega_{prototype}} \propto \frac{\sqrt{\frac{G_m A_m / h_m}{M_m}}}{\sqrt{\frac{G_p A_p / h_p}{M_p}}} = \frac{\sqrt{\frac{G_p A_p \alpha^2 / h_p \alpha}{\rho_p L_p{}^3 \alpha^3}}}{\sqrt{\frac{G_p A_p / h_p}{\rho_p L_p{}^3}}} = \sqrt{\frac{1}{\alpha^2}} = \frac{1}{\alpha} \qquad \textbf{(5-2)}$$

Where:

L = unit of length

M = unit of mass

$\omega_n$ = natural frequency

$\alpha$ = scale factor = 1/2

A = area

h = wall height

G = shear modulus

So, the relationship between the period of the half-scale specimen and that of the prototype structure is

$$\frac{T_{model}}{T_{prototype}} = \alpha \qquad \textbf{(5-3)}$$

In this case, the scaling factor $\alpha$ equals 1/2, so the period of the half-scale specimen is one-half that of the prototype. This same relationship can be shown to be true when the stiffness terms in Equation 5-2 involve flexural stiffness of the transverse shear walls or in-plane stiffness of the diaphragm.

Figure 5.3 and Figure 5.4 show the modified input records for the half-scale specimens. Figure 5.5, Figure 5.6, Figure 5.7, and Figure 5.8 show the acceleration and displacement response spectra for those modified input records.

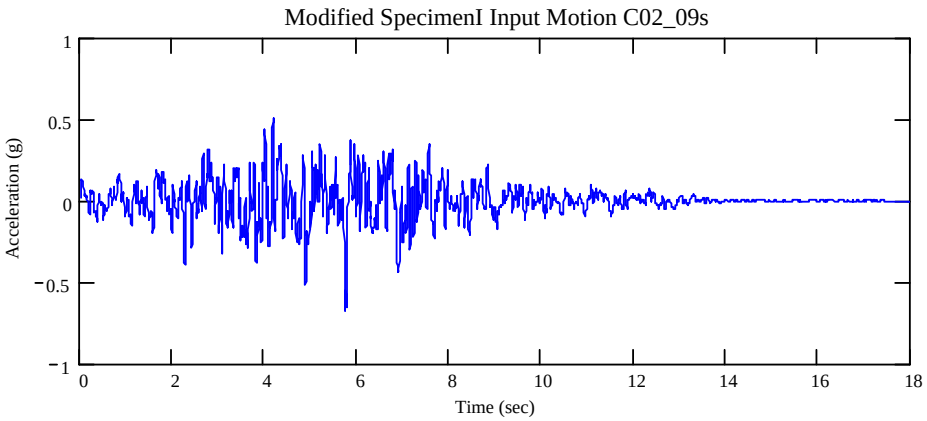


**Figure 5.3. Time-scaled input record for transverse excitation of half-scale specimens.**

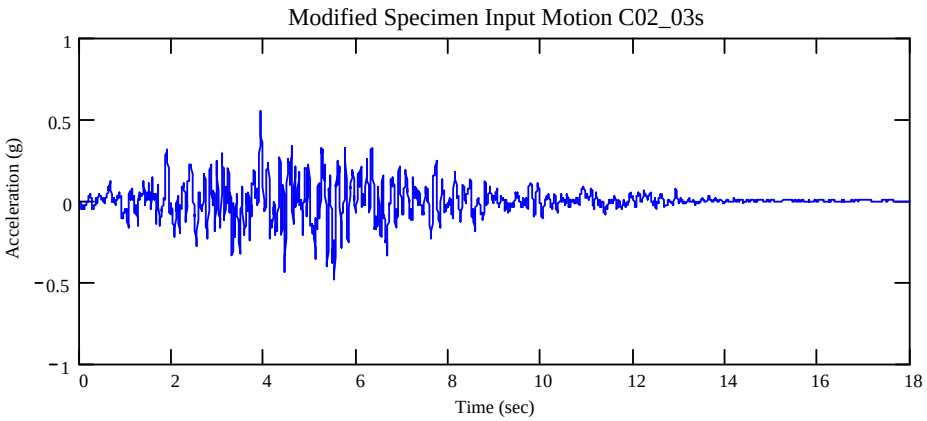


**Figure 5.4. Time-scaled input record for longitudinal excitation of half-scale specimens.**

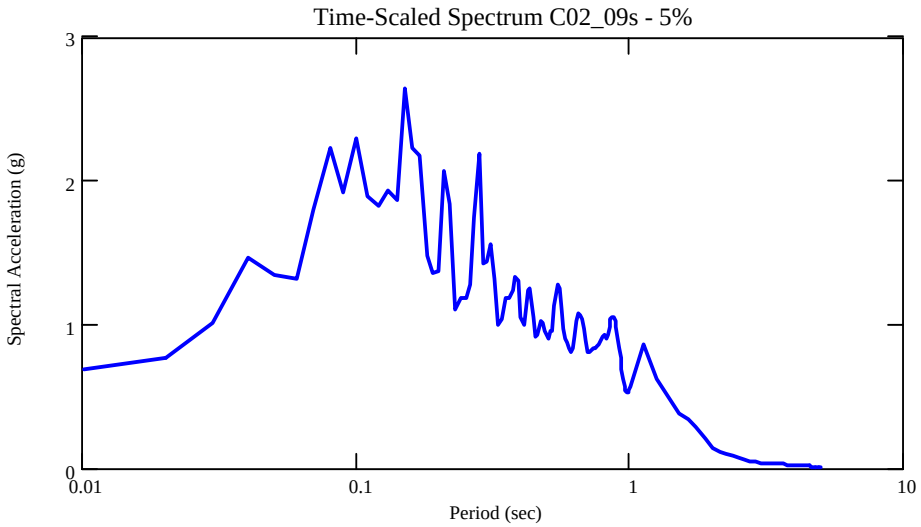


**Figure 5.5. Acceleration response spectrum of time-scaled input record used for transverse excitation of half-scale specimens.**

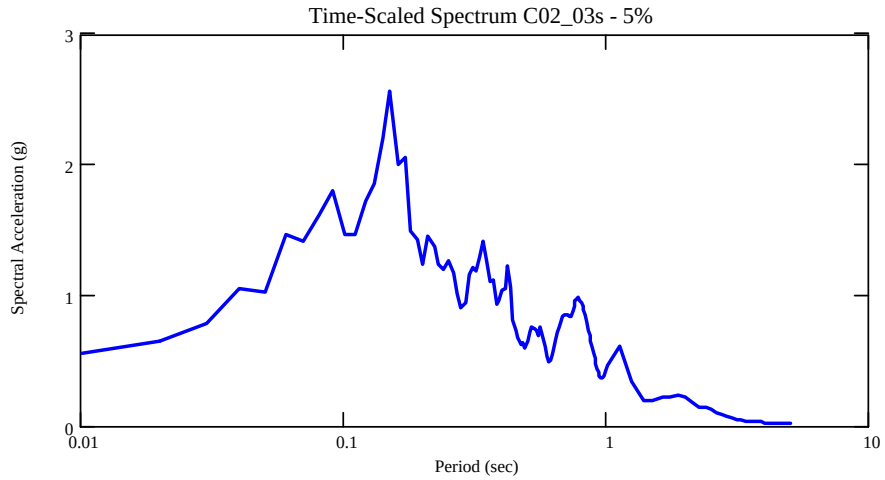


**Figure 5.6. Acceleration response spectrum of time-scaled input record used for longitudinal excitation of half-scale specimens.**

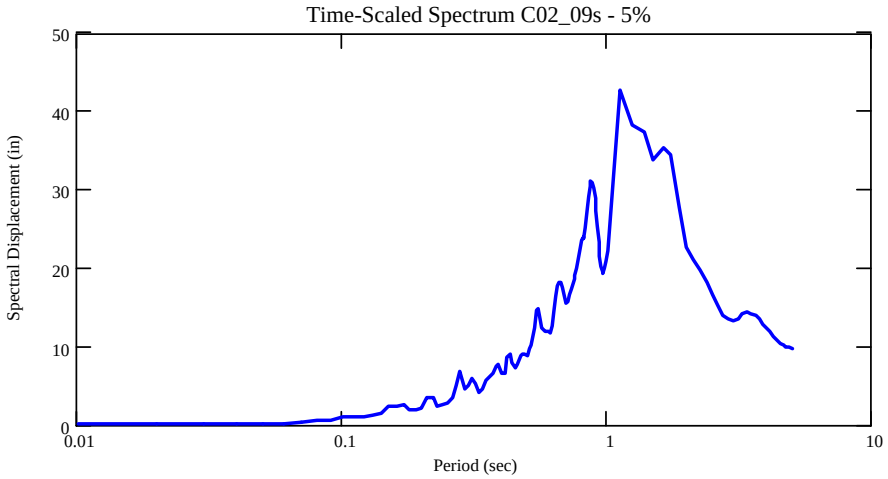


**Figure 5.7. Displacement response spectrum of time-scaled input record used for transverse excitation of half-scale specimens.**

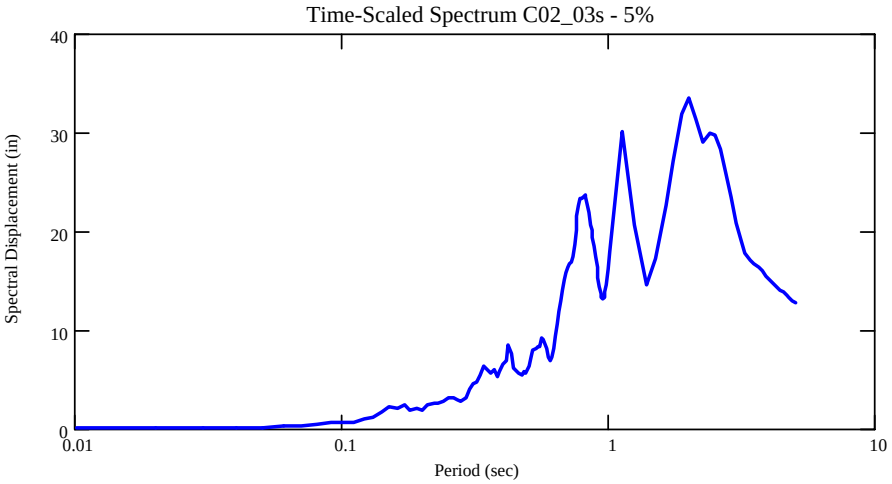


**Figure 5.8. Displacement response spectrum of time-scaled input record used for longitudinal excitation of half-scale specimens.**

# 6 White-Noise, Sine-Sweep and Sine-Decay Testing

The half-scale specimens were subjected to a series of dynamic tests intended to measure their natural frequencies and equivalent viscous damping ratios. White-noise excitation and sine-sweep/resonant-search excitation were performed prior to seismic testing to obtain information about the natural frequencies of the specimens. Sine-decay testing performed prior to seismic testing provided the equivalent viscous damping ratios of the half-scale specimens. White-noise tests performed following each seismic test detected changes in the natural frequencies of the specimens. Table 6-1 and Table 6-2 summarize the low-level test series for each half-scale specimen.

**Table 6-1. Low-level testing of Specimen #1**

| Preceding Seismic Test | Low-Level Test Type and Number | Directions |
|---|---|---|
| - | White Noise 1, 2, 3 | Y, X, Z |
| - | Sine Sweep 1, 2, 3 | X, Y, Z |
| - | Sine Decay 1, 2, 3 | X, Y, Z |
| Seismic Test 3 | White Noise 4, 5 | Y, X |
| Seismic Test 4 | White Noise 6, 7 | Y, X |
| Seismic Test 5 | White Noise 8, 9 | Y, X |
| Seismic Test 6 | White Noise 10, 11 | Y, X |
| Seismic Test 7 | White Noise 12, 13 | Y, X |
| Seismic Test 8 | White Noise 14, 15 | Y, X |
| Seismic Test 9 | White Noise 16, 17 | Y, X |
| Seismic Test 10 | White Noise 18, 19 | Y, X |
| Seismic Test 11 | White Noise 20, 21 | Y, X |

**Table 6-2. Low-level testing of Specimen #2.**

| Preceding Seismic Test | Low-Level Test Type and Number | Directions |
|---|---|---|
| - | White Noise 22, 23, 24 | Y, X, Z |
| - | Sine Sweep 4, 5, 6 | X, Y, Z |
| - | Sine Decay 4, 5 | X, Y |
| Seismic Test 2 | White Noise 25, 26 | Y, X |
| Seismic Test 4 | White Noise 27, 28 | Y, X |
| Seismic Test 5 | White Noise 29, 30 | Y, X |
| Seismic Test 6 | White Noise 31, 32 | Y, X |
| Seismic Test 7 | White Noise 33, 34 | Y, X |
| Seismic Test 8a | White Noise 35, 36 | Y, X |
| Seismic Test 8b | White Noise 37, 38 | Y, X |
| Seismic Test 9 | White Noise 39, 40 | Y, X |
| Seismic Test 10 | White Noise 41, 42 | Y, X |

## 6.1 Natural Frequencies

CERL personnel used a random vector generation algorithm to develop the white-noise input waveforms*. Each white-noise test ran for 60 seconds. The sine-sweep testing varied between 10 Hz and 80 Hz at a maximum table acceleration of about 0.10*g*. Each sine-sweep test ran for 90 seconds. Figure 6.2 is intended to describe only the shape of a typical sine-sweep input record and not typical acceleration or time values. The white-noise and sine-sweep tests ran in the three principal plan directions of the specimens (east-west, north-south, and up-down). Acceleration response data were recorded during those tests. Table 6.3 summarizes the findings from the white noise and sine sweep tests.

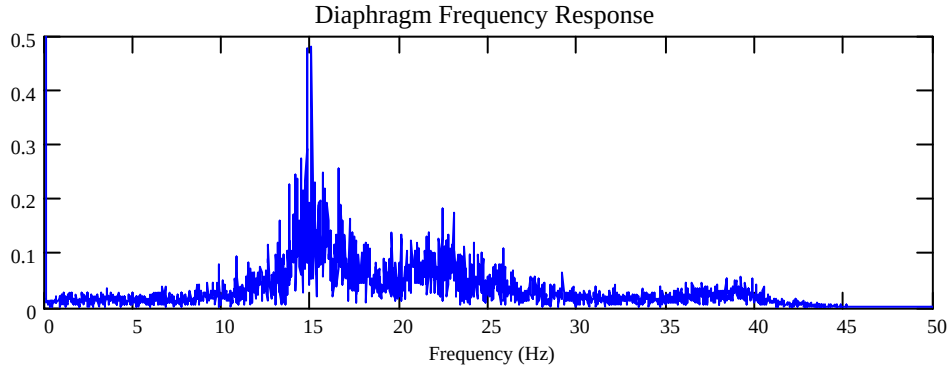


**Figure 6.1. Typical transverse frequency response of the diaphragm to white noise excitation.**

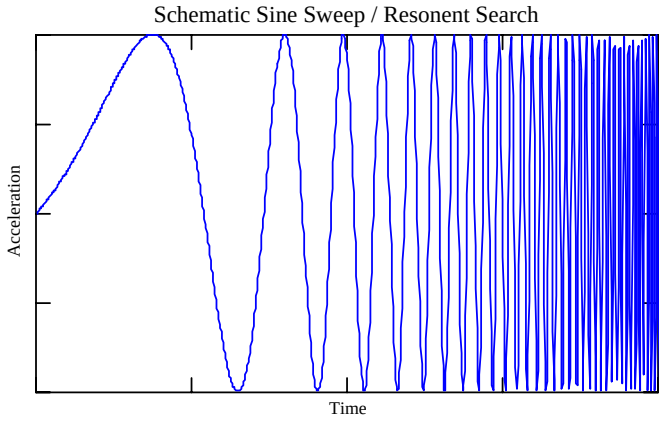


**Figure 6.2. Typical sine-sweep input record.**

* Personal communication, James Gambill, US Army ERDC/CERL.

**Table 6-3. Results of sine-sweep and white-noise testing.**

| Principal Direction | Specimen #1 (Lumber) lowest frequency | Specimen #2 (Metal) lowest frequency |
|---|---|---|
| X (longitudinal) | 20 Hz | 20 Hz |
| Y (transverse) | 14 Hz | 12 Hz |
| Z (vertical) | 38 Hz | 25 Hz |

## 6.2 Equivalent Viscous Damping

The CERL personnel excited each specimen three times, in each principal plan direction, at the lowest measured natural frequency associated with that direction. Excitation was abruptly halted and decay of the specimen's acceleration response was recorded. Figure 6.3 is intended to describe only the shape of a typical sine-decay response and not typical acceleration or time values. An equivalent viscous damping ratio was then calculated from the decaying portion of the response. Table 6-4 summarizes the findings from the sine-decay tests.

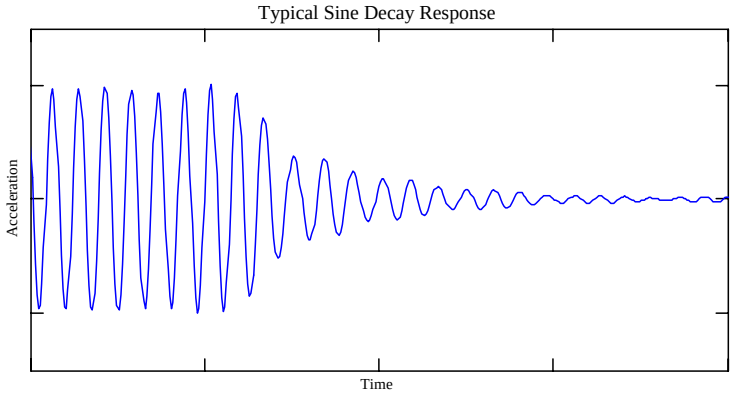


**Figure 6.3. Typical sine-decay response.**

**Table 6-4. Results of sine-decay testing.**

| Principal Direction | Specimen #1 (Lumber) damping ratio | Specimen #2 (Metal) damping ratio |
|---|---|---|
| X (longitudinal) | 7 % | 5 % |
| Y (transverse) | 3 % | 5 % |
| Z (vertical) | 3 % | N/A* |

* Data from this test were inadvertently corrupted.

# 7 Testing of Half-Scale Specimen #1 *(Diagonal Lumber Sheathing)*

## 7.1 Specimen Instrumentation

Instrumentation of half-scale Specimen #1 required 78 data channels, measuring:

- deflections relative to a stationary frame off the shaking table using 9 spiral potentiometers;
- lateral, vertical, and out-of-plane accelerations using 19 accelerometers; and
- shearing deformations, uplift, and pier rocking using 50 linear potentiometers.

Figure 7.1 through Figure 7.6 show the instrumentation of Specimen #1.

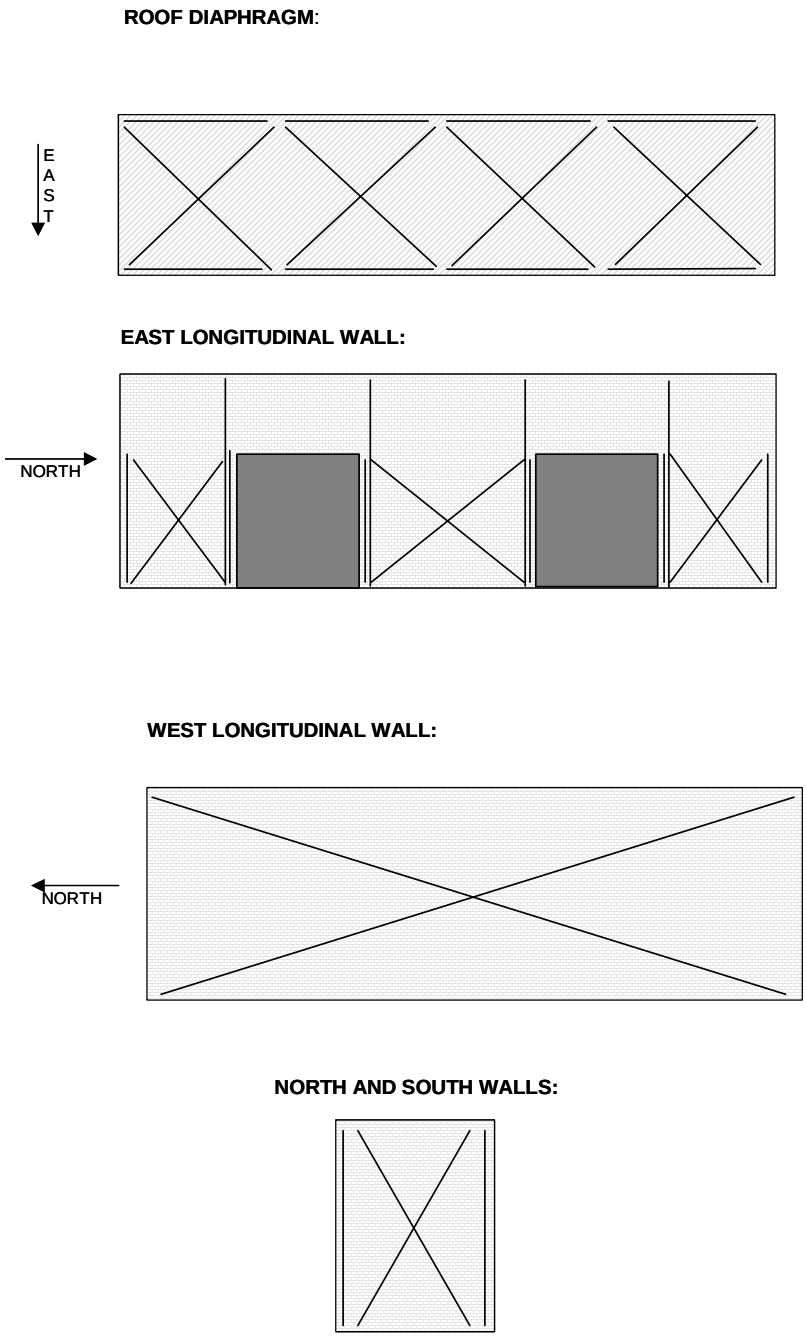


**Figure 7.1. Instrumentation for measuring in-plane shear deformations using linear potentiometers (Specimen #1).**

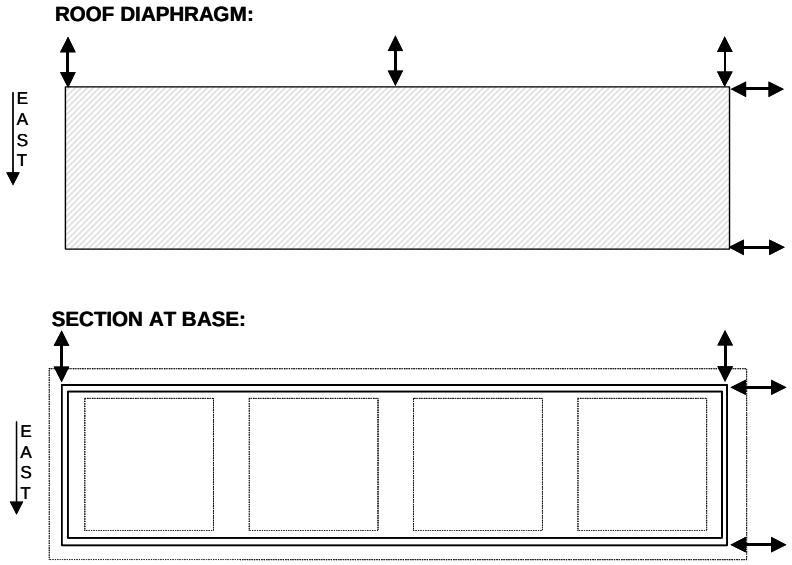


**Figure 7.2. Instrumentation for measuring global point displacements using spiral potentiometers (Specimen #1).**

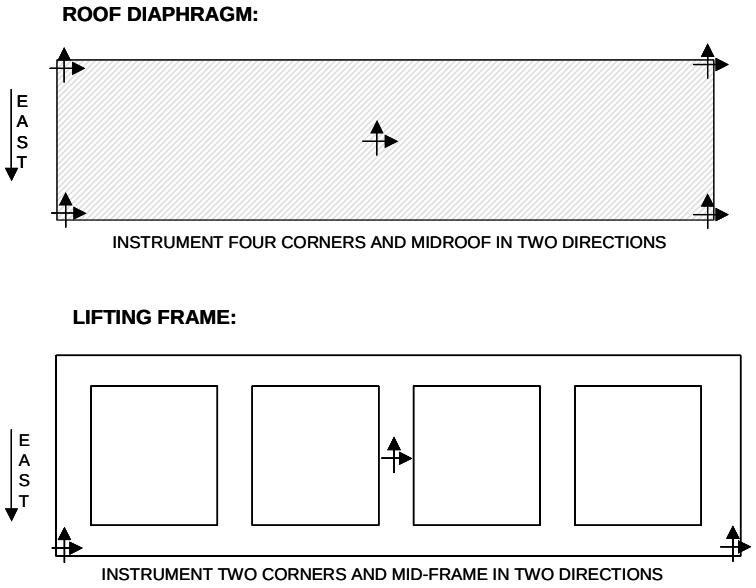


**Figure 7.3. Instrumentation for measuring horizontal accelerations (Specimen #1).**

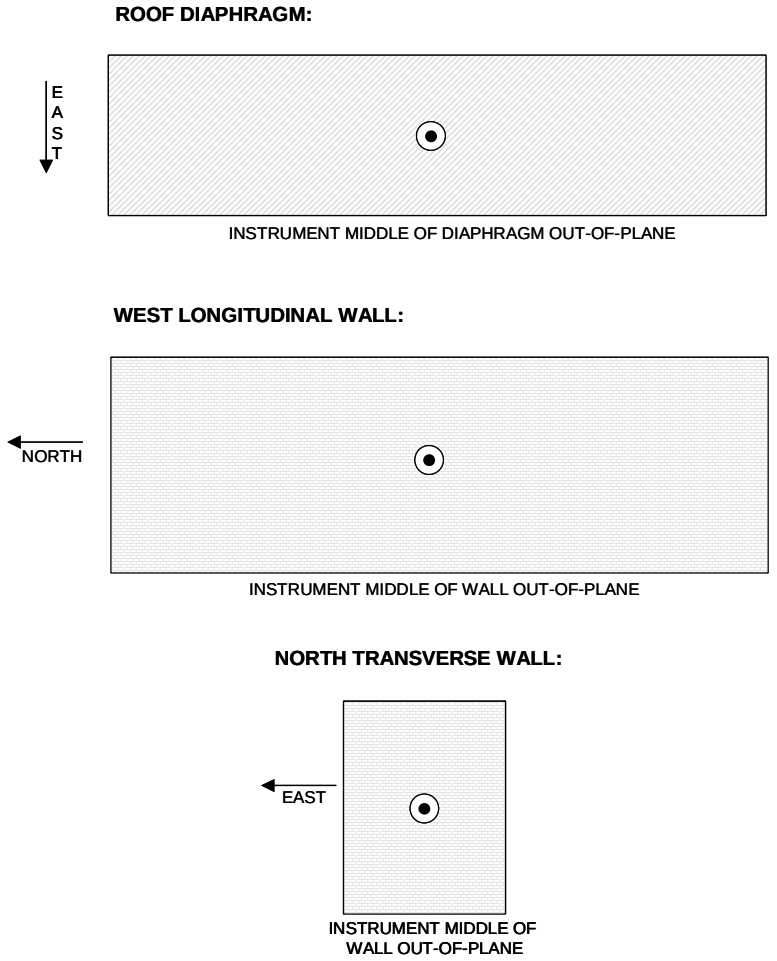


**Figure 7.4. Instrumentation for measuring out-of-plane accelerations (Specimen #1).**


**Figure 7.5. Linear potentiometers mounted on lower southeast corner of perforated masonry wall (Specimen #1).**

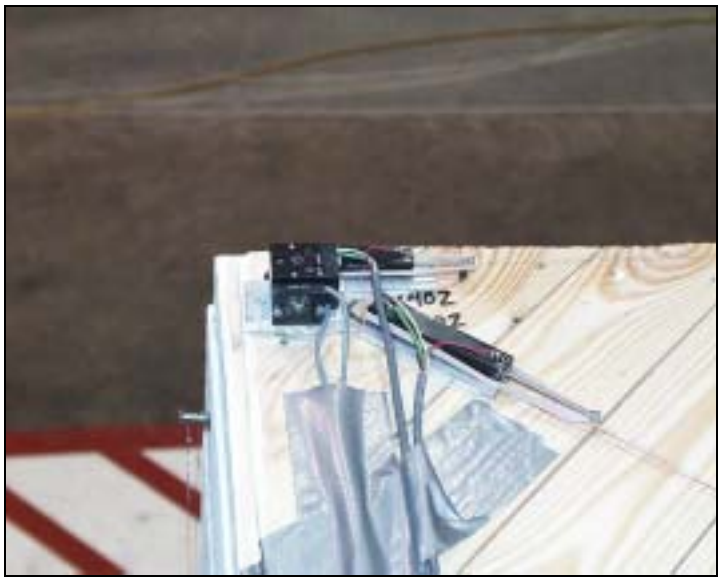

**Figure 7.6. Accelerometers and linear potentiometers mounted on southeast corner of roof diaphragm (Specimen #1).**

## 7.2 Preparation of Shaking Table (TESS)

CERL personnel subjected TESS to ground motions without the specimen to check agreement between input motions and table output motions. The CERL electronics technician discovered that the east-west acceleration response at a frequency of about 40 Hz was approximately twice what it should have been. Troubleshooting showed that this discrepancy occurred only in the south table accelerometer. It was determined that full control of the shaking table could be maintained using only the north table accelerometer. The south accelerometer was disconnected and testing was continued as planned.

The specimen and lifting girder were secured to TESS with six large tie-down bolts (Figure 7.7).

**Figure 7.7. Lifting of Specimen #1 onto shaking table.**

## 7.3 Seismic Ground Motion Tests

CERL personnel and the University of Texas at Austin researchers subjected the specimen to a suite of 11 seismic tests at increasing levels of maximum input acceleration. From each uniaxial test to the next, the direction of excitation was alternated from longitudinal to transverse, or vice-versa. This was done so that the structure would experience similar deterioration in both directions as the test series progressed. Table 7-1 summarizes the input used for each of the 11 tests. For example, Seismic Test 7 of Specimen #1 was biaxial. The longitudinal excitation was the modified C02_03s record with its acceleration ordinates scaled by 50% and a PGA of 0.28*g*. The transverse excitation was the modified C02_09s record with its acceleration ordinates scaled by 50% and a PGA of 0.33*g*.

**Table 7-1. 11 test motions for Specimen #1 ( X = Longitudinal, Y = Transverse).**

| Test | Direction | Input Acceleration | X $\ddot{u}_{g\,MAX}$ | Y $\ddot{u}_{g\,MAX}$ |
|---|---|---|---|---|
| 1 | Y | 0.15 * C02_09s | - | 0.10g |
| 2 | X | 0.15 * C02_03s | 0.08g | - |
| 3 | Y | 0.75 * C02_09s | - | 0.50g |
| 4 | X | 0.75 * C02_03s | 0.41g | - |
| 5 | Y | 1.00 * C02_09s | - | 0.67g |
| 6 | X | 1.00 * C02_03s | 0.55g | - |
| 7 | X + Y | 0.50 * C02_03s + 0.50 * C02_09s | 0.28g | 0.33g |
| 8 | X + Y | 1.00 * C02_03s + 1.00 * C02_09s | 0.55g | 0.67g |
| 9 | Y | 1.50 * C02_09s | - | 1.00g |
| 10 | Y | 2.00 * C02_09s | - | 1.33g |
| 11 | X + Y | 2.00 * C02_03s + 2.00 * C02_09s | 1.10g | 1.33g |

## 7.4 Preliminary Observations

### 7.4.1 Damage at Low Levels of Excitation (PGA < 0.67 g)

#### 7.4.1.1 Transverse Shaking

Visible and audible damage to the half-scale specimen occurred during Test 5, with a maximum ground acceleration of 0.67*g*. The specimen popped and cracked loudly, and the longitudinal walls visibly responded out-of-plane. Inspection of the half-scale specimen following Test 5 revealed a 12-inch vertical crack in the middle of the west wall. No other damage was apparent.

#### 7.4.1.2 Longitudinal Shaking

Visible damage to the half-scale specimen occurred during Test 6, with a maximum acceleration of 0.55*g*. Inspection following the test revealed cracking along the base of the center pier in the perforated wall, and along the base of one of the transverse walls. No other damage was apparent.

### 7.4.2 Damage at High Levels of Excitation (PGA > 0.67g)

#### 7.4.2.1 Transverse and Longitudinal Shaking

Visible and audible damage increased with increasing excitation. At input acceleration levels greater than 1.0*g*, cracking propagated throughout the structure along what became evident as out-of-plane yield lines. Figure 7.8 shows idealized yield lines for the longitudinal walls based on that observed cracking pattern. Also, the transverse walls developed prominent bed-joint cracks, characteristic of pier rocking (Figure 7.9). Figure 7.10 shows the actual cracking pattern for the perforated longitudinal wall. Visible damage finally occurred to the roof diaphragm during Test 10, at a maximum acceleration of 1.33*g* in the transverse direction. Inspection revealed some cracking at nailing points, and the end of one piece of sheathing lumber pulled loose. No other visible damage occurred to the diaphragm.

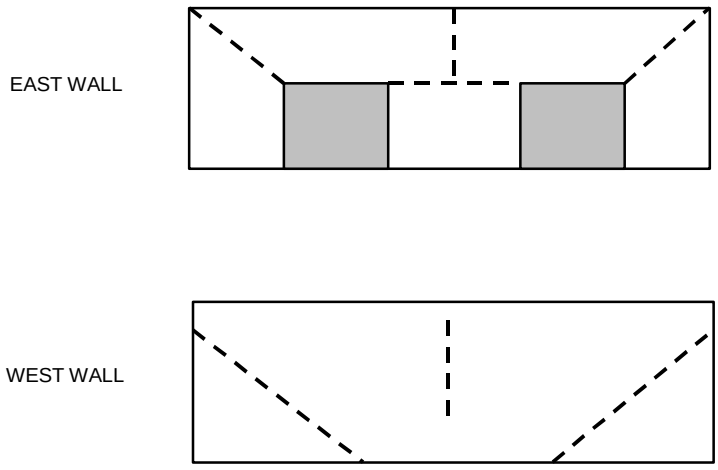


**Figure 7.8. Probable yield lines of east perforated wall and west wall (Test 11, Specimen #1).**

**Figure 7.9. Actual bed-joint cracking characteristic of pier rocking (Test 11, Specimen #1).**

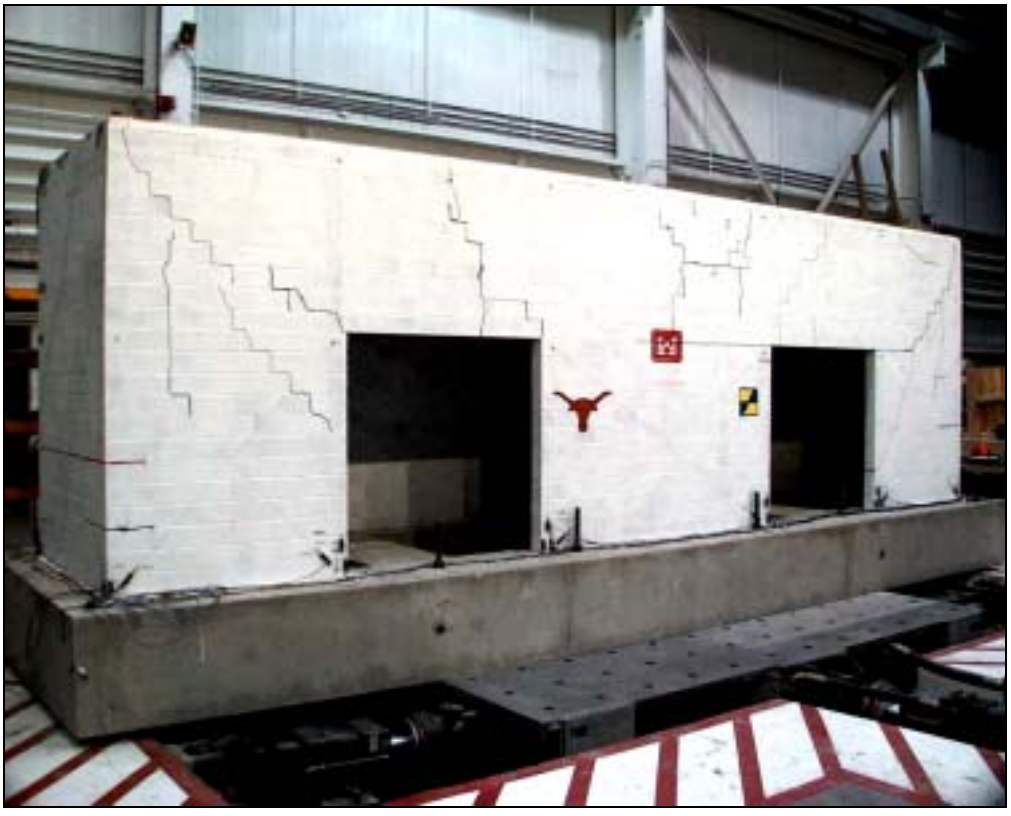

**Figure 7.10. Actual cracking pattern of perforated wall (Test 11, Specimen #1).**

## 7.5 Evaluation of Nails and Nail Holes in Lumber Diaphragm

CERL personnel performed a visual inspection of the sheathing nails and the associated nail holes following the seismic testing. The goal of the nail-hole investigation was to detect deformations of the nails and their holes that might reduce the in-plane stiffness of the diaphragm. The inspection searched for:

- withdrawal of nails;
- flexural deformation of nails;
- bearing deformation (ovalling) at the nail holes in the sheathing lumber;
- bearing deformation at the nail holes in the joist lumber; and
- splitting of sheathing and joist lumber at nailing points.

The study included five sheathing boards, shown schematically in Figure 7.11*, which sustained damage during the testing.

Removing the boards without increasing any existing damage required grinding off the heads of the nails connecting the board to the underlying joists. The sheathing boards were then carefully removed and analyzed. Slight damage in the form of ovalling and splitting was found in several boards.

Distinguishing load-induced damage from pre-existing damage proved very difficult, however. Construction of the diaphragm inevitably produced some damage, which was unfortunately indistinguishable from the damage incurred by seismic actions. Thus, the study of the nail holes provided no conclusive information regarding damage to the diaphragm in the form of splitting, ovalling of holes, or deformation of the nails.

* Drawing done by Scott Voss, graduate student at University of Illinois and employee of ERDC/CERL.

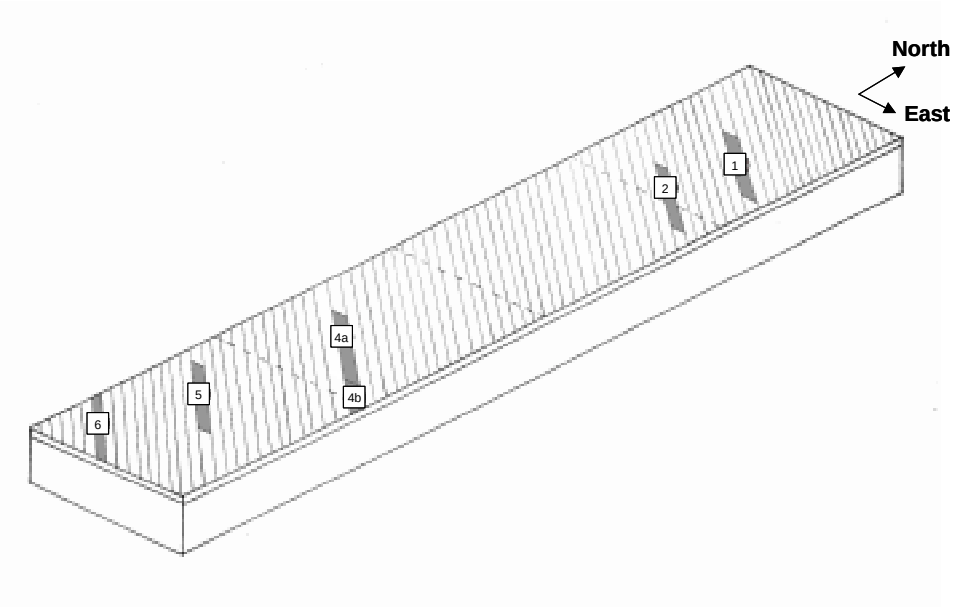


**Figure 7.11. Sheathing boards investigated in nail-hole evaluation.**

# 8 Testing of Half-Scale Specimen #2 (Corrugated Metal Deck)

## 8.1 Specimen Instrumentation

Instrumentation of half-scale Specimen #2 required 82 data channels, measuring:

- deflections relative to a stationary frame off the shaking table using 9 spiral potentiometers;
- slip across end laps of decking sheets using 4 linear potentiometers;
- lateral, vertical and out-of-plane accelerations using 19 accelerometers; and
- shearing deformations, uplift and pier rocking using 50 linear potentiometers.

Figure 8.1 through Figure 8.6 show the instrumentation plan for Specimen #2.

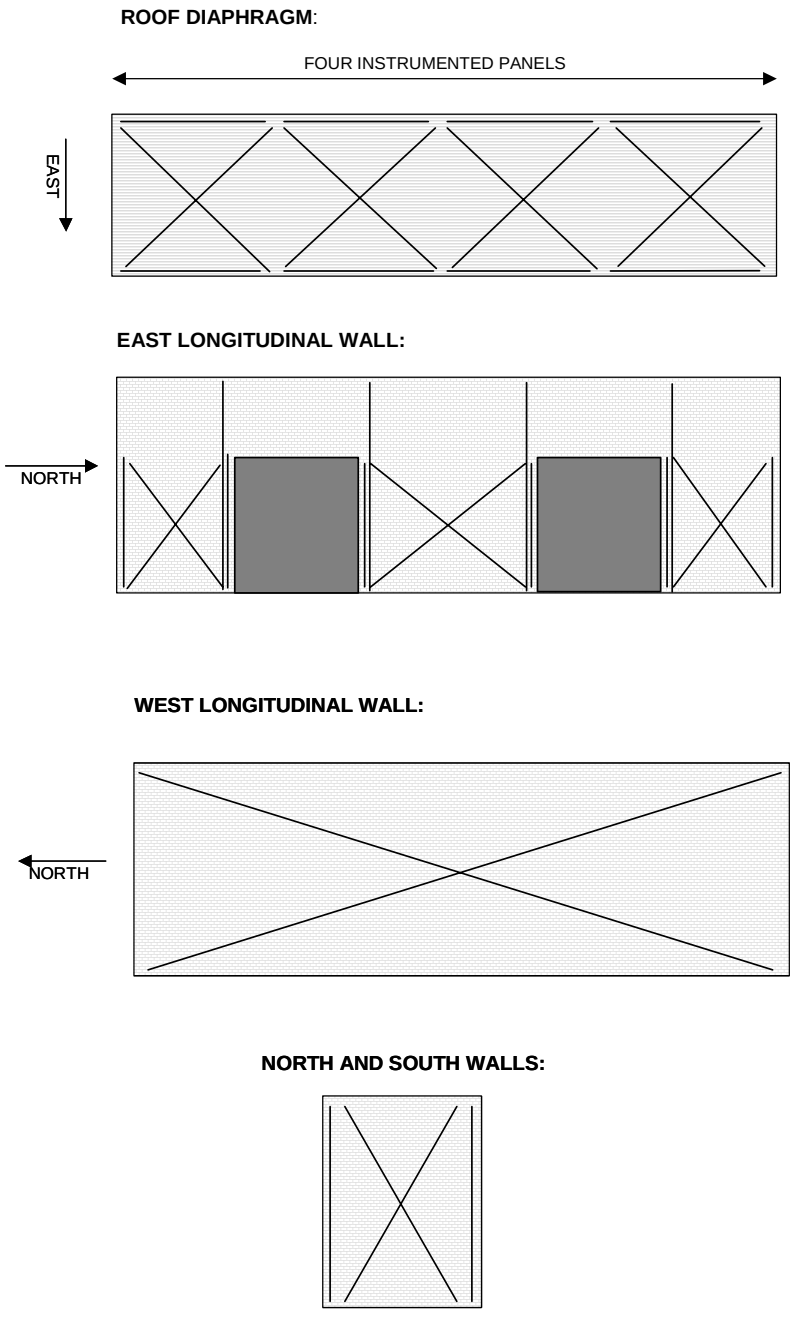


**Figure 8.1. Instrumentation for measuring in-plane shear deformations using linear potentiometers (Specimen #2).**

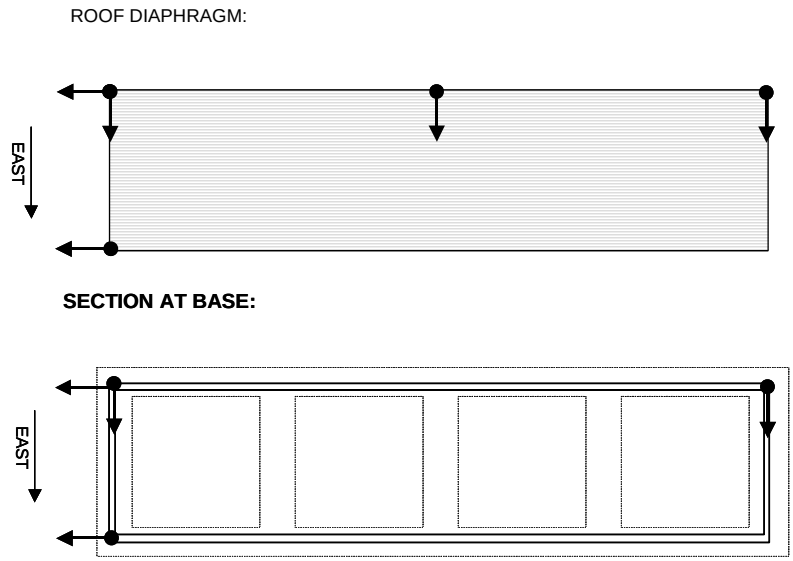


**Figure 8.2. Instrumentation for measuring global point displacements using spiral potentiometers (Specimen #2).**

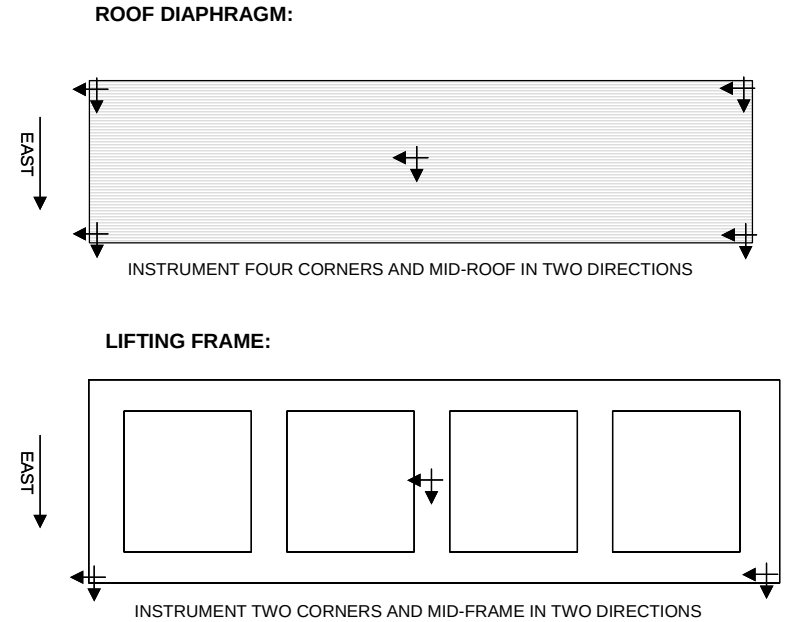


**Figure 8.3. Instrumentation for measuring horizontal accelerations (Specimen #2).**

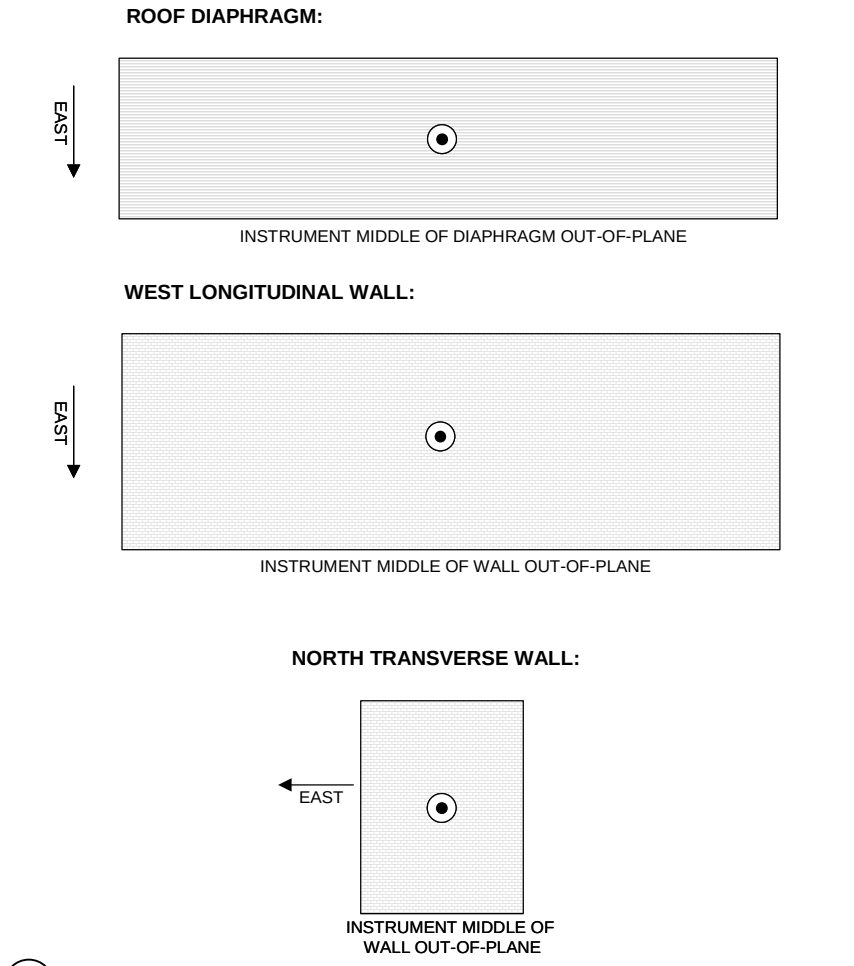


**Figure 8.4. Instrumentation for measuring out-of-plane accelerations (Specimen #2).**

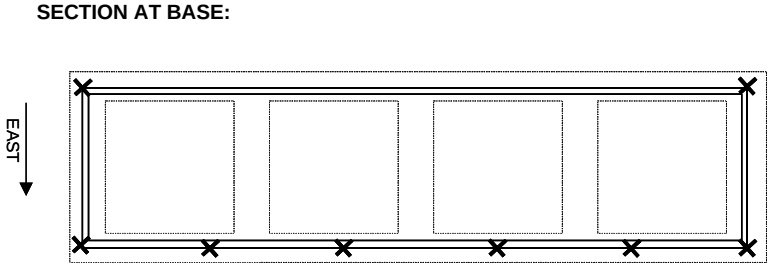


**Figure 8.5. Instrumentation for measuring uplift (Specimen #2).**

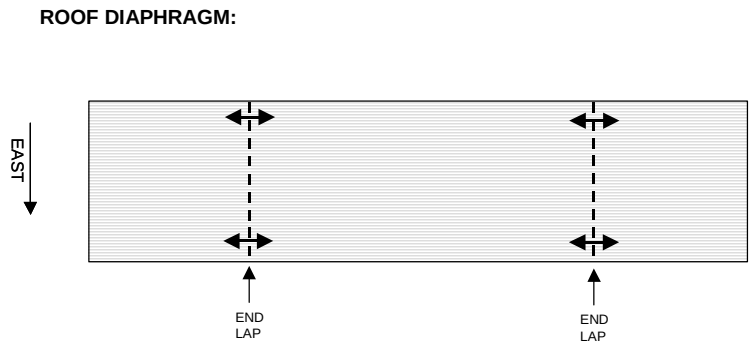


**Figure 8.6. Instrumentation for measuring slip across sheet end laps (Specimen #2).**

## 8.2 Digital Video Recording

A digital video camera set up above the north side of the diaphragm provided a visual record of the testing. The camera angle captured the entire diaphragm during testing (Figure 8.7). Digital video systems offer significant advantages over analog video systems, including:

- digital picture quality is far superior to that of traditional analog systems;
- digital copies of digitally recorded images are identical to the original;
- digital images can be efficiently transferred to personal computers for straightforward video editing and subsequent export as AVI files; and
- individual frames of digital video can be exported and used in reports. For an example of this, see Figure 8.7. The in-plane flexibility of the roof deck is clearly evident from the bending of the corrugations during dynamic response.

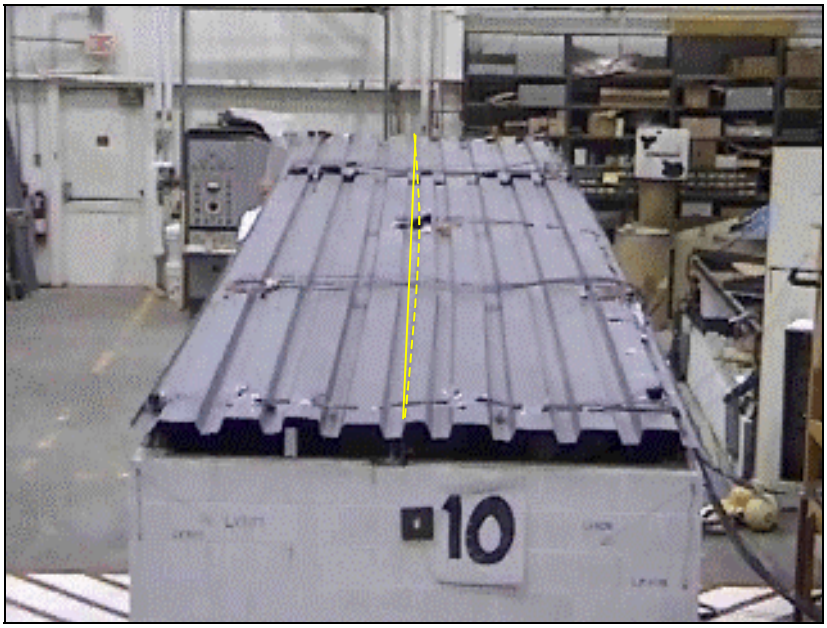


**Figure 8.7. Exported digital video frame from Test 10 of Specimen #2. The solid light line represents the undeformed shape and the dashed light line represents the deformed shape.**

## 8.3 Preparation of Shaking Table (TESS)

After analyzing acceleration data from the testing of Specimen #1, it became apparent that the table itself, and therefore the specimen as well, had experienced some unanticipated coupling among all six of the table's degrees of freedom. The tests performed on Specimen #1, most of which were intended to involve excitation of one table degree of freedom only, were in fact at least bi-axial and probably multi-axial tests. The unintended coupled input motions ranged from 5% to 15% of the intended input motions.

To understand the possible reasons for this coupling, and its probable consequences, it is useful to briefly review how a shaking table is controlled, what can cause coupling, and how that coupling is addressed.

A shaking table is basically a closed-loop loading system in which the controlled parameter is table acceleration. In a single-axis shaking table, table accelerations in the active degree of freedom are controlled, and the remaining degrees of freedom are eliminated mechanically using rollers or other constraints. The active degree of freedom is controlled using an electronic feedback loop in which errors between instantaneous response and desired input are detected, reversed, amplified, and used to adjust the servo-valve attached to the actuator. Modern systems usually base corrective servo-valve inputs on other considerations as

well, including the instantaneous rate of change of the error. Remaining relative errors between the prescribed motion and the response of the table (ideally one percent or less) are due to oscillation of the oil column within the hydraulic lines, to limitations in servo-valve capacity, to the response of the underlying reaction mass, and to the response of the mounted specimen itself, which applies inertial forces to the table.

In a multi-axis table, mechanical constraints cannot be used, and table movement is possible in all degrees of freedom. This complicates the control situation, because all degrees of freedom, including non-excited ones, must be controlled actively to eliminate possible influences from mechanical coupling, hydraulic interaction and inertial forces produced by specimen response. Ideally, inactive degrees of freedom (those that are intended to have zero values) can be maintained at zero either by not prescribing any input for them, or by specifically prescribing zero input.

The TESS facility also has the capability of "software compensation." The table is run using the prescribed input motion at a low level, and the table response is measured for inactive degrees of freedom. Those values can in fact differ from zero. The relationship between the prescribed input in the active degree of freedom, and possible non-zero response in the inactive degrees of freedom, can be used to generate a matrix of cross-coupling waveforms for the table under that particular ground motion and specimen. The cross-coupling waveforms are then used to generate inputs which, when applied to the inactive degrees of freedom, correct their actual values to zero.

In an attempt to eliminate the unwanted response of non-active degrees of freedom, researchers from the University of Texas and CERL ran TESS through the same longitudinal (N-S) sine sweep motion under three different control conditions:

1. null files in the five non-active degrees of freedom, and no software compensation;

2. null files in the five non-active degrees of freedom, and software compensation obtained using the base girder only; and

3. null files in the non-active degrees of freedom, and software compensation obtained using the specimen.

Surprisingly, Fast Fourier Transforms (FFT) of table response under the three control conditions suggested that the least cross-coupling occurred under the

first control condition (no software compensation). Thus, the research team opted to run the tests under that condition.

## 8.4 Seismic Ground Motion Tests

CERL personnel and the University of Texas researchers chose to subject Specimen #2 to 12 seismic tests at increasing levels of maximum acceleration. The logic behind the test plan, summarized in Table 8-1, is as follows:

- Tests 0-6: use ground-motion amplitudes selected to leave the specimen essentially undamaged and hence elastic.

- Tests 7-8b: use ground-motion amplitudes selected to cause large amounts of damage associated with the longitudinal response of the building. At this point in the testing plan the specimen should be essentially undamaged. Damage should be in the form of pier rocking and diaphragm racking.

- Tests 9 and 10: use ground-motion amplitudes selected to cause large amounts of damage associated with the transverse response of the building. At this point in the testing plan the specimen should have incurred significant damage associated with the longitudinal response but should be essentially undamaged with respect to the transverse response. Damage to the masonry should be in the form of significant out-of-plane deflections of the longitudinal walls and associated cracking. Damage to the diaphragm should consist of broken welds and buckled decking.

The above test plan was intended to eliminate the possible influence of prior damage in each of the specimen's two principal directions.

During half-scale motion at high levels of excitation (Test 8b) the research team ran the input record through a high-pass filter so that higher levels of input acceleration could be imposed without exceeding the displacement limits of TESS. The filtering did not affect the input motion in the probable frequency range of importance for the specimen as identified by the preliminary analytical study discussed in Section 10 of this report.

**Table 8-1. 12 test motions for Specimen #2 ( X = Longitudinal, Y = Transverse).**

| Test | Direction | Input Acceleration | X $\ddot{u}_{g\,MAX}$ | Y $\ddot{u}_{g\,MAX}$ |
|---|---|---|---|---|
| 0 | X | 0.10*C02_03s | 0.05g | - |
| 1 | X | 0.30*C02_03s | 0.16g | - |
| 2 | Y | 0.30*C02_09s | - | 0.20g |
| 3 | X + Y | 0.21*C02_03s + 0.30*C02_09s | 0.11g | 0.20g |
| 4 | X | 0.60*C02_03s | 0.32g | - |
| 5 | Y | 0.60*C02_09s | - | 0.40g |
| 6 | X +Y | 0.42*C02_03s + 0.60*C02_09s | 0.22g | 0.40g |
| 7 | X | 1.50*C02_03s | 0.82g | - |
| 8a | X | 2.25*C02_03s | 1.23g | - |
| 8b | X | 4.00*C02_03s | 1.56g | - |
| 9 | Y | 1.50*C02_03s | - | 1.00g |
| 10 | Y | 2.00*C02_03s | - | 1.33g |

## 8.5 Preliminary Observations

### 8.5.1 Damage Prior to Testing

Specimen #2 was slightly damaged prior to testing. Pre-test inspection of the specimen revealed several long vertical and diagonal hairline cracks in the west longitudinal wall. These may have formed during construction, during placement of the specimen on the shaking table, or from other causes. Whatever its origin, this damage did not significantly affect either the consistency of the test program or the subsequent response of the specimen.

### 8.5.2 Damage at Low Levels of Excitation (PGA < 0.40g)

Specimen #2 sustained very little damage from low-level Tests 0-6. Pre-existing cracks extended a small amount and some other slight cracks appeared in areas such as at the bases of the transverse walls. The low level of damage suggested predominantly elastic behavior. This was the goal of the early testing (see Section 8.4 of this report).

### 8.5.3 Damage at High Levels of Excitation (PGA > 0.40g)

#### 8.5.3.1 Longitudinal Excitation

Visible and audible damage occurred during Test 8a with a peak longitudinal ground acceleration of 1.23*g*. Two puddle welds connecting the metal deck to the diaphragm fractured. Diaphragm damage increased with Test 8b and a peak longitudinal ground acceleration of 1.56*g*. During this test an additional puddle weld fractured and a shear crack formed above the north opening in the east longitudinal wall (Figure 8.9). The masonry walls sustained very little additional cracking, however.

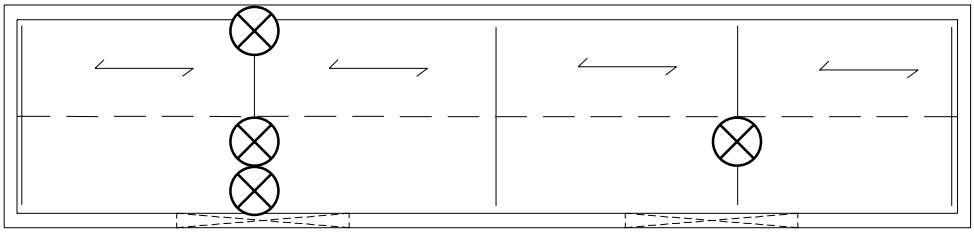

**Figure 8.8. Location of fractured puddle welds (Test 8b, Specimen #2).**

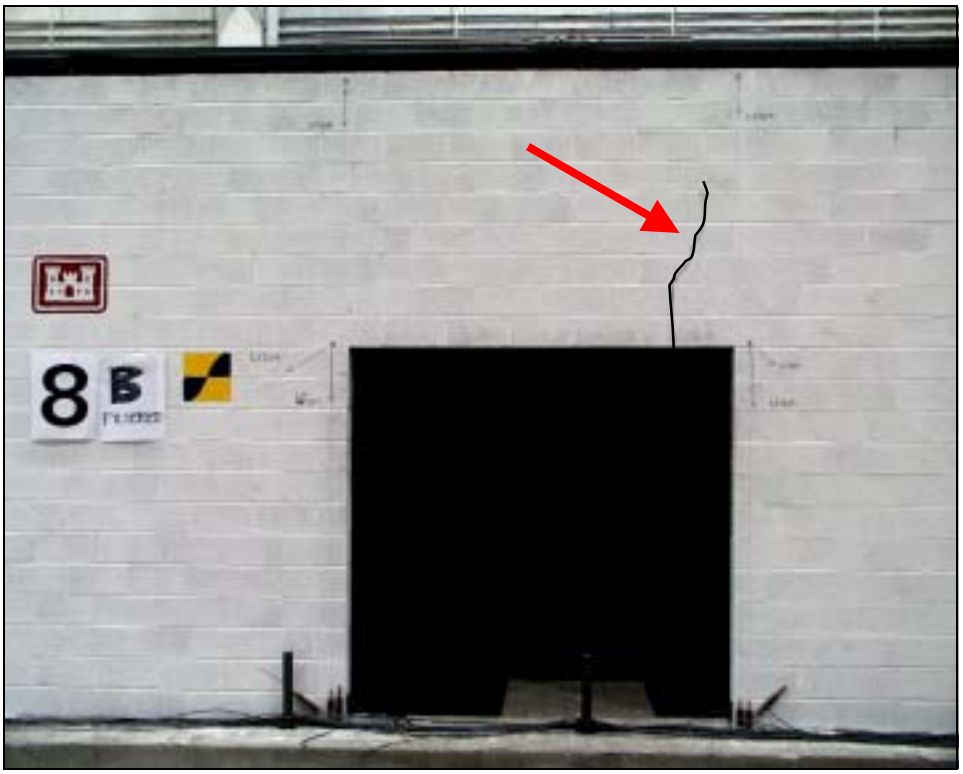


**Figure 8.9. Shear crack above north perforation in east wall (Test 8b, Specimen #2).**

#### 8.5.3.2 Transverse Excitation

Damage spread quickly and extensively throughout the structure during strong transverse excitation. Cracking propagated through the structure along what became evident out-of-plane yield lines. Figure 8.12 shows idealized yield lines for the longitudinal walls. Figure 8.10 shows the actual cracking pattern for the perforated longitudinal wall.

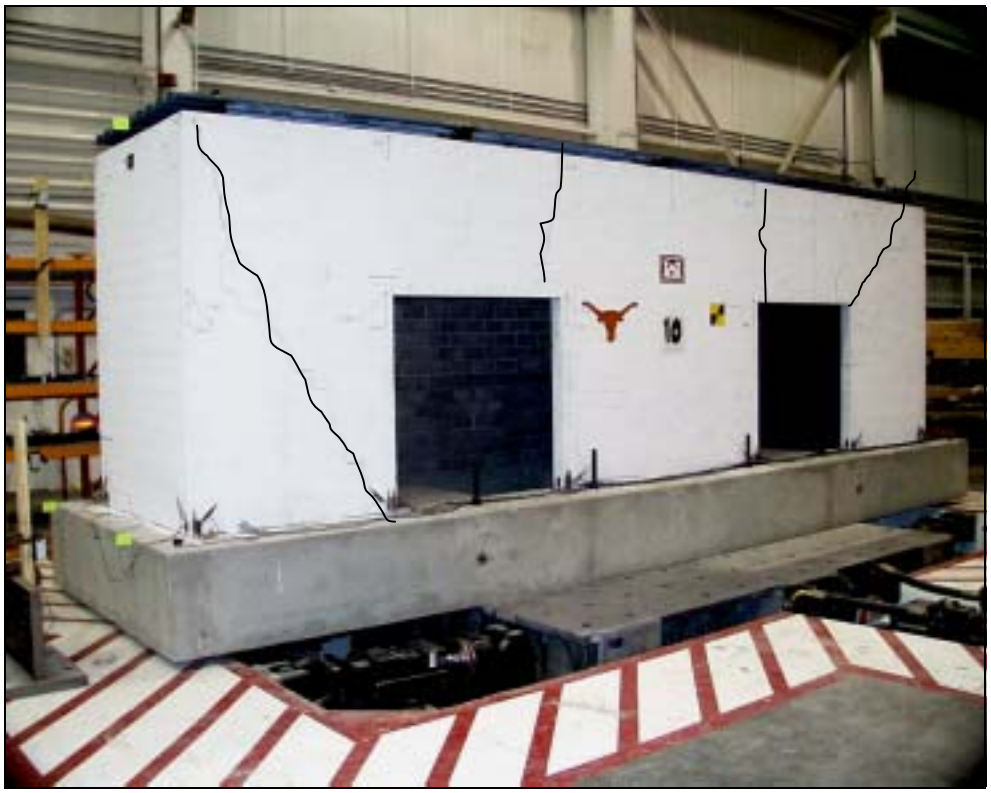

**Figure 8.10. Actual cracking pattern of east (perforated) wall (Test 10, Specimen #2).**

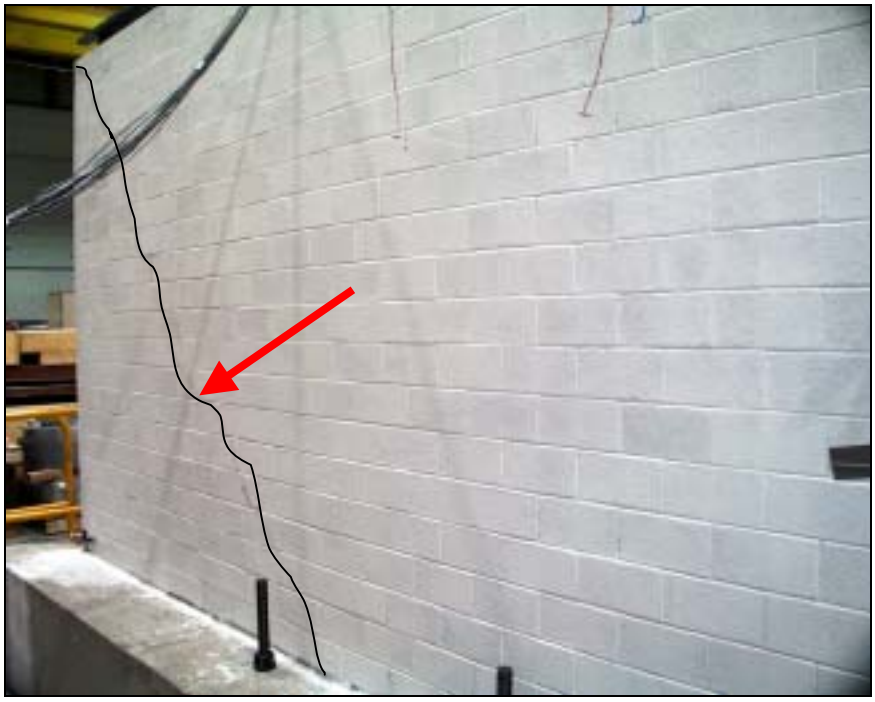

**Figure 8.11. North end of west wall showing out-of-plane yield line (Test 10, Specimen #2).**

Extensive damage occurred to the roof diaphragm and diaphragm instrumentation during Test 10 at a maximum acceleration of 1.33*g* in the transverse direction. Inspection revealed that two side-lap screws at the north and south ends of the diaphragm had pulled out and subsequently severed several of the linear potentiometer wires running diagonally across the roof (Figure 8.1 and Figure 8.14). Furthermore, several of the linear potentiometers measuring end-lap slip and three of the five diaphragm accelerometers broke free from their mounts (Figure 8.3, Figure 8.6, Figure 8.14, and Figure 8.15).

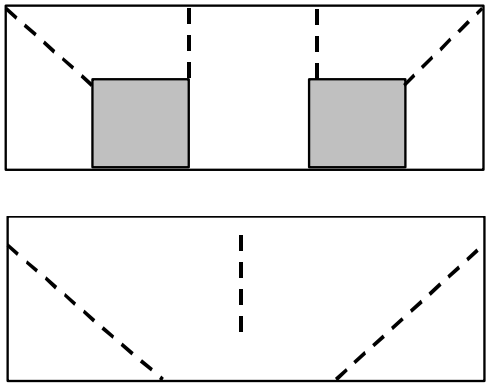

**Figure 8.12. Probable yield lines of east (perforated) wall and west wall (Test 11, Specimen #2).**

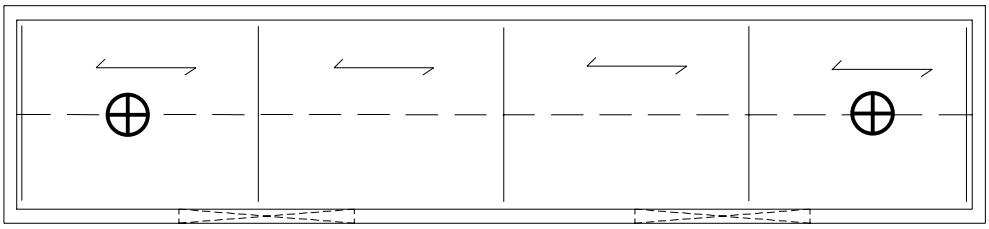

**Figure 8.13. Location of damaged side-lap screws (Test 10, Specimen #2).**

**Figure 8.14. Side-lap screw pulled loose and severed instrumentation wire (Test 10, Specimen #2).**

**Figure 8.15. Detail of side-lap screw (Test 10, Specimen #2).**

**Figure 8.16. Loss of several instruments during Test 10.**

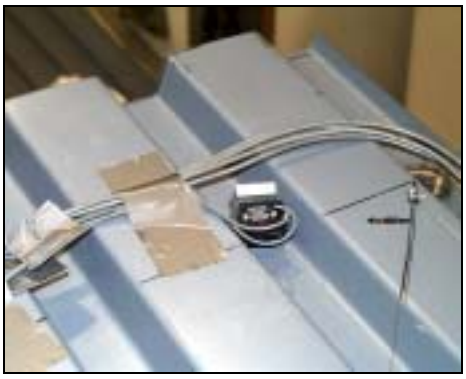

**Figure 8.17. Loss of accelerometer during Test 10.**

# 9 Evaluation of Test Data

Instrumentation of the half-scale specimens measured deformations, displacements, and accelerations. Evaluation of the gathered data particularly examined:

- internal consistency of data;
- natural frequencies of half-scale specimens and their relationship to observed damage;
- in-plane deformation responses of roof diaphragms;
- dynamic amplification of structural elements and its relationship to observed damage; and
- in-plane behavior of transverse shear walls; and
- relationship between measured drift and observed damage.

Mechanical properties of the masonry used in the half-scale specimens were also measured. The evaluation and results of the gathered data are now discussed.

## 9.1 Material Properties

CERL personnel tested 11 three-block masonry prisms in compression. Table 9-1 summarizes the results of those compression tests.

**Table 9-1. Masonry prism compression tests.**

| Specimen | Construction | Strength | Usable Strain | Elastic Modulus |
|---|---|---|---|---|
| #1 | grouted | 1400 psi | 0.0029 | 330 ksi |
| #1 | ungrouted | 900 psi | 0.0029 | 320 ksi |
| #2 | grouted | 1800 psi | 0.0031 | 550 ksi |
| #2 | ungrouted | 1000 psi | 0.0027 | 420 ksi |

The measured elastic modulus of the masonry used in half-scale Specimen #1 was approximately one-quarter of the expected modulus of about 1200 ksi. The measured elastic modulus of the masonry used in half-scale Specimen #2 was approximately one-half to one-third of the expected modulus of about 1200 ksi.

CERL personnel also performed compression tests on 2 in. by 2 in. masonry coupons taken from the face shells of the half-scale CMU. Imprecision in the testing instrumentation resulted in a lack of useful information regarding the elastic modulus of the masonry, however.

## 9.2 Relationship Between Drift and Damage

In this report, damage sustained by the half-scale specimens is characterized using drift ratios. Traditionally, drift ratios are calculated by dividing the inter-story drift between the two floors of interest by the corresponding inter-story height. That procedure is widely accepted by the structural engineering community as an index of structural damage for framed structures with rigid floor diaphragms. Seismic damage in walled structures with flexible horizontal diaphragms, however, cannot be completely characterized by inter-story drift. It must also be characterized by a measure of the in-plane deformation of the horizontal diaphragms themselves (Figure 9.1).

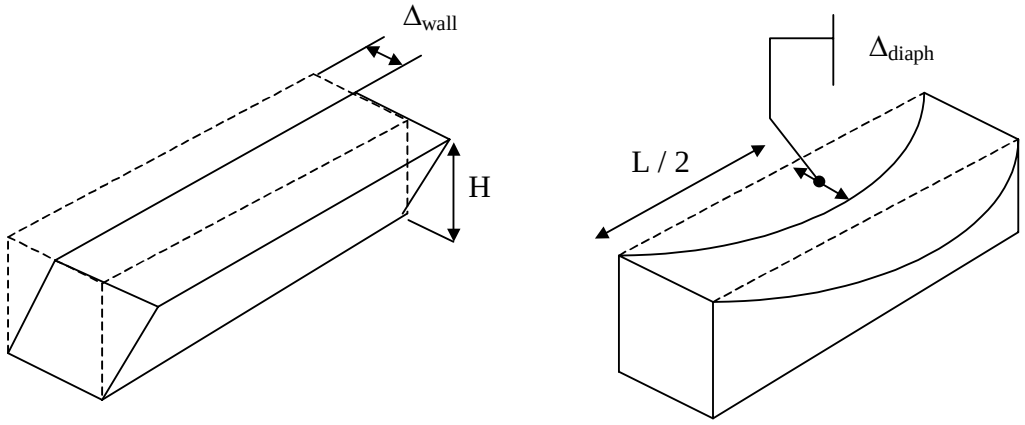


**Figure 9.1. Characteristic deflections and dimensions of half-scale specimens used to define drift ratios.**

In this report, the diaphragm drift ratio, $\delta_{diaph}$, describing damage to the horizontal diaphragm and to the longitudinal walls due to in-plane deformations of the roof diaphragm, is defined:

$$\delta_{diaph} = \frac{\Delta_{diaph}}{L/2} \qquad \textbf{(9-1)}$$

where,

$\Delta_{diaph}$ = in-plane deflection of diaphragm relative to tops of supporting shear walls (Figure 9.1)

$L$ = length of diaphragm

The wall drift ratio, $\delta_{wall}$, describing damage to the transverse shear walls due to in-plane deformations, is defined here and elsewhere as:

$$\delta_{wall} = \frac{\Delta_{wall}}{H} \quad \text{(9-2)}$$

where,

$\Delta_{wall}$ = inter-story drift

$H$ = inter-story height

In the case of the two, half-scale test specimens, $H$ is 84 in. (7 ft), $L$ is 264 in. (22 ft), and the characteristic deflections, $\Delta$, are taken as the measured spectral values.

In this report, diaphragm drift ratios are evaluated using Equation 9-1 and shear wall drift ratios are evaluated using Equation 9-2.

## 9.3 Testing of Specimen #1 (Lumber Diaphragm)

### 9.3.1 Consistency of Data

To check the internal consistency of the test data, the measured diaphragm displacement histories from a given seismic test were compared with displacements calculated by the numerical double integration of the measured diaphragm accelerations. As shown in Figure 9.2 and Figure 9.3, the two records are very comparable, substantiating the consistency of the data.

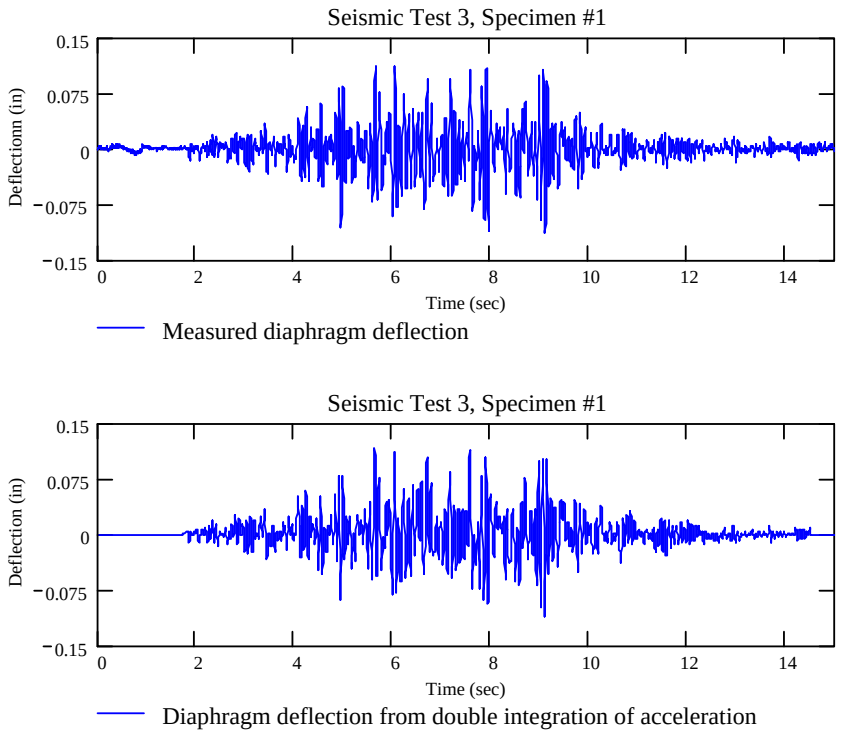


**Figure 9.2. Comparison of measured displacement history for Test 3 of Specimen #1 with double integration of acceleration record.**

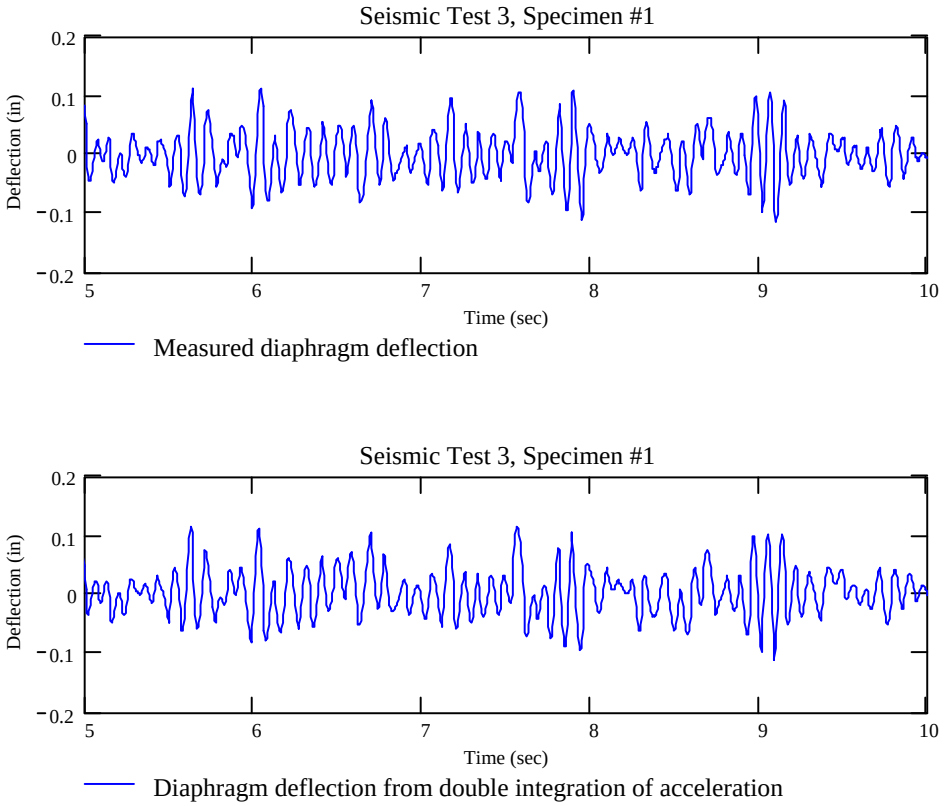


**Figure 9.3. Five-second detail of Figure 9.2.**

### 9.3.2 Accumulation of Damage and Decrease in Frequencies

Half-scale Specimen #1 accumulated significant damage during high levels of excitation. As a result, its natural frequencies decreased. Changes in the natural frequencies were detected test-to-test using white-noise excitation in the specimen's two principal plan directions, following each test.

The analytical study, described in Section 10 of this report, showed that the fundamental frequency of the specimen was characteristic to its transverse response. Therefore, relative changes in the fundamental frequency were meaningful only when they occurred following transverse excitation. Figure 9.4 shows the test-to-test decrease in the measured fundamental frequency of half-scale Specimen #1 following transverse seismic tests.

The specimen did not accumulate sufficient damage from longitudinal response to exhibit a significant test-to-test decrease in its longitudinal frequencies of response (Figure 9.5).

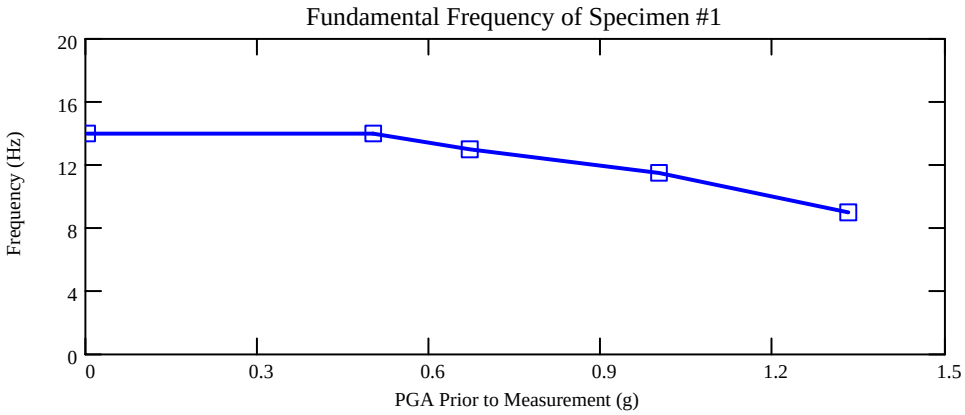


**Figure 9.4. Test-to-test decrease in fundamental frequency due to accumulation of damage from transverse response of Specimen #1.**

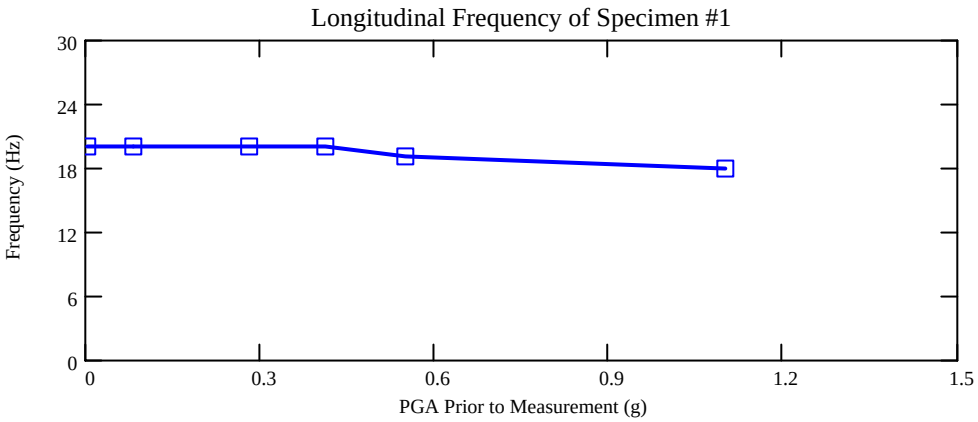


**Figure 9.5. Test-to-test decrease in lowest identifiable mode associated with longitudinal response of half-scale Specimen #1.**

### 9.3.3 Dynamic Response

#### 9.3.3.1 Diaphragm Response during Transverse Excitation

The approximate deformed shape of the diaphragm at any point during the simulation could be determined by analyzing the in-plane diaphragm response data. Figure 9.6 illustrates characteristic deformations of the instrumented diaphragm panels. The approximate shear deformation of each panel was determined using the extension and contraction of the linear potentiometers placed along the panel diagonals. The approximate flexural deformation of each panel was determined using the extension and contraction of the linear potentiometers placed along the panel chords. These deformations were then summed from panel to panel along the length of the diaphragm to obtain an approximate deformed shape during transverse response. Figure 9.7 shows the approximate shape of the diaphragm during the peak response of Test 9.

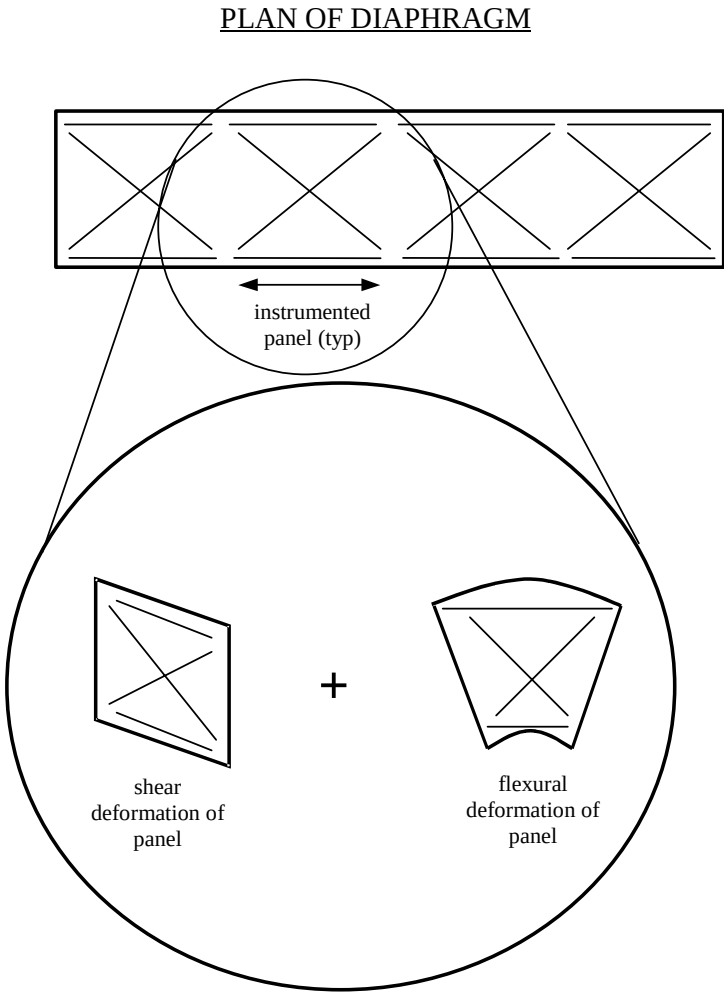


**Figure 9.6. Characteristic deformations of instrumented diaphragm panels.**

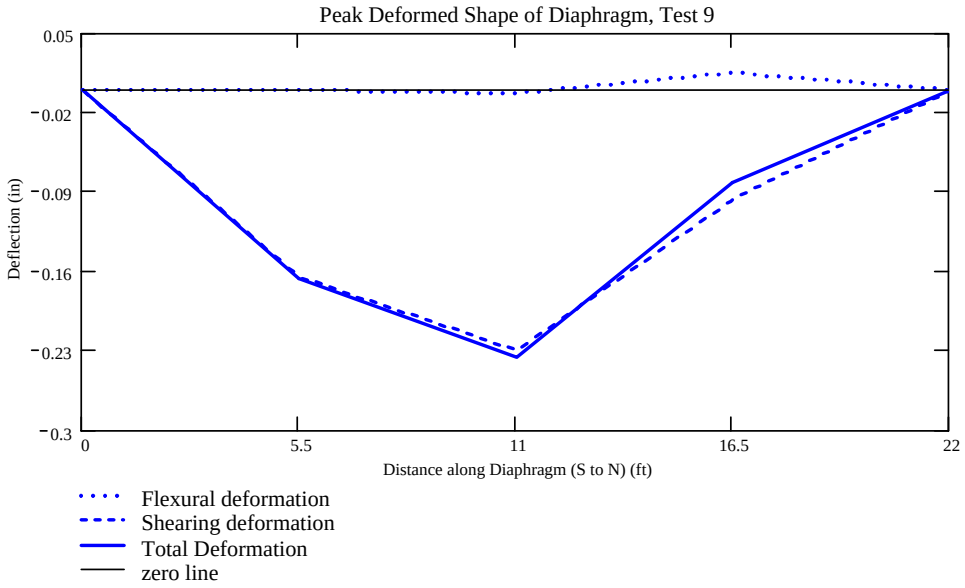


**Figure 9.7. Deformed shape of diaphragm during peak response (Test 9, Specimen #1).**

Analytical studies discussed in Section 10 of this report calculated a fundamental mode of response controlled by the in-phase, in-plane, and single-curvature response of the roof diaphragm and the transverse shear walls. Figure 9.7 shows that the roof diaphragm responded in-plane approximately in single curvature. Figure 9.8 shows that the plan center of the diaphragm and the tops of the transverse shear walls responded primarily in-phase during transverse response. Those observations imply that the transverse response of the diaphragm was dominated by the fundamental mode of the specimen. The arrows in Figure 9.9 mark several typical regions of amplitude cancellation ("beating") in the diaphragm acceleration response of Specimen #1, during Test 5. Such cancellations are generally attributable to the superposition of two sinusoids with different frequencies. Therefore, Figure 9.9 suggests that a higher mode participated to the acceleration response of the specimen at a detectable level. This contribution was small, however.

Figure 9.7 shows that shearing deformations dominated the overall in-plane response of the diaphragm. Considering the high, in-plane shearing flexibility of the diaphragm compared to its low, in-plane flexural flexibility corroborates this observation.

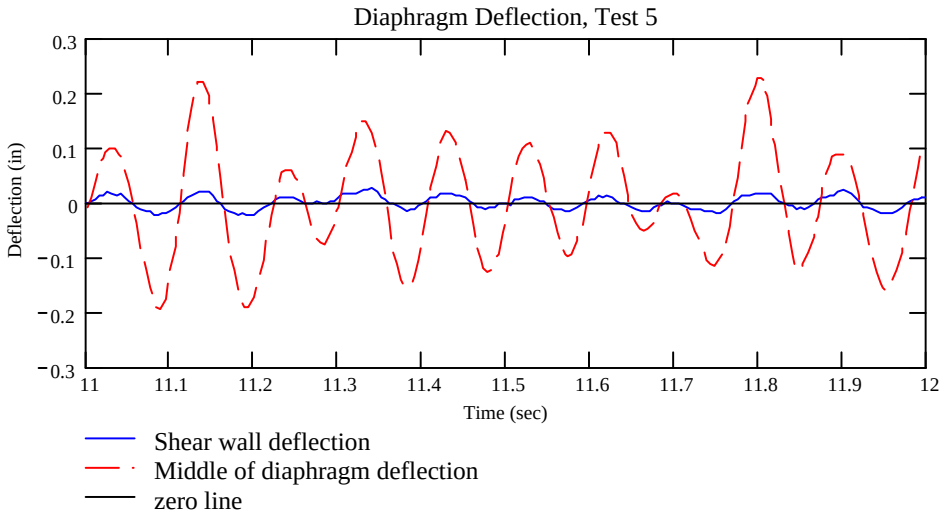


**Figure 9.8. Transverse displacement response of center of diaphragm and tops of transverse shear walls as measured relative to base of specimen (Test 5, Specimen #1).**

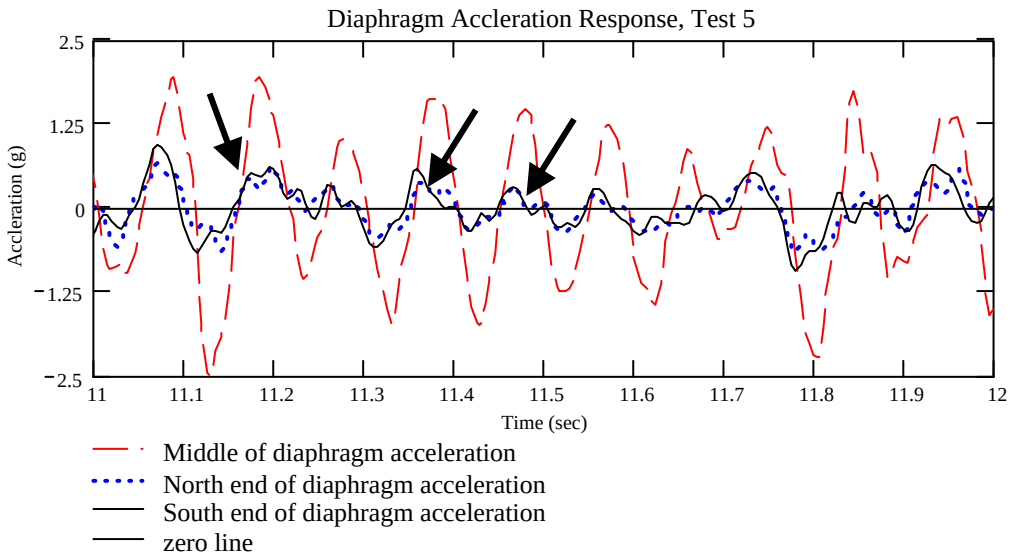


**Figure 9.9. Transverse acceleration response of center of diaphragm and tops of transverse shear walls (Test 5, Specimen #1).**

### 9.3.3.2 Dynamic Amplification and Damage

Spectral accelerations at a given point on a structure are often considered in terms of the Dynamic Amplification Factor (DAF), the ratio of the measured spectral acceleration to the peak input acceleration. Figure 9.11 and Figure 9.12 respectively show the DAFs measured at the roof diaphragm and at mid-height of the unperforated west longitudinal wall. Dynamic amplification decreased with increasing levels of input acceleration above 0.67*g*. Visible damage to the diaphragm was not detected until Test 10, at a PGA of 1.33*g* and a diaphragm drift ratio of about 0.7%. Visible damage to the masonry walls, however, occurred earlier, during Test 5, at a PGA of about 0.67*g* and a diaphragm drift ratio (Equation 9-1) of about 0.2% (Figure 9.1 and Figure 9.10). Significant damage to the masonry walls occurred during Test 9 at a PGA of 1.00*g* and a diaphragm drift ratio of 0.35%. Table 9-2 summarizes the observed diaphragm drift ratios and corresponding damage to the longitudinal walls and the diaphragm itself.

**Table 9-2. Observed drift and related damage (Specimen #1).**

| Element | Test | PGA | Diaphragm Drift Ratio (%) | Damage |
|---|---|---|---|---|
| Longitudinal Walls | 5 | 0.67*g* | 0.2 | Slight cracking |
| Longitudinal Walls | 9 | 1.00*g* | 0.35 | Extensive cracking |
| Longitudinal Walls | 10 | 1.33*g* | 0.7 | Extensive cracking, hinging |
| Diaphragm | 10 | 1.33*g* | 0.7 | Splitting, nail pulling |

Damage to the masonry walls was much more extensive and significant than to the lumber diaphragm. The decrease in diaphragm DAF was likely due to damage in the masonry walls, not in the diaphragm itself. Flexural cracking of the reinforced masonry walls led to significant stiffness degradation and a consequent reduction in dynamic amplification. This has been noted in other studies as well (Tomazevic and Weiss 1994, Abrams and Paulson 1991).

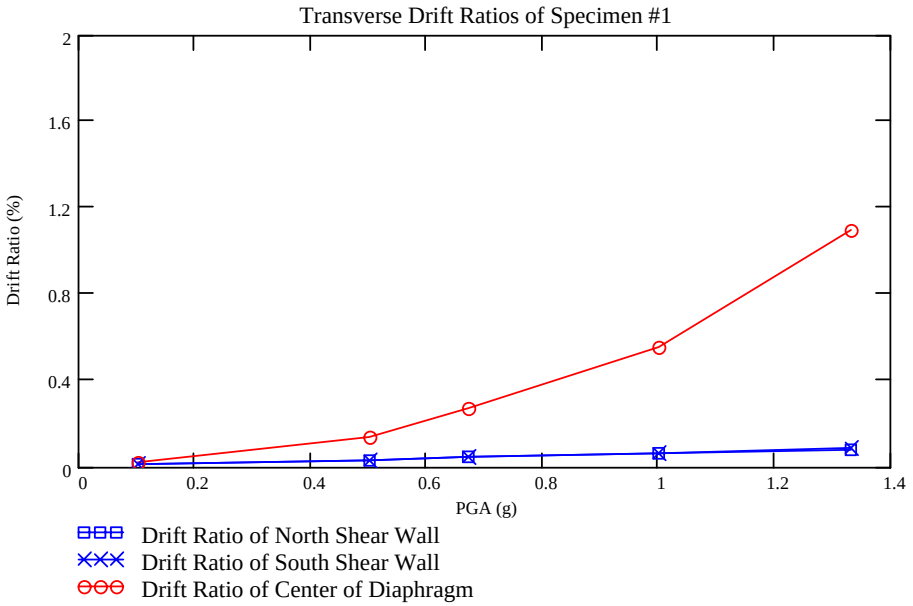


**Figure 9.10. Measured drift ratios of diaphragm and transverse shear walls during transverse excitation (Specimen #1).**

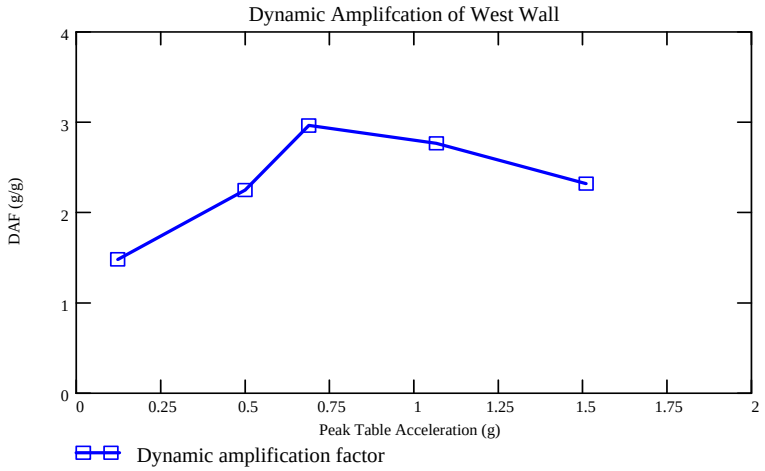


**Figure 9.11. Out-of-plane dynamic amplification of west longitudinal wall at mid-height during transverse excitation (Specimen #1).**

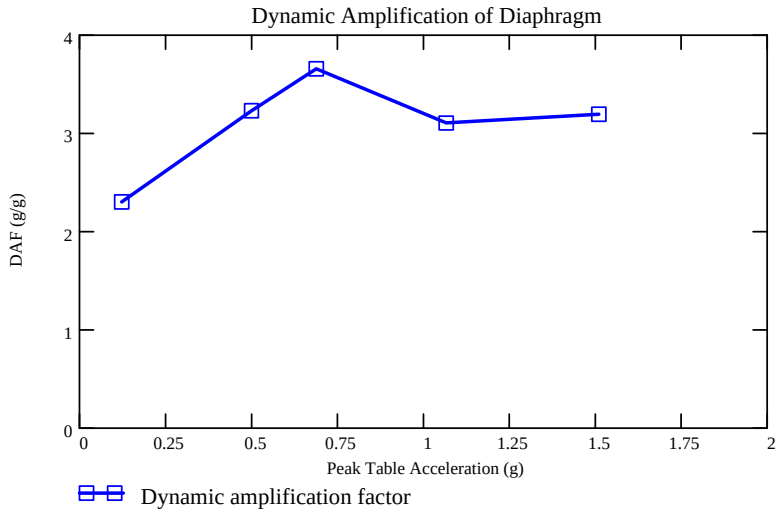


**Figure 9.12. In-plane dynamic amplification of roof diaphragm during transverse excitation (Specimen #1).**

### 9.3.4 Behavior of Shear Walls During Strong Transverse Excitation

The transverse shear walls remained elastic during low levels of excitation, with no visible cracking or permanent deformation. This observation is substantiated by the fact that even at high input accelerations, wall drift ratios are less than 0.1 % (Equation 9-1 and Figure 9.10). During strong seismic tests (PGA >0.67*g*) a continuous bed-joint crack developed along the entire plan length of the south shear wall (Figure 9.13). This crack was characteristic of rigid-body rotation of the shear wall about its base (wall rocking). Data from the vertical linear potentiometers on either side of the shear wall (Figure 7.1) confirmed the hypothesis of wall rocking (Figure 9.14). Closing of the bed-joint crack results in the sharp, downward peaks in the data. Opening of the bed-joint crack and eventual reversal of the direction of rotation of the wall causes the smoother, half-sinusoidal portions of the data record. The transverse shear walls sustained very little additional damage.

**Figure 9.13. Bed-joint crack characteristic of wall rocking (Test 9, Specimen #1).**

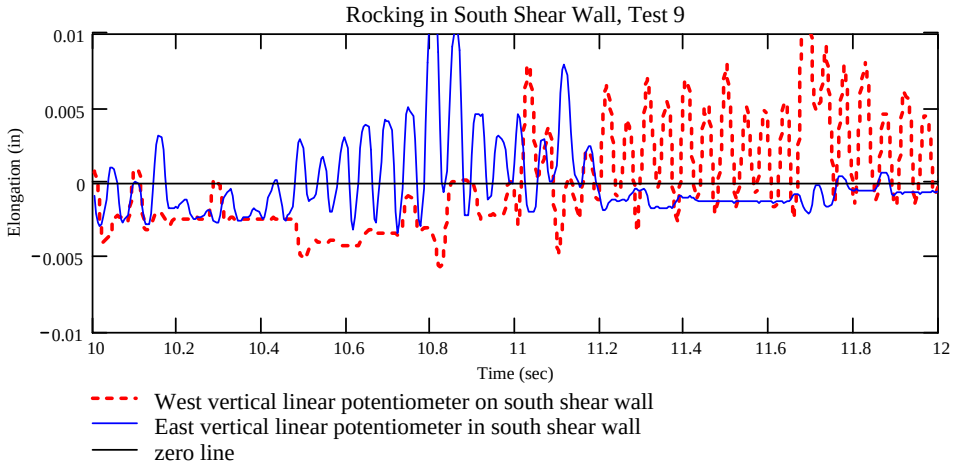


**Figure 9.14. Rocking of south shear wall (Test 9, Specimen #1).**

## 9.4 Testing of Specimen #2 (Metal Diaphragm)

### 9.4.1 Consistency of Data

As discussed in more detail in Section 10.2.2 of this report, measured diaphragm accelerations were dominated by local, high-frequency, high-acceleration response of the metal decking. Data were made more usable by filtering the high

frequency (>20 Hz) acceleration response from the measured data, using a square low-pass filter (Figure 10.15).

### 9.4.2 Accumulation of Damage and Decrease in Frequencies

Half-scale Specimen #2 accumulated significant damage during high levels of transverse excitation. Changes in the natural frequencies were detected test-to-test using white-noise excitation in the specimen's two principal plan directions. Figure 9.15 shows the measured fundamental frequency of the half-scale specimen following each transverse seismic test.

The specimen did not accumulate sufficient damage from longitudinal response to exhibit a significant test-to-test decrease in its longitudinal frequencies of response (Figure 9.16).

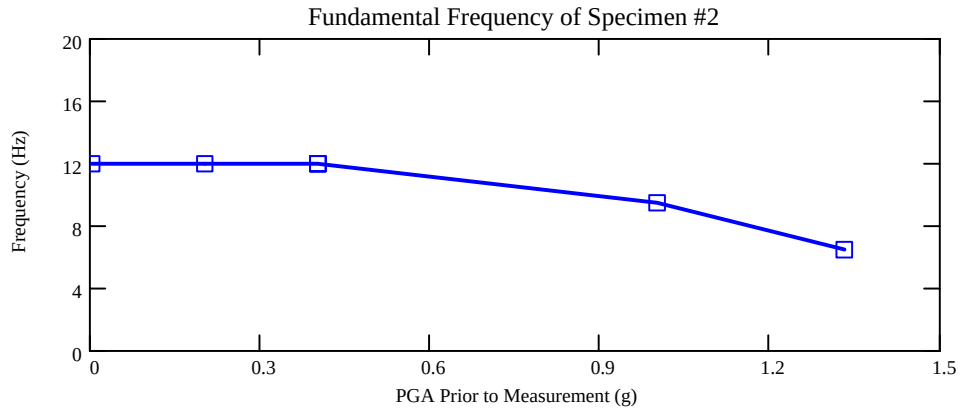


**Figure 9.15. Test-to-test decrease in fundamental frequency due to accumulation of damage characteristic to the transverse response of Specimen #2.**

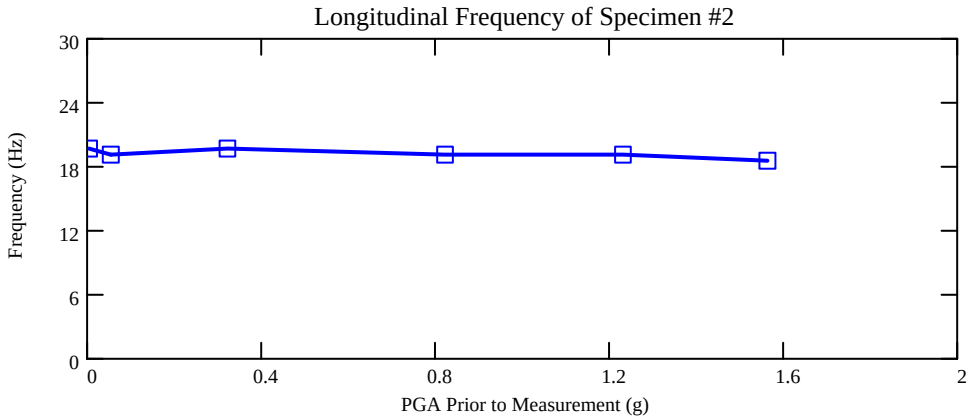


**Figure 9.16. Test-to-test decrease in lowest identifiable frequency associated with longitudinal response of half-scale Specimen #2.**

### 9.4.3 Dynamic Response

#### 9.4.3.1 Diaphragm Response During Transverse Excitation

Using the in-plane response data as discussed in Section 9.3.3.1 of this report, the approximate deformed shape of the diaphragm on Specimen #2 at any point in the time history was determined. Figure 9.17, showing the approximate shape of the diaphragm during the peak response of Test 9, implies that the in-plane response of the diaphragm was dominated by the first mode of the structures dominated for the same reasons discussed in Section 9.3.3.1 of this report. The in-phase, in-plane displacement response of the center of the diaphragm and the two transverse shear walls during Test 9 (Figure 9.18) suggests this as well, again for the same reasons discussed in Section 9.3.3.1 of this report.

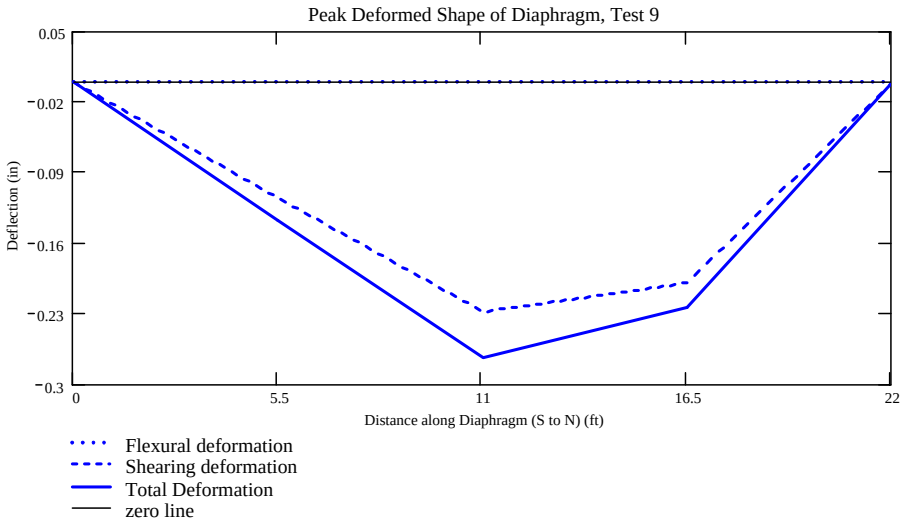


**Figure 9.17. Deformed shape of diaphragm during peak response (Test 9, Specimen #2).**

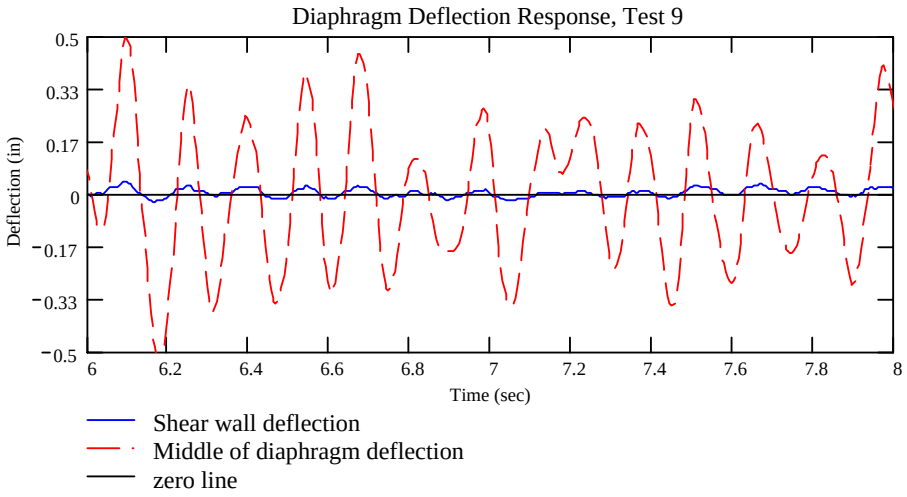


**Figure 9.18. Transverse displacement response of center of diaphragm and tops of transverse shear walls as measured relative to base of specimen (Test 9, Specimen #2).**

Figure 9.17 shows that shearing deformations dominated the overall in-plane response of the diaphragm. Considering the large, in-plane shearing flexibility of the diaphragm compared to its small, in-plane flexural flexibility corroborates this observation.

#### 9.4.3.2 Dynamic Amplification and Damage

Figure 9.20 and Figure 9.21 present the Dynamic Amplification Factor (DAF) measured during transverse excitation at the roof diaphragm level and at mid-height of the west longitudinal wall. The dynamic amplification of the diaphragm and the west longitudinal wall decreased following strong transverse excitation (Test 10). Visible damage to the diaphragm was detected following Test 8a, at a longitudinal PGA of 1.23*g*. Significant visible damage to the longitudinal masonry walls occurred later, during Test 9, at a transverse PGA of about 1.00*g* and a diaphragm drift ratio of about 0.4% (Equation 9-1). Therefore, the decrease in diaphragm DAF was likely due to damage in the masonry walls, and not in the diaphragm itself. Table 9-3 summarizes the observed diaphragm drift ratios and corresponding damage to the longitudinal walls and the diaphragm itself.

**Table 9-3. Observed drift and related damage (Specimen #2).**

| *Element* | *Test* | *PGA* | *Diaphragm Drift Ratio (%)* | *Damage* |
|---|---|---|---|---|
| *Longitudinal Walls* | *5* | *0.40g* | *0.09* | *Negligible* |
| *Longitudinal Walls* | *9* | *1.00g* | *0.40* | *Extensive cracking* |
| *Longitudinal Walls* | *10* | *1.33g* | *1.00* | *Extensive cracking, hinging* |

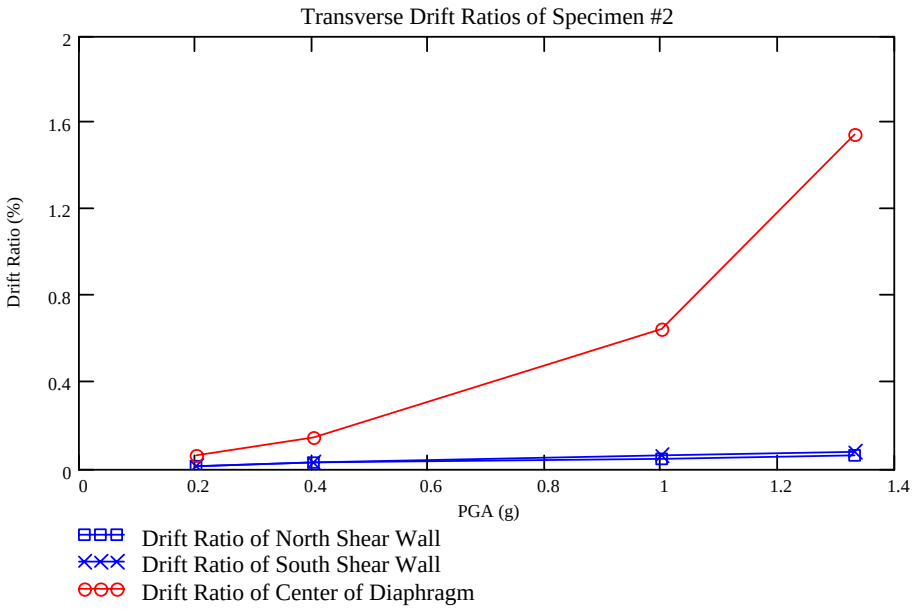


**Figure 9.19. Measured drift ratios of diaphragm and transverse shear walls during transverse excitation (Specimen #2).**

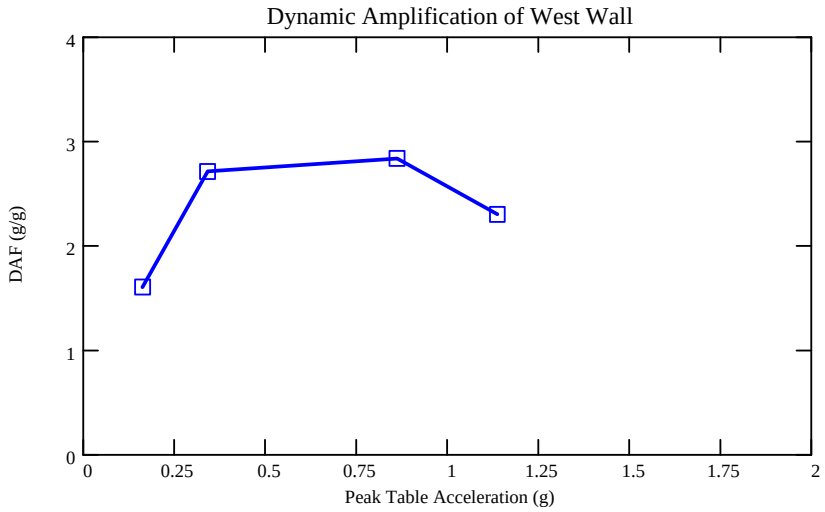


**Figure 9.20. Out-of-plane dynamic amplification of west longitudinal wall at mid-height during transverse excitation (Specimen #2).**

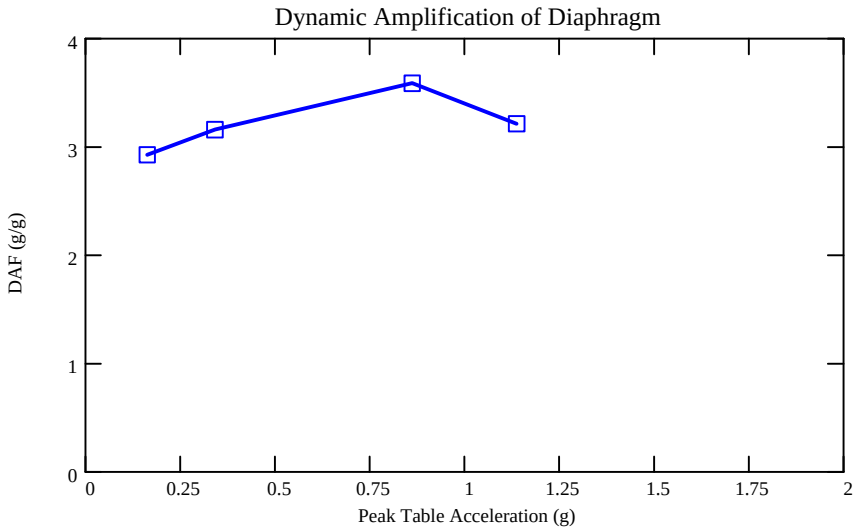


**Figure 9.21. In-plane dynamic amplification of roof diaphragm during transverse excitation (Specimen #2).**

### 9.4.4 Behavior of Shear Walls During Strong Transverse Excitation

The masonry shear walls of Specimen #2 incurred no significant cracking or permanent deformation during high levels of excitation. This observation is substantiated by the fact that even at high input accelerations, drift ratios of the walls are less than 0.1 % (Equation 9-2 and Figure 9.19). The transverse shear walls of Specimen #2 did not rock during strong transverse excitation.

### 9.4.5 Longitudinal Response

Specimen #2 had two large openings in the east perforated wall, each four feet by four feet, and no openings in the west wall. Asymmetry in plan layout of masonry walls implies torsional response. Analytical studies described in Section 10 of this report, however, suggest that the structure did not have a well-defined torsional mode of response, in spite of its plan asymmetry. The lowest mode shape characteristic to the longitudinal response of the specimen is shown in Figure 9.22. In this mode, the two longitudinal masonry walls respond in phase but at different amplitudes. This implies racking of the diaphragm due to in-phase differential displacement of the longitudinal walls.

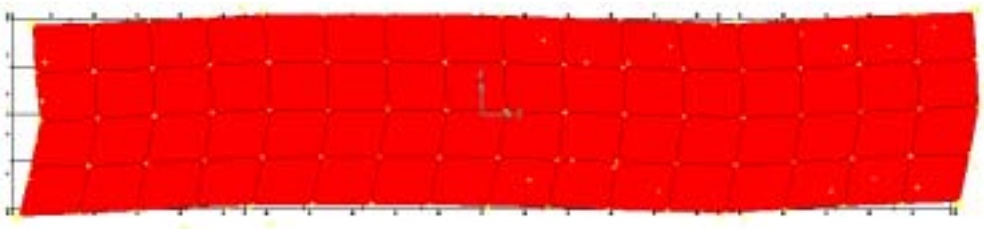

**Figure 9.22. Lowest identifiable mode of response characteristic to the longitudinal response of Specimen #2 (plan view at roof diaphragm level).**

The longitudinal walls were extremely stiff in-plane, and deformations during the strongest longitudinal excitation (PGA = 1.56*g*) were about 0.02 in. The instrumentation was not sensitive enough to detect the behavior suggested by Figure 9.22.

# 10 Analytical Modeling

Several different analytical models representing the half-scale test specimens were developed with the following objectives:

- review different available analysis techniques;
- substantiate the observed responses of the half-scale specimens;
- compare the accuracy of predictions from different techniques to the observed responses of the half-scale specimens;
- investigate the parametric sensitivity of the calculated results; and
- assess the viability of the techniques as design tools.

A typical seismic design, as outlined in the IBC-2000, was carried out in order to review how the buildings addressed in this report would typically be analyzed in design practice and also to identify possible deficiencies in that procedure.

Linear elastic finite element models of the two, half-scale specimens were created using the program SAP2000 (1999). The models were first created using material and dimensional parameters developed much as they would be in typical design. The models then were modified using available measured material properties, and then finally modified to better predict the observed responses. Results of those models were assessed for their sensitivity to error in key assumptions. Finally, the technique's viability as a typical design tool was evaluated.

Also for purposes of design, a simplified design approach was developed, in which low-rise structures with flexible roof diaphragms were idealized as two-degree-of-freedom systems. This approach was first developed mathematically and was then implemented using the two, half-scale specimens tested here as representative models. The calculated and measured responses were compared and the sensitivity of those results to error in the initial assumptions was assessed.

## 10.1 Typical Seismic Design of Prototype Structure

For reference, a typical seismic design process for the prototype building, as outlined in the IBC-2000, is presented here. The response spectrum used in this analysis, Figure 10.1, was developed using the procedures outlined in IBC-2000. The spectrum in Figure 10.1 corresponds to a 10% probability of expected exceedence in 50 years; the spectra in Figure 5.1 and Figure 5.2 represent a 2% probability of expected exceedence in 50 years. Multiplying the ordinates in Figure 10.1 by 3/2 would shift the expected probability of exceedence to about 2% in 50 years.

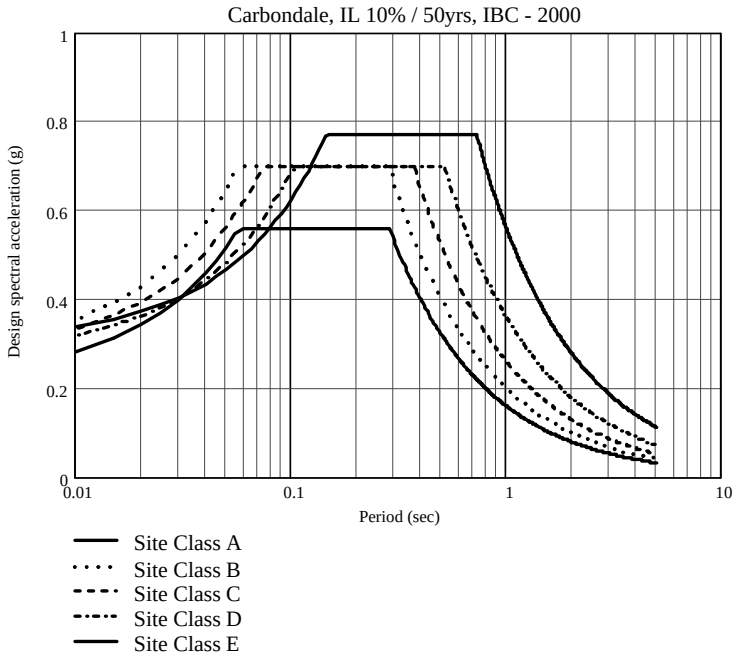


**Figure 10.1. IBC-2000 design response spectrum for Carbondale, IL.**

Designers have the option to use the Simplified Analysis (SA) procedure (IBC-2000 1617.5) in lieu of more rigorous dynamic analysis when the structure under consideration meets the criteria of Seismic Use Group I, as defined in the IBC-2000, as well as a number of other limitations (IBC-2000 1616.6). The warehouse and storage facilities represented by the prototype structure typically meet these criteria, and thus may be designed using the SA procedure.

The design base shear is:

$$V = \frac{1.2 \cdot S_{DS} \cdot W}{R} \qquad \textbf{(10-1)}$$

where,

$S_{DS}$= short-period design spectral acceleration ($g$)

$W$ = effective seismic weight of structure

$R$ = response modification factor (IBC 2000 Table 1617.6)

In the case of the prototype building,

- $W$ is 34,000 lb, approximated as one-half the total weight of the masonry walls plus the weight of the diaphragm;
- $S_{DS}$ is about 0.70 $g$, approximated from Figure 10.1 for Site Class B, Site Class C or Site Class D; and
- $R$ is 2.5, determined from Table 1617.6 in the IBC-2000 for ordinary reinforced masonry bearing wall buildings.

The design base shear is then:

$$V_{prototype} = \frac{1.2 \cdot S_{DS} \cdot W}{R} = \frac{1.2 \cdot 0.70 \cdot 34{,}000}{2.5} \approx 11{,}400\ lb \qquad \textbf{(10-2)}$$

This base shear would then be applied at the roof diaphragm level as an equivalent lateral force, and design would proceed.

The Simplified Analysis procedure also states that the design story drift shall be taken as:

$$\Delta = 0.01 \cdot H \qquad \textbf{(10-3)}$$

where $H$ is the story height of the structure. In the case of the prototype building,

$$\Delta_{prototype} = 0.01 \cdot 168\ in. = 1.68\ in. \qquad \textbf{(10-4)}$$

It is shown in Section 11 of this report, that the effective inertia forces on the half-scale specimen are one-eighth those that would exist in the prototype structure (Equation 11-5), and the drifts in the half-scale specimen are one-quarter those that would occur in the prototype structure (Equation 11-8).

Thus, the design shear to be applied at the roof diaphragm level for the half-scale specimen is:

$$V_{specimen} = \frac{1}{8} \cdot V_{prototype} = \frac{1}{8} \cdot 11{,}400\ lb = 1400\ lb \qquad \textbf{(10-5)}$$

Likewise, the design story drift for the half-scale specimen is:

$$\Delta_{specimen} = \frac{1}{4} \cdot \Delta_{prototype} = \frac{1}{4} \cdot 1.68\ in. = 0.42\ in. \qquad \textbf{(10-6)}$$

Low-rise masonry buildings with flexible diaphragms have distributed mass and stiffness. If the designer elects to perform a more rigorous multi-degree-of-freedom analysis, however, sufficient guidance is not available in the IBC-2000 for idealization as a multi-degree-of-freedom system. That deficiency is addressed in the following sections.

## 10.2 Linear-Elastic Finite Element Models

### 10.2.1 Specimen #1 (lumber diaphragm)

The linear-elastic finite element method (FEM) model used to calculate the time-history response of Specimen #1 initially used assumed values for some of the model parameters. Those assumed values were determined much as they would be in typical design practice (Table 10-1). For purposes of this report, a FEM model with these assumed parameters is referred to as an "Original FEM" model.

The value for the shear modulus of lumber was initially chosen because it represents a typical ratio of shear modulus to elastic modulus for materials often used in structural design. For monolithic lumber elements, a better initial assumption would have been, $G = E/16$. As discussed later in this report, however, the best value for a complex lumber subassemblage can be very difficult to estimate, and may be quite different from either $0.40E$ or $E/16$.

**Table 10-1. Original assumptions for FEM modeling of Specimen #1.**

| Parameter | Typical Design Value |
|---|---|
| elastic modulus of masonry, *E* | 1200 ksi |
| shear modulus of masonry, *G* | 40% of *E* = 480 ksi |
| elastic modulus of lumber, *E* | 1200 ksi |
| shear modulus of lumber, *G* | 40% of *E* = 480 ksi |
| diaphragm thickness, $t_d$ | specified thickness of sheathing, 3/8 in. |
| effective masonry thickness in shear, $t_m$ | 2.2 in. |
| effective masonry thickness in bending, $t_b$ | 3.5 in. |
| equivalent viscous damping | 5% |

Since the FEM model is linear elastic, it was useful to compare the calculated model response and the measured specimen response only at low levels of input acceleration. Observations of cracking patterns during testing suggested that the half-scale specimen remained basically elastic during Seismic Test 1 through Seismic Test 5 with PGAs of 0.10*g* and 0.67*g*, respectively. In general, Seismic Test 3 provided the basis for most of the analytical modeling (Figure 10.2).

The FEM model used the measured table accelerations in both the longitudinal and transverse directions for input accelerations. Using the measured table accelerations as opposed to the table input accelerations eliminated the possibility of spurious table accelerations causing disagreement between the calculated and measured responses. Section 8.3 of this report offers a complete discussion of the possible sources of such unintended table accelerations and the techniques used to reduce these accelerations.

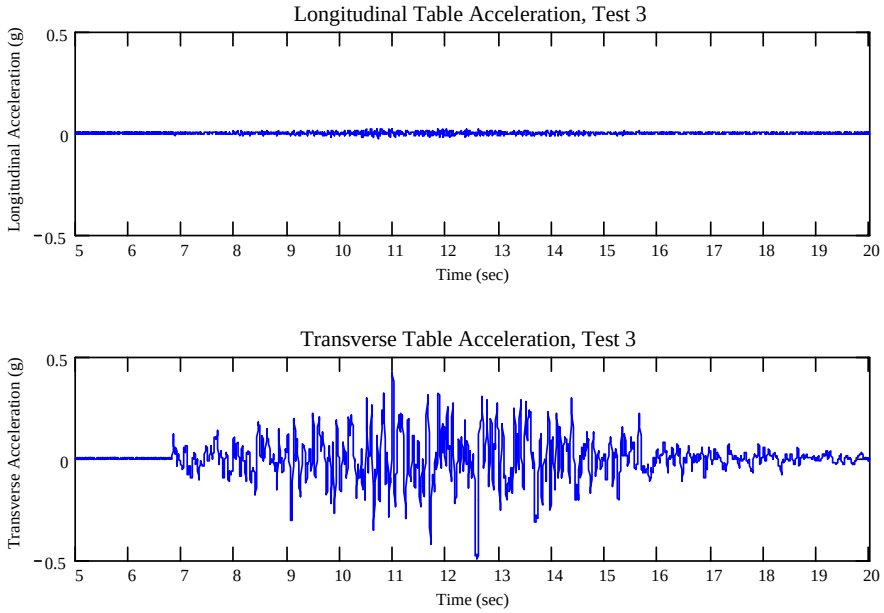


**Figure 10.2. Measured transverse table accelerations (Specimen #1, Test 3).**

Preliminary comparisons of measured and calculated responses showed significant differences. The Original FEM model consistently calculated a higher fundamental frequency (25 Hz) than that measured (14 Hz), and significantly smaller accelerations and deflections than those measured. These observations suggested that the Original FEM model was much stiffer than the experimental specimen.

Following the development of the Original FEM model, CERL personnel conducted compression tests on a series of masonry prisms, which showed that the actual elastic modulus of the half-scale CMU was only 325 ksi, one-quarter the assumed modulus of 1200 ksi. No material data were collected on the lumber sheathing.

To better compare the calculated and measured responses, a new FEM model was developed using the measured modulus of elasticity of the masonry. In particular, goals were to calibrate that new FEM model to achieve:

- sufficient agreement between the calculated fundamental frequency and the measured fundamental frequency;

- sufficient agreement between calculated displacements and accelerations and measured displacements and accelerations in regions of peak response; and

- sufficient agreement between calculated displacements and accelerations and measured displacements and accelerations in regions of non-peak response.

A flow chart describing calibration of the new FEM model is shown schematically in Figure 10.3.

Varying the assumed thickness of the diaphragm shell elements, and using the measured modulus of the masonry, led to a sufficient level of agreement between the calculated values of peak response and the measured values of peak response. The diaphragm shell element thickness was systematically decreased from the specified value of 3/8 inch to zero, in increments of 1/16 inch. At each step in the calibration process, the FEM model was run and the calculated and measured responses compared. The FEM model based on the measured modulus of the masonry accurately calculated the fundamental period of the building over the wide range of assumed diaphragm thicknesses.

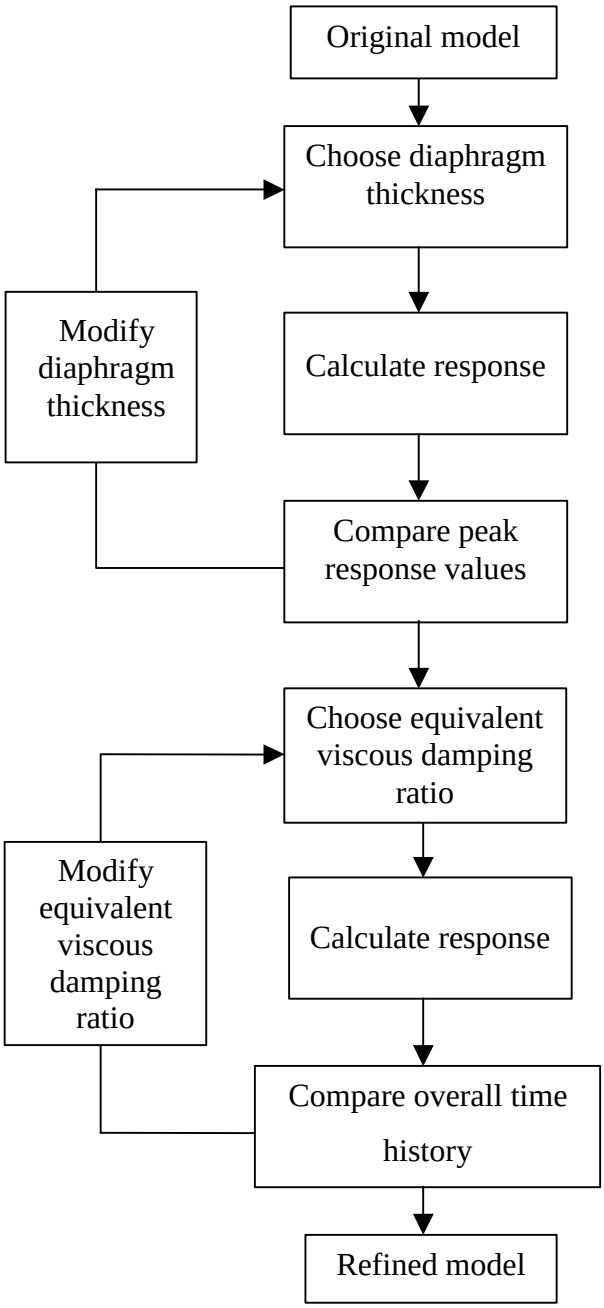


**Figure 10.3. Refinement process used for FEM model of Specimen #1.**

Varying the equivalent viscous damping ratio achieved consistent overall agreement in the time history. The damping ratio was systematically increased from 0% to 5.0%, in increments of 0.5%. The FEM model described in the preceding paragraphs is referred to as the "Refined FEM" model. Table 10-2 summarizes the key parameters of both the Original FEM model and the Refined FEM model.

Some parameters used in the Refined FEM model differed significantly from those used in the Original FEM model. Chief among those was the elastic modulus of the masonry. Differences between the assumed and the measured modulus of masonry may exist for a number of reasons:

- higher than typical porosity in the half-scale CMU;
- lower than typical elastic modulus of aggregates in the half-scale CMU; and
- lower than typical elastic modulus of mortar.

Another parameter that differed significantly from that used in the Original FEM model was the diaphragm thickness. Differences between the originally assumed diaphragm thickness and that used in the Refined FEM model were also expected, because:

- wood is an orthotropic material and thus it does not maintain the proportion of shearing modulus to elastic modulus for isotropic materials, $G = \frac{E}{2(1+\upsilon)}$; and
- mechanisms other than material deformations contribute to deformation of the diaphragm (Section 10.3.2 of this report).

These differences are significant but justified. Section 10.2.3 of this report discusses the sensitivity of analysis results to changes in assumed diaphragm thickness.

The Refined FEM model calculated the response of Specimen #1 quite well. The measured and calculated values of peak response correspond in both their location in the time history and their overall magnitude. Moreover, the overall shape and magnitude of the calculated and measured time-histories are also in general agreement. Figure 10.4 through Figure 10.7 compare the measured and calculated transverse responses of the diaphragm, at its plan center, during Seismic Test 3.

**Table 10-2. Key parameters for Original and Refined FEM models.**

| FEM Model | Diaphragm thickness | Elastic Modulus of Masonry | Equivalent viscous damping |
|---|---|---|---|
| Original | 3/8 in. | 1200 ksi | 5% |
| Refined | 1/16 in. | 325 ksi | 5% |

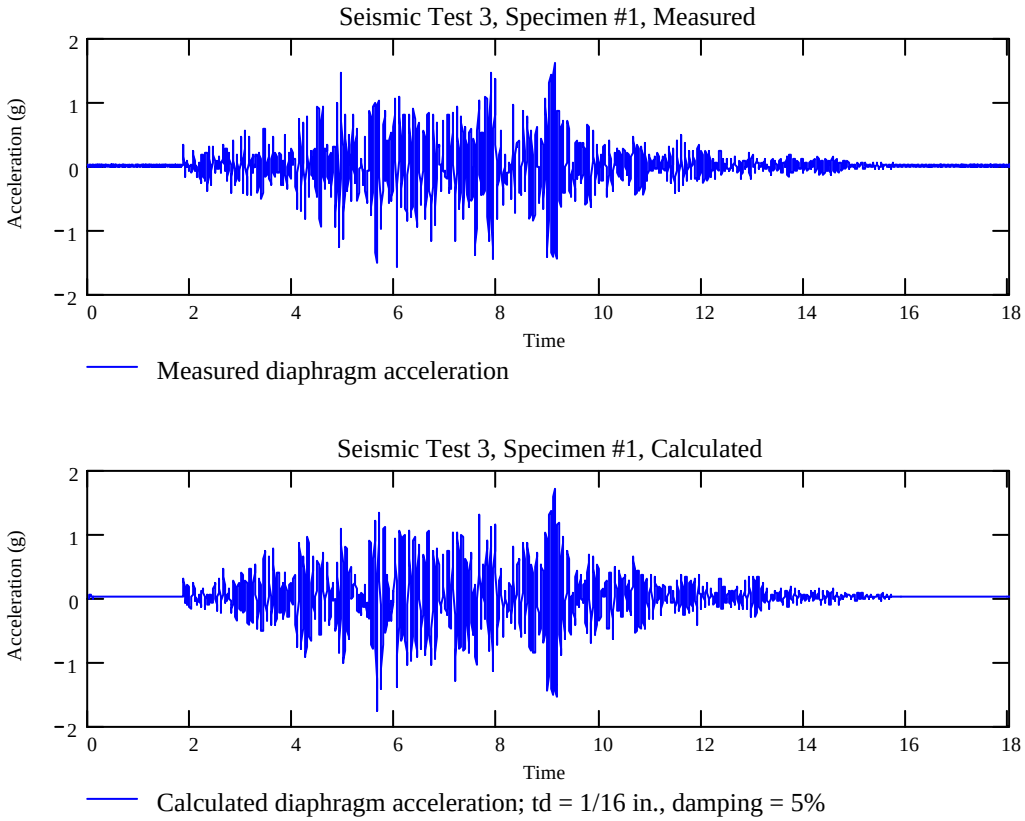


**Figure 10.4. Measured and calculated diaphragm acceleration response (Refined FEM model, Specimen #1).**

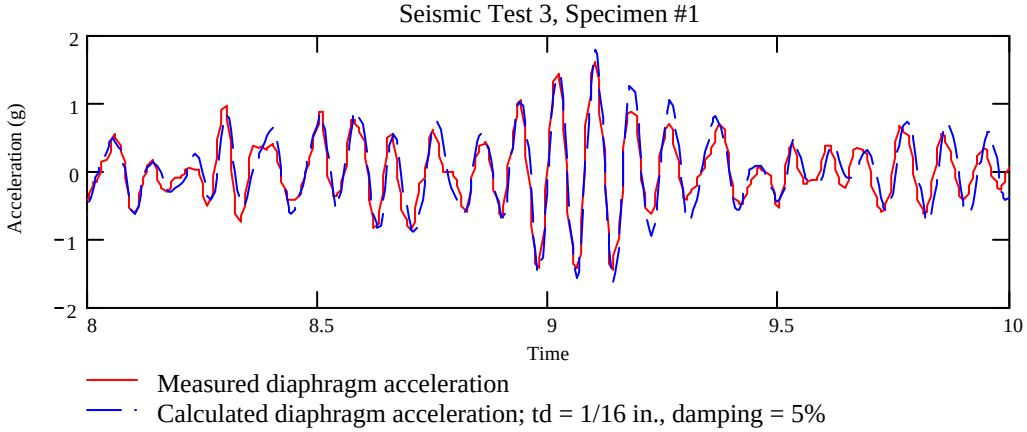


**Figure 10.5. Two-second comparison of measured and calculated diaphragm acceleration during peak response (Refined FEM model, Specimen #1).**

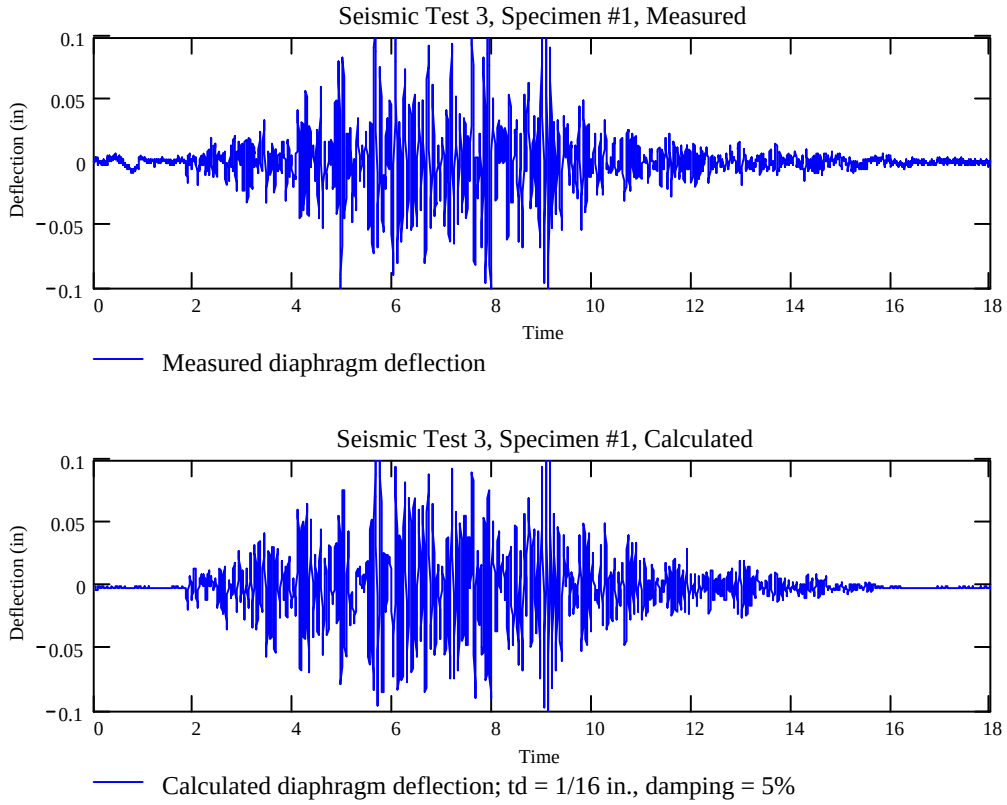


**Figure 10.6. Measured and calculated diaphragm displacement response as measured relative to base of specimen (Refined FEM model, Specimen #1).**

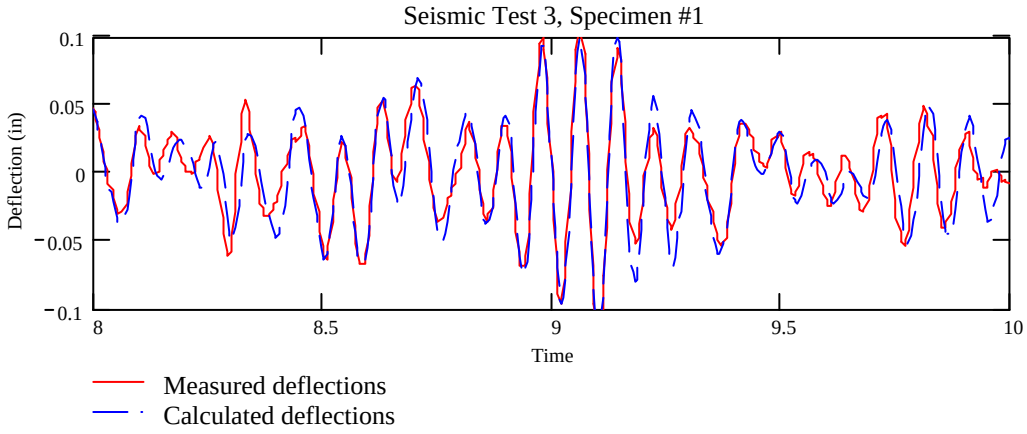


**Figure 10.7. Two-second comparison of measured and calculated diaphragm deflection during peak response as measured relative to base of specimen (Refined FEM model, Specimen #1).**

The finite-element analysis provided base shears and diaphragm shears for both models. Overall base shears were estimated by summing the base-reaction envelopes of both transverse shear walls. Similarly, diaphragm reaction shears were estimated by summing the shell-element shear-stress envelopes (or shell-element force-resultant envelopes) at both ends of the diaphragm, across given cross-sectional planes (Figure 10.8). Figure 10.8 was only used to calculate approximate diaphragm shears, as discussed, and is not intended to represent the actual distribution of shear stress in the diaphragm of half-scale Specimen #1 during seismic testing. Table 10-3 summarizes those calculated shears for simulated Seismic Test 3.

**Table 10-3. Calculated base shears (Test 3, Specimen #1).**

| Diaphragm Shear | Overall Base Shear |
|---|---|
| 2500 lb | 3600 lb |

The Refined FEM model also calculated elastic stress patterns, and thus expected cracking patterns, in the masonry walls for any given ground motion. Those stress patterns implied flexural cracking at the top course and the base of the center pier (Figure 10.9). They also implied cracking at the base and interior of the unperforated west longitudinal wall (Figure 10.10 and Figure 10.11). Figure 10.9, Figure 10.10 and Figure 10.11 suggest that the highest joint stresses occur within the wall height. This implies that the largest out-of-plane dynamic amplification occurs in the walls' interior, and not at the roof diaphragm level. These analytical predictions concurred with the cracking patterns observed in half-scale Specimen #1.

The Refined FEM model of half-scale Specimen #1 achieved the following:

- it accurately calculated the natural frequencies of the half-scale specimen;
- it accurately calculated the displacement and acceleration responses of the half-scale specimen;
- it accurately determined cracking locations for any given ground motion; and
- it provided a way to estimate diaphragm shear and overall base shear for any given ground motion.

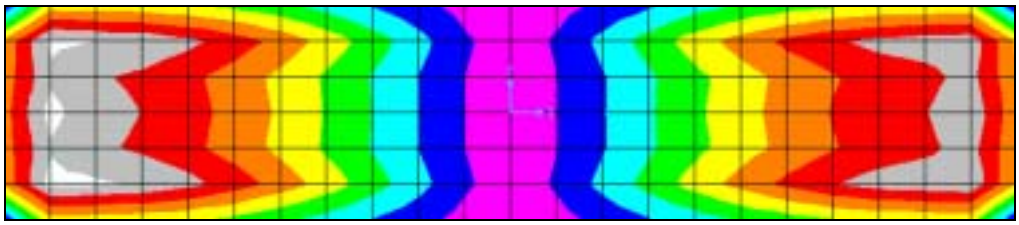

**Figure 10.8. Example of calculated in-plane shear-diaphragm stress (Refined FEM model, Specimen #1).**

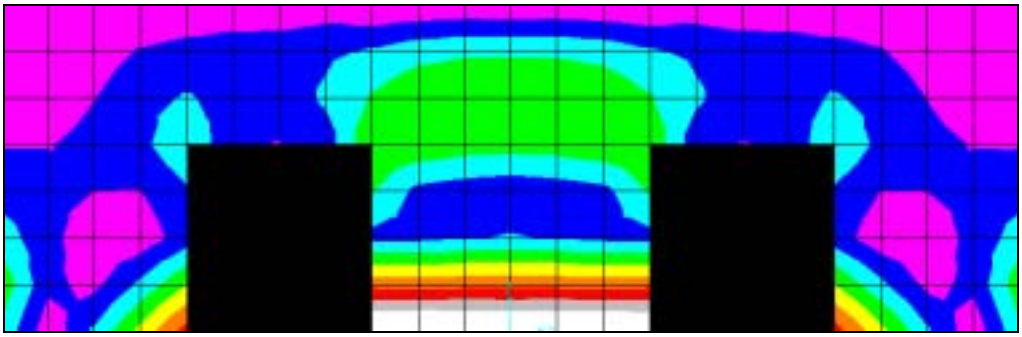

**Figure 10.9. Example of calculated bed-joint normal-stress contours in east perforated longitudinal wall (Refined FEM model, Specimen #1).**

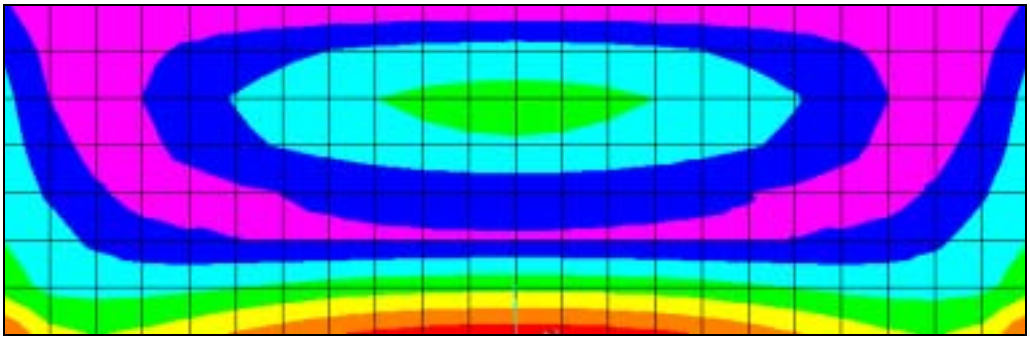

**Figure 10.10. Example of calculated bed-joint normal-stress contours in west longitudinal wall (Refined FEM model, Specimen #1).**

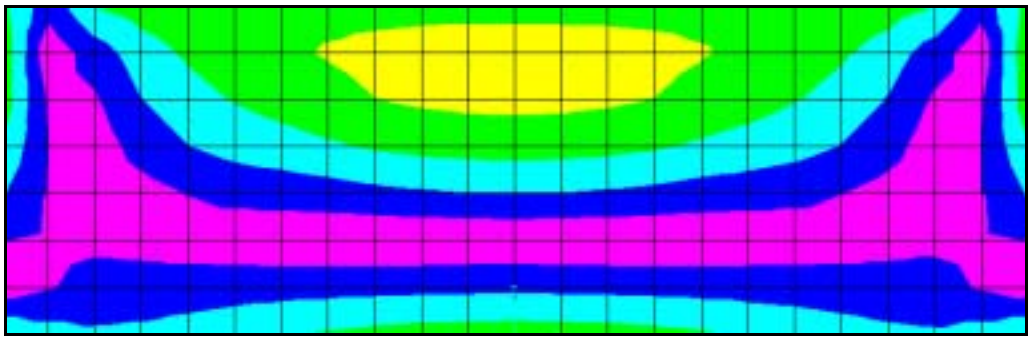

**Figure 10.11. Example of calculated head-joint normal-stress contours in west longitudinal wall (Refined FEM model, Specimen #1).**

### 10.2.2 Specimen #2 (metal diaphragm)

The linear elastic FEM used to calculate the time-history response of Specimen #2 initially used assumed values for some parameters. Those assumed values were determined much as they would be in typical design practice, Table 10-4. For purposes of this report, a FEM model with these assumed parameters is referred to as an "Original FEM."

**Table 10-4. Original assumptions for FEM modeling of Specimen #2.**

| Parameter | Typical Design Value |
|---|---|
| elastic modulus of masonry, $E$ | 1200 ksi |
| shear modulus of masonry, $G$ | 40 % of $E$ = 480 ksi |
| elastic modulus of metal deck, $E$ | 29000 ksi |
| shear modulus of metal deck, $G$ | 40% of $E$ = 11600 ksi |
| diaphragm thickness in shear, $t_d$ | specified gauge thickness of decking, 0.030 in. |
| diaphragm thickness in bending | 1.34 in. |
| effective masonry thickness in shear, $t_m$ | 2.2 in. |
| effective masonry thickness in bending, $t_b$ | 3.5 in. |
| equivalent viscous damping | 5 % |

Since the analytical model is linear elastic, it was useful to compare the analytical model response and the experimental specimen response only at low levels of input acceleration. Observations of cracking patterns during testing of Specimen #2 suggested that the structure remained basically elastic during Seismic Test 0 (zero) through Seismic Test 8a with PGAs of 0.05$g$ and 1.23$g$ (longitudinal), respectively. In general, Test 5 provided the basis for most of the analytical modeling (Figure 10.12) with a PGA of 0.40$g$.

For the same reasons discussed in Section 8.3 of this report, the analytical modeling of Specimen #2 used the measured table accelerations in the longitudinal and transverse directions for the input accelerations.

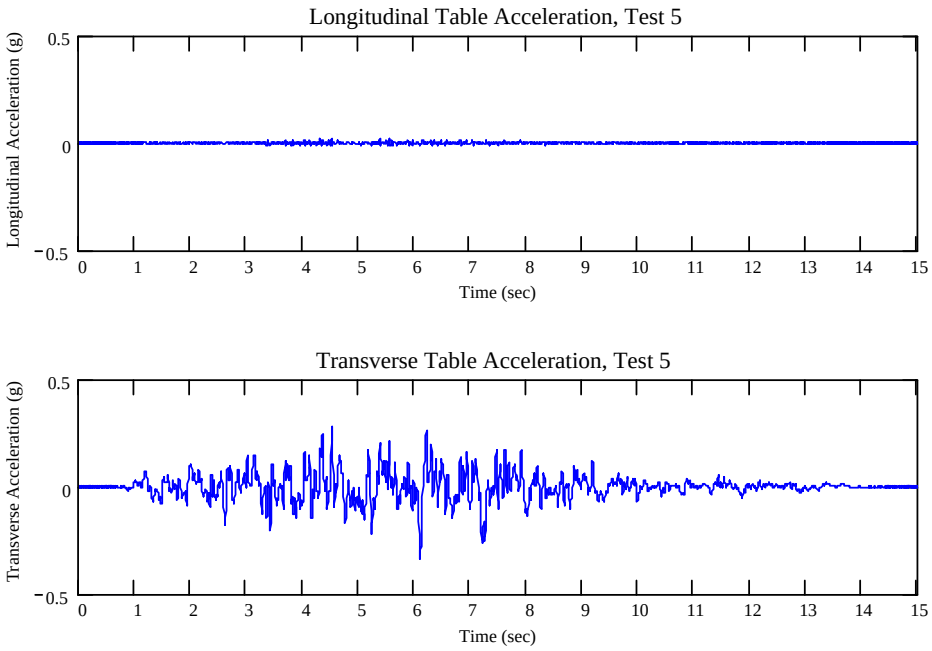


**Figure 10.12. Measured transverse table accelerations (Specimen #2, Test 5).**

Preliminary comparisons of measured and calculated responses showed very significant differences. The Original FEM consistently calculated a higher fundamental frequency (20 Hz) than that measured (12 Hz), and significantly smaller accelerations and deflections that those measured. These observations suggested that the Original FEM was much stiffer than the experimental specimen.

Compression tests conducted at CERL on masonry prisms showed that the actual elastic modulus of the half-scale CMU from Specimen #2 was 480 ksi, about one-third of the assumed modulus of 1200 ksi. No material data were collected on the metal decking.

Metal deck design manuals often tabulate the $G'$ value as a measure of shear stiffness for different welding and screwing patterns, $G' = G_{effective} \times thickness$ (United Steel Deck Co. 1999). A typical value of $G'$ for light gauge, lightly connected (36 / 3 welding and one side lap screw per span) is about 10 kip/inch. Given the specified gauge thickness of the decking, 0.030 in., an effective shear modulus, $G_{effective}$, was established as 333 ksi, far less than the initially assumed value of 11,600 ksi.

To better compare the measured responses, a new FEM model was developed using the measured elastic modulus of the masonry and the estimated shear modulus of the metal decking. This new FEM is referred to, as before, as the "Refined FEM" model.

Some parameters used in the Refined FEM model differed significantly from those used in the Original FEM model. Chief among those was the modulus of the masonry. Difference between the assumed and the measured elastic modulus of masonry may exist for the same reasons discussed in Section 10.2.1 of this report. Another was the assumed diaphragm thickness. Difference between the originally assumed diaphragm material elastic modulus and that used in the Refined FEM model was expected, because:

- steel deck is an orthotropic assembly and thus it does not maintain the usual proportion of shearing modulus to elastic modulus ($G = 0.40\ E$); and

- mechanisms other than material deformations contribute to deformation of the diaphragm (Section 10.3.2 of this report).

Therefore, these differences are significant but justified.

The Refined FEM model accurately calculated the fundamental frequency of the system (12 Hz). The model did not, however, predict the time-history response of Specimen #2 well. The measured diaphragm response contained radically larger magnitudes of accelerations throughout the time-history. Inspection of the measured frequency response of the diaphragm to Seismic Test 5 revealed a significant amount of energy at frequencies between about 40 and 70 Hz (Figure 10.13). Presumably, local, high-frequency, high-acceleration response of the metal decking dominated the measured response (Figure 10.14) and resulted in the observed difference between the measured and calculated diaphragm behavior. Removing the high-frequency (>20 Hz) acceleration response from the measured data, using a square low-pass filter (Figure 10.15), made the data more usable and made the calculated responses closer to that observed.

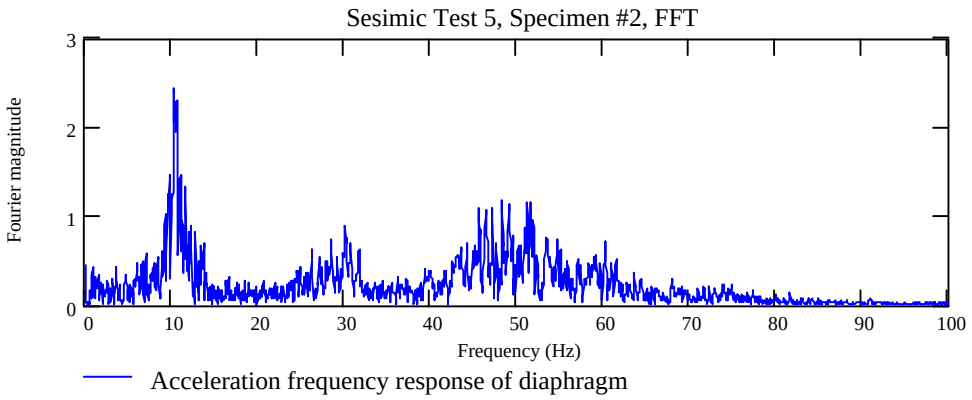


**Figure 10.13. Unfiltered, measured acceleration frequency response of diaphragm (Specimen #2, Test 5).**

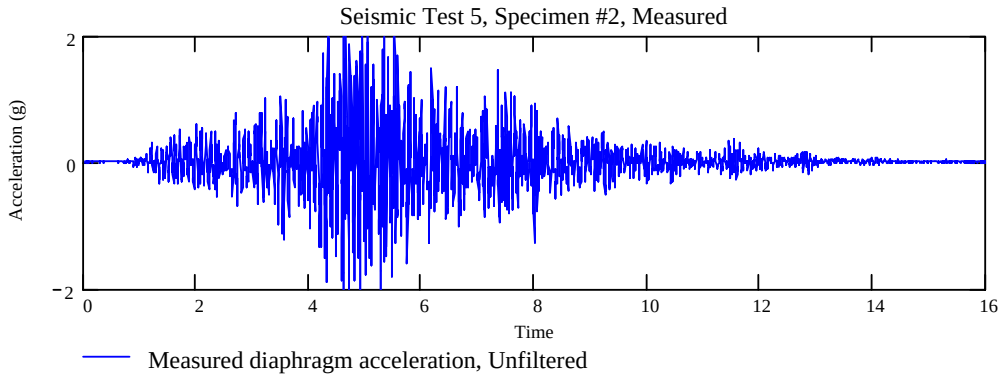


**Figure 10.14. Unfiltered, measured acceleration response of diaphragm (Specimen #2, Test 5).**

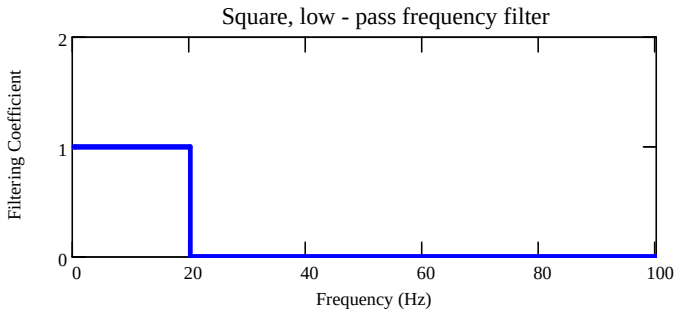


**Figure 10.15. Low-pass filter used to modify measured acceleration response of diaphragm (Specimen #2).**

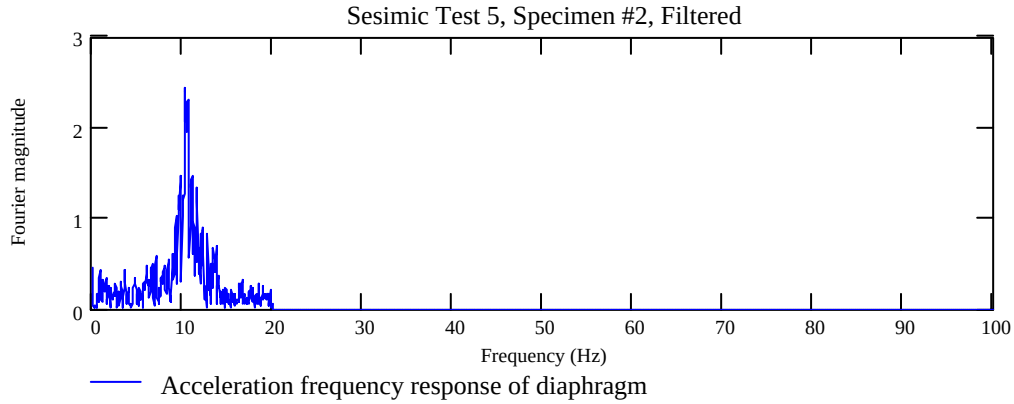


**Figure 10.16. Filtered, measured acceleration frequency response of diaphragm (Specimen #2, Test 5).**

The measured and the calculated responses of Specimen #2 matched well after filtering. The measured and calculated spectral responses correspond in their location in the time history and in their overall amplitude (Figure 10.17 and Figure 10.18). Table 10.5 compares the key parameters of the Original FEM model and the Refined FEM model of Specimen #2.

**Table 10-5. Key parameters for Original FEM and Refined FEM models.**

| FEM Model | Diaphragm Shear Modulus | Elastic Modulus of Masonry | Equivalent viscous damping |
|---|---|---|---|
| Original | 40% of 29000 ksi | 1200 ksi | 5% |
| Refined | 333 ksi | 480 ksi | 5% |

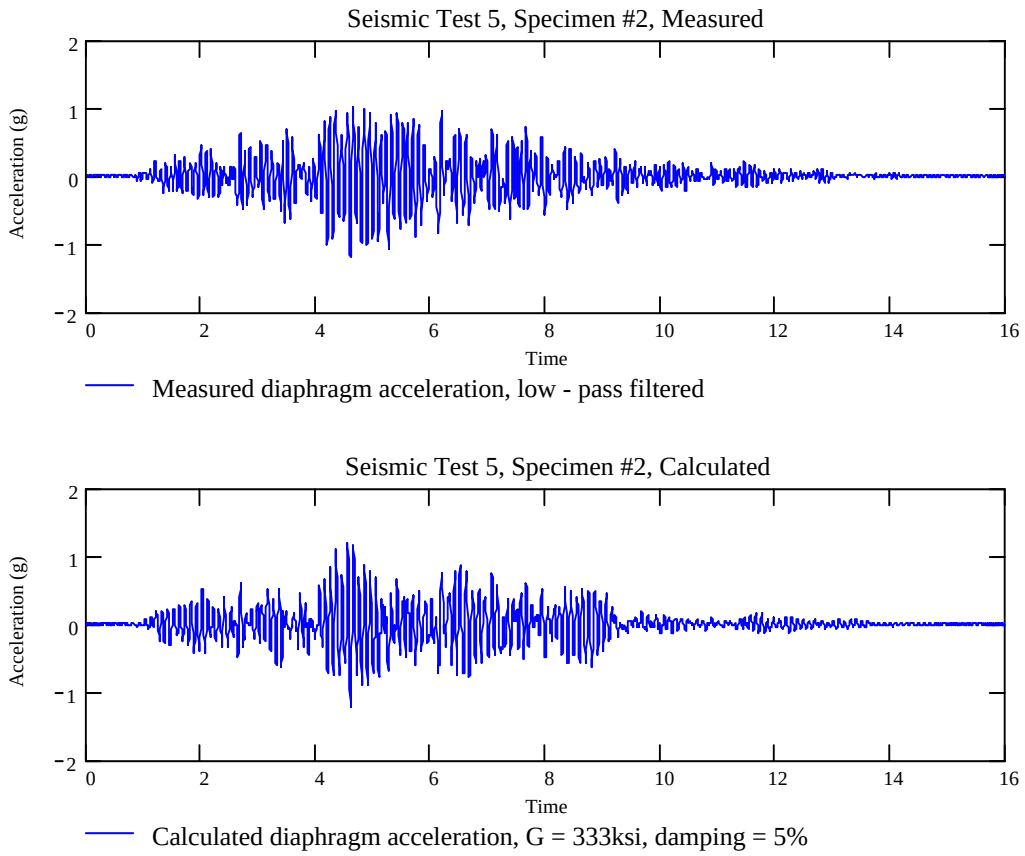


**Figure 10.17. Measured and calculated diaphragm acceleration response (Specimen #2, Test 5, Refined FEM model).**

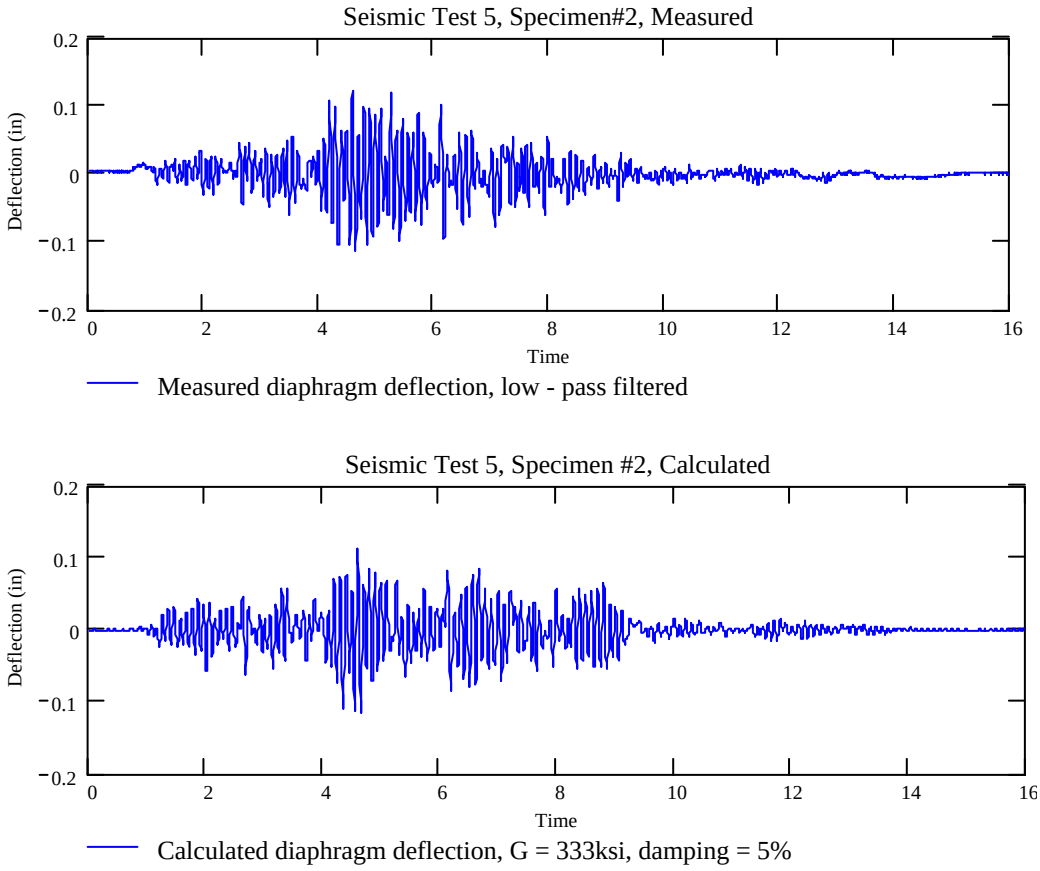


**Figure 10.18. Measured and calculated diaphragm deflection response measured relative to base of specimen (Specimen #2, Test 5, Refined FEM model).**

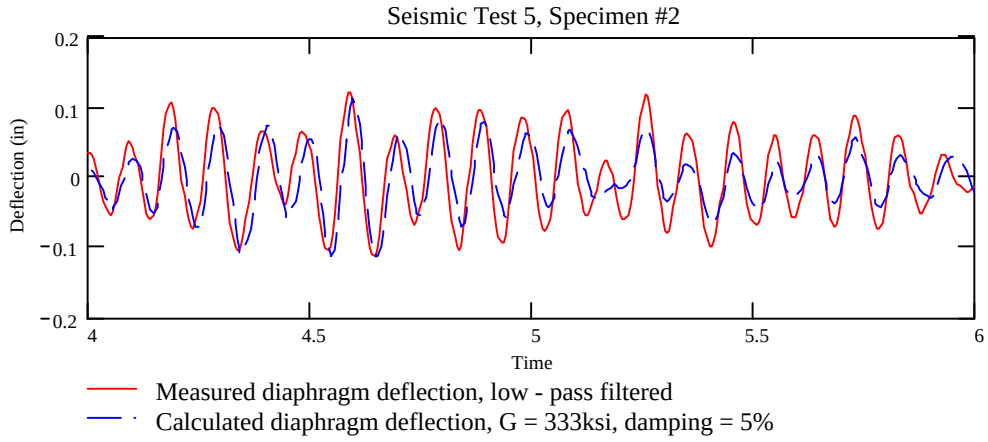


**Figure 10.19. Two-second comparison, during peak response, of measured and calculated diaphragm displacement measured relative to the base of the specimen (Specimen #2, Test 5, Refined FEM model).**

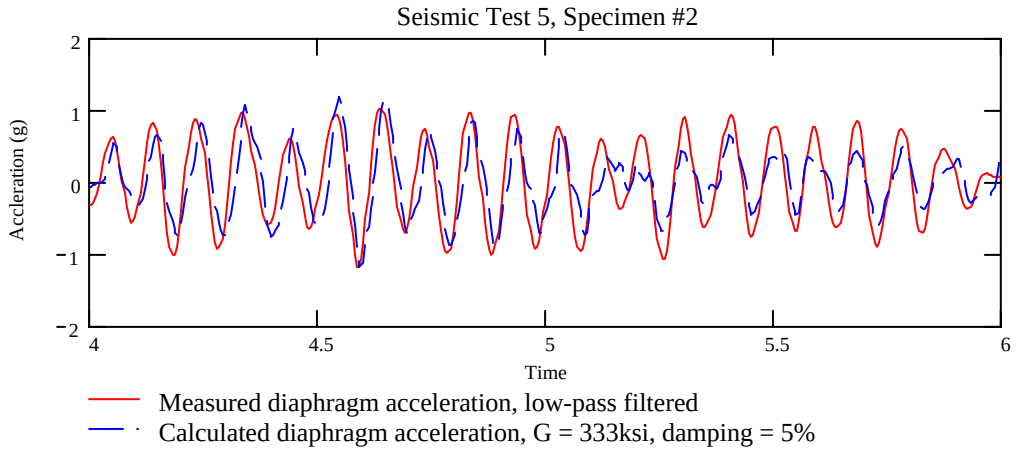


**Figure 10.20. Two-second comparison of measured and calculated diaphragm acceleration during peak response (Specimen #2, Test 5, Refined FEM model).**

The finite-element analysis provided base shears and diaphragm shears, as described in Section 10.2.1 of this report. Table 10-6 summarizes those resulting base shears.

**Table 10-6. Calculated base shears (Specimen #2, Test 3).**

| Diaphragm Shear | Overall Base Shear |
|---|---|
| 1100 lb | 1600 lb |

The Refined FEM model also calculated elastic stress patterns, and thus expected cracking patterns, in the masonry walls for any given ground motion. The analytical predictions concurred with the observed cracking patterns in Specimen #2.

The refined linear-elastic FEM model of Specimen #2 achieved the following:

- it accurately calculated the natural frequencies of the half-scale system;
- it accurately calculated both the displacement and acceleration responses of the half-scale specimen;
- it accurately calculated where cracks could be expected for a particular ground motion; and
- it provided a way to estimate diaphragm shear and overall base shear for any given ground motion.

### 10.2.3 Sensitivity Analysis of the Results from FEM Models

The calibration process used for the FEM model of Specimen #1 provided a measure of the sensitivity of the finite element results to different initial assumptions. This sensitivity analysis included the effects of assumed diaphragm element thickness and assumed equivalent viscous damping ratio. For instance, the Refined FEM model consistently calculated a reasonably accurate fundamental period almost independently of the assumed diaphragm thickness (Figure 10.21). This implied that as long as the analytical roof diaphragm imposed reasonable compatibility between transverse deflections of longitudinal walls, the FEM model would predict a sufficiently accurate fundamental period. Similarly, FEM analysis consistently calculated accurate spectral displacements and accelerations, almost independently of the assumed diaphragm thickness (Figure 10.22). This implies that, again, as long as the analytical roof diaphragm imposed reasonable compatibility between transverse deflections of longitudinal walls, the FEM would predict sufficiently accurate spectral response.

Figure 10.23 suggests that the modeling was somewhat more sensitive to changes in the assumed value of equivalent viscous damping. The calculated spectral response quantities increased by roughly 15% for every percentage-point decrease in the assumed damping ratio. At the typical design value of 5% damping, the FEM model calculated values near those measured.

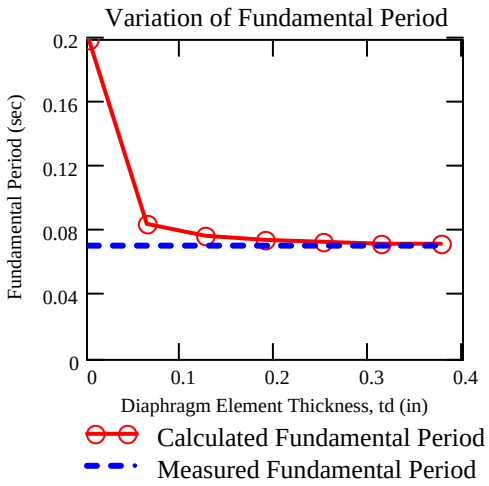


**Figure 10.21. Sensitivity of calculated fundamental period to assumed thickness of diaphragm shell elements (Specimen #1).**

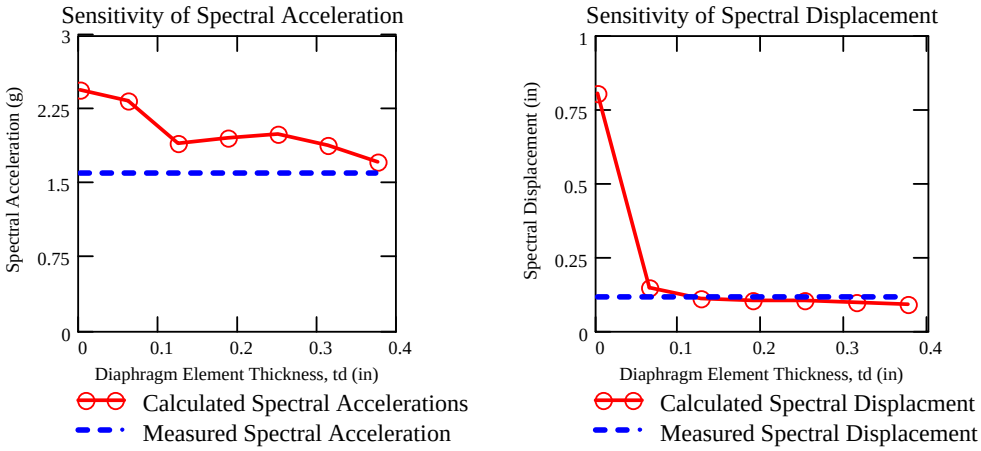


**Figure 10.22. Sensitivity of calculated spectral response quantities to assumed thickness of diaphragm shell elements (damping = 5%, Seismic Test 3, Specimen #1).**

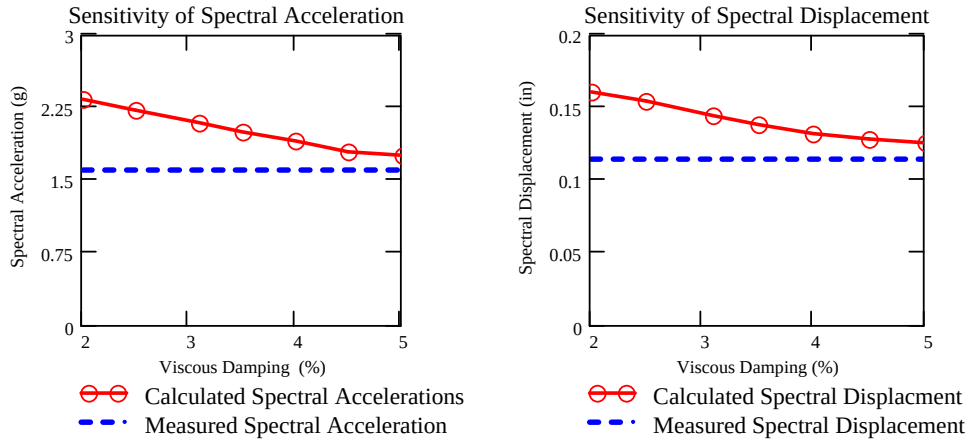


**Figure 10.23. Sensitivity of calculated spectral response quantities to assumed equivalent viscous damping ratio (diaphragm thickness = 1/16 in., Seismic Test 3, Specimen #1).**

## 10.3 Equivalent Two-DOF Generalization and Response-Spectrum Analysis

Comparison of calculated and measured responses suggested that the half-scale test specimens, and the analytical models representing them, behaved as multi-degree-of-freedom systems. The roof diaphragm tends to respond independently of the transverse shear walls, and the transverse shear walls tend to respond together, in-phase. To investigate this behavior and the possibility of developing a simplified design approach based on it, it was useful to idealize the specimens as two-degree-of-freedom (2-DOF) systems.

### 10.3.1 General Approach

To idealize the half-scale specimens as 2-DOF systems, the generalized coordinates $q_1$ and $q_2$, described in Figure 10.24, were chosen. Degree of freedom 1 is associated with the in-plane deformation of the transverse shear walls. Degree of freedom 2 is associated with the in-plane deformation of the diaphragm.

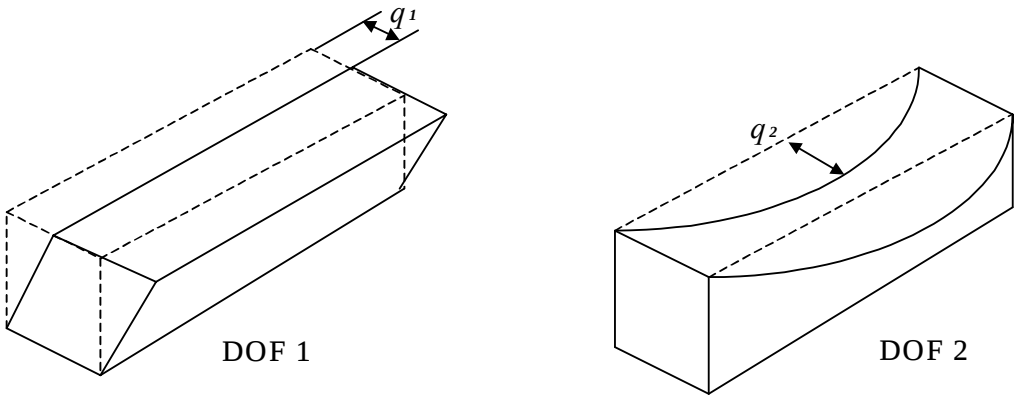


**Figure 10.24. Generalized coordinates for 2-DOF idealization.**

#### 10.3.1.1 First Degree of Freedom, $q_1$

The transverse shear walls have an aspect ratio of 88 in. / 56 in., or about 1.5. It can be shown that both flexural and shearing deformations significantly contribute to the deflection of a cantilever shear wall at this aspect ratio. Thus, the chosen shape function $\phi(y)$ had non-uniform first and second derivatives.

$$\phi(y) = 1 - \cos\left(\frac{y\pi}{2H}\right) \qquad \textbf{(10-7)}$$

where, $H$ = height of half-scale specimen

$y$ = vertical coordinate

The generalized mass $M^*_1$ associated with $q_1$ (Chopra 1995) is:

$$M^*_1 = \int_0^H \mu(y)\left[\phi(y)\right]^2 dy \qquad \textbf{(10-8)}$$

where, $\mu(y)$, the mass of the specimen per unit height, is piecewise continuous because it must include the concentrated mass of the diaphragm $M_{diaphragm}$ at $y = H$. Evaluation of the integral gives:

$$M^*_1 = \frac{1}{5}\mu H + M_{diaphragm} \quad \textbf{(10-9)}$$

The generalized stiffnesses $K^*_{S1}$ and $K^*_{f1}$, representing respectively the shearing stiffness and the flexural stiffness of one transverse shear wall associated with DOF $q_1$, are defined by the definite integrals

$$K^*_{S1} = A'G\int_0^H \left[\phi'(y)\right]^2 dy \quad \textbf{(10-10)}$$

and

$$K^*_{f1} = EI\int_0^H \left[\phi''(y)\right]^2 dy \quad \textbf{(10-11)}$$

where, $G$ = shearing modulus of the masonry

$E$ = elastic modulus of the masonry

$A'$ = effective shear area of the transverse walls

$I$ = in-plane moment of inertia of the transverse walls

Evaluation of these integrals gives:

$$K^*_{S1} = \frac{A'G}{H}\frac{\pi^2}{8} \quad \textbf{(10-12)}$$

$$K^*_{f1} = \frac{EI}{H^3}\frac{\pi^4}{32} \quad \textbf{(10-13)}$$

Flexibility is the reciprocal of stiffness. Thus, the total generalized stiffness for the two transverse shear walls is:

$$K^*_1 = 2\cdot\frac{K^*_{S1}K^*_{f1}}{K^*_{S1}+K^*_{f1}} \quad \textbf{(10-14)}$$

#### 10.3.1.2 Second Degree of Freedom, $q_2$

The shape function chosen to represent the deflected shape of the diaphragm during transverse excitation should, again, have non-uniform first and second derivatives. A suitable shape function is:

$$\phi(x) = \sin\left(\frac{\pi}{L}x\right) \qquad \text{(10-15)}$$

where, $L$ = longitudinal dimension of half-scale specimen

$x$ = horizontal coordinate

The expression for the generalized mass $M^*_2$ associated with the second degree of freedom $q_2$ is:

$$M^*_2 = \int_0^L \mu(x)[\phi(x)]^2 dx \qquad \text{(10-16)}$$

where $\mu(x)$, the mass per unit length of the diaphragm plus one-half the mass per unit length of the longitudinal walls, is taken as a constant $\mu$,. Evaluation of this integral gives:

$$M^*_2 = \frac{1}{2}\mu L \qquad \text{(10-17)}$$

This report has shown that the in-plane responses of the half-scale diaphragms were dominated by shearing deformations. Thus, the generalized stiffness $K^*_2$ associated with the second degree of freedom $q_2$ is:

$$K^*_2 = A'G\int_0^L [\phi'(x)]^2 dx \qquad \text{(10-18)}$$

Evaluation of this integral gives:

$$K^*_2 = A'G\frac{\pi^2}{2L} \qquad \text{(10-19)}$$

#### 10.3.1.3 Response-Spectrum Analysis

To use this generalized 2-DOF system for response-spectrum analysis, the response spectrum (in this case Carbondale Ground Motion C02_09s, Figure 5.2) must be scaled in two ways:

1. The period axis (abscissa) must be multiplied by the dimensional scaling factor, $\alpha = 1/2$ (see Section 5.2 of this report); and

2. The response spectral ordinates must be scaled according to the input that the analysis is intended to represent (Table 7-1 and Table 8-1).

For example, if the RSA is intended to represent Seismic Test 3 of Specimen #1, then the period axis of the response spectrum (Carbondale ground motion C02_09s) must be factored by 0.50, and the spectral ordinates must be factored by 0.75.

Response-spectrum analysis conducted for this report used standard computer techniques and the SRSS combination of modal responses. Use of the SRSS technique requires that natural frequencies of the system be sufficiently separated to ensure statistically independent contributions to response. Analytical studies discussed in Section 10 of this report showed that the natural frequencies of the half-scale specimens, as calculated by FEM modeling, were well separated. Therefore, use of the SRSS combination is justified.

### 10.3.2 Response Spectrum Analysis of Generalized 2-DOF System for Specimen #1 (lumber diaphragm)

The expressions for $M^*_1$, $M^*_2$, $K^*_1$ were readily evaluated using:

- known dimensions of the half-scale specimen;

- measured elastic modulus E of masonry in the half-scale specimen;

- estimated shearing modulus G of masonry in the half-scale specimen, taken as 0.40E (FEMA 273 1997); and

- estimated values of unit mass for the masonry and lumber.

Evaluation of $K^*_2$ (Equation 10-17) required an estimate of the in-plane shearing rigidity ($A'G$) of the diaphragm. This is the inverse of diaphragm flexibility, which derives from several mechanisms:

- in-plane shearing deformation of lumber sheathing;
- in-plane flexural deformation of the diaphragm assembly (lumber web and masonry chords);
- slip at nailed connections; and
- slip at chord member splices.

The consensus of the technical community dealing with wood is that the in-plane stiffness of lumber-sheathed diaphragms cannot be predicted by simple rational analysis (FEMA 1997a,b and *Western Woods Use Book* 1973). FEMA (1997a,b) documents contain formulas for the shearing modulus of lumber-sheathed diaphragms, $G_d$, and the in-plane deflection of those diaphragms. These formulas are empirical, however, and are not intended to provide an accurate representation of the different mechanisms contributing to diaphragm stiffness. In particular, the contribution of nail slip to the deflection of a lumber-sheathed diaphragm is not well modeled (ATC-7 1981). In the case of diagonally sheathed lumber diaphragms, the distribution of shear stress, the value of shearing modulus $G$, and hence the shear rigidity $A'G$, are not well understood or modeled.

To skirt the difficulty of predicting an accurate shearing stiffness, the effective shearing rigidity $A'G_{eff}$ of the half-scale diaphragm was derived empirically from the experimental data, using the process explained below.

The diaphragm shear $V(t)$ at any time $t$, at any distance $x$ along the length of the diaphragm is:

$$V(x,t) = \int_0^x \mu(\xi)\ddot{u}(\xi,t)d\xi \qquad \textbf{(10-20)}$$

Where:

$\mu(x)$ = mass associated with the response of the diaphragm, approximated here as the mass per unit length of the diaphragm plus one-half the mass per unit length of the longitudinal masonry walls

$\ddot{u}(x,t)$ = lateral acceleration of the diaphragm

The transverse diaphragm acceleration is known at only three points: the two ends of the diaphragm and its plan center. The transverse diaphragm acceleration can be estimated using a Ritz function $\Psi(x)$:

$$\ddot{u}(x,t) \approx \ddot{q}_1(t) + \Psi(x)\ddot{q}_2(t) \qquad \textbf{(10-21)}$$

Where,

$\Psi(\xi)$ = $\sin\left(\frac{\pi}{L}x\right)$

$\ddot{q}_1(t)$ = known acceleration history at the tops of the transverse walls

$\ddot{q}_2(t)$ = known acceleration history at the plan center of the diaphragm

The selected Ritz function approximating the diaphragm shear is consistent with the recommendation of FEMA 274 C3.2.4 (1997) for the distribution of inertial forces and inertial shear forces in a flexible diaphragm (Figure 10.25).

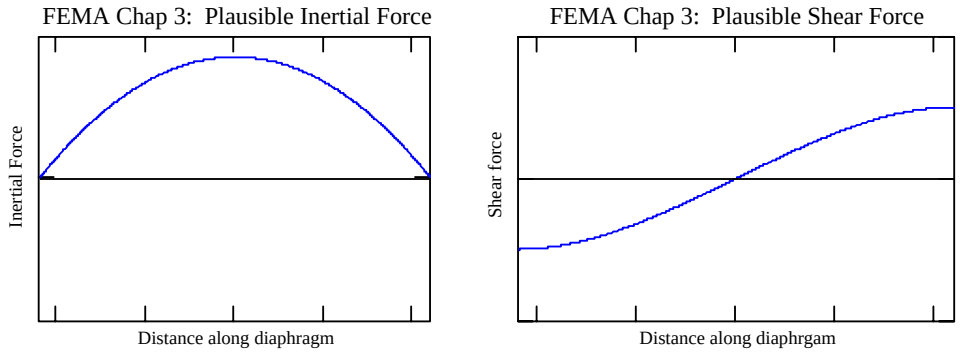


**Figure 10.25. Recommended distribution of inertial forces for flexible diaphragm (FEMA 274).**

At the plan center of the diaphragm, the in-plane deflection due to shearing deformation is:

$$q_2(t) = \frac{1}{A'G_{eff}} \int_0^{L/2} \left[ \int_0^x \mu(\xi)\ddot{u}(\xi,t)d\xi \right] dx \qquad \textbf{(10-22)}$$

**or**

$$q_2(t) = \frac{1}{A'G_{eff}} \int_0^{L/2} \int_0^x \mu(\xi)\{\ddot{q}_1(t) + \Psi(\xi)[\ddot{q}_2(t)]\}d\xi dx \qquad \textbf{(10-23)}$$

Evaluation of this integral gives

$$q_2(t) = \frac{\mu L^2}{8A'G_{eff}}\left[\ddot{q}_1(t) + \left(\frac{4\pi - 8}{\pi^2}\right)\ddot{q}_2(t)\right] \quad \textbf{(10-24)}$$

**or**

$$q_2(t) = \frac{\mu L^2}{8A'G_{eff}}\left[\ddot{q}_1(t) + 0.463 \cdot \ddot{q}_2(t)\right] \quad \textbf{(10-25)}$$

Using measured spectral values of displacement and acceleration at the plan center and at the ends of the diaphragm, the expression for $A'G_{eff}$ is

$$A'G_{eff} = \frac{\mu L^2}{8}\frac{\left(Sa_{q1} + 0.463 \cdot \left(Sa_{q2} - Sa_{q1}\right)\right)}{Sd_{q2}} \quad \textbf{(10-26)}$$

For Test 3 of Specimen #1, $Sa_{q1} = 0.74g$, $Sa_{q2} = 1.6g$ and $Sd_{q2} = 0.12\ in$. Thus,

$$A'G_{eff} = 1300\ kip \quad \textbf{(10-27)}$$

That value for $A'G_{eff}$ was then substituted into $K^*_2$ (Equation 10-17).

Using the mass and stiffness values summarized in Table 10-7, calculated spectral responses were close to those measured. The analysis calculated a fundamental frequency of response, 10.5 Hz, within 25% of the observed value of 14 Hz. The 5% damped spectral acceleration of the Test 3 transverse input motion at 10.5 Hz,1.5*g*, is approximately equal to the measured transverse spectral response of Specimen #1 during Test 3, 1.6*g*. Table 10-8 summarizes the calculated and measured spectral responses.

**Table 10-7. DOF mass and stiffness values used for RSA (Specimen #1).**

| Degree of Freedom | Mass | Stiffness |
|---|---|---|
| $q_1$ - Shear Walls | 2100 lb (force) | 320,000 lb / in. |
| $q_2$ - Diaphragm | 2050 lb (force) | 24,000 lb / in. |

**Table 10-8. Measured and calculated spectral responses (Specimen #1, Test 3).**

| Model | Fundamental Frequency | Diaphragm Acceleration, *Sa* | Diaphragm Deflection, *Sd* |
|---|---|---|---|
| Measured | 14 Hz (0.07 sec) | 1.6*g* | 0.120 in. |
| 2-DOF RSA | 10.5 Hz (0.097 sec) | $Sa_1$ = 1.5*g* | 0.148 in. |
| Refined FEM | 12 Hz (0.08 sec) | 1.8*g* | 0.128 in. |
| Original FEM | 25 Hz (0.04 sec) | 1.1*g* | 0.020 in. |

The diaphragm shear and the overall base shear (Table 10-9) calculated by the RSA are in general agreement with the values calculated by FEM models (Section 10.2 ).

**Table 10-9. Calculated seismic shears (Specimen #1, Test 3).**

| Model | Diaphragm Shear | Overall Base Shear |
|---|---|---|
| Refined FEM | 2500 lb | 3600 lb |
| 2-DOF | 3200 lb | 3700 lb |

### 10.3.3 Response Spectrum Analysis of Generalized Specimen #2 (metal diaphragm)

The expressions for $M^*_1$, $M^*_2$, $K^*_1$ were readily evaluated using:

- known dimensions of the half-scale specimen;
- measured elastic modulus E masonry used in the half-scale specimen;
- estimated shearing modulus G of masonry used in half-scale specimen, taken as 0.40E (FEMA 1997a); and
- estimated values of unit mass for the masonry and steel components.

Evaluation of $K^*_2$ (Equation 10-17) required an estimate of the in-plane shearing rigidity ($A'G$) of the diaphragm. This is the inverse of flexibility, which derives from several mechanisms:

- in-plane shearing deformation of metal deck;
- in-plane flexural deformation of the diaphragm assembly (metal deck and masonry chords);
- broadening and narrowing of deck deformations;

- out-of-plane buckling deformation of metal deck panels;
- local deformation at weld points;
- local deformation and slip at side-lap screws; and
- slip at OWJ-to-masonry interface.

To skirt the difficulty of predicting an accurate shearing stiffness for the metal diaphragm, the effective shearing rigidity $A'G_{eff}$ of the half-scale diaphragm was derived empirically from the experimental data using the same technique developed in Section 10.3.2 of this report.

Recall Equation 10-24:

$$A'G_{eff} = \frac{\mu L^2}{8}\frac{\left(Sa_{q1} + 0.463 \cdot \left(Sa_{q2} - Sa_{q1}\right)\right)}{Sd_{q2}}$$

For Test 5 of Specimen #2, $Sa_{q1} = 0.62g$, $Sa_{q2} = 1.2g$ and $Sd_{q2} = 0.12\ in.$ Thus,

$$A'G_{eff} = 610\ kip \qquad \textbf{(10-28)}$$

The value for $A'G_{eff}$ was then substituted into $K^*_2$ (Equation 10-17). It is interesting to note that $A'G_{eff}$ is about equal to the same quantity calculated using the actual cross-sectional area of the diaphragm, $A$, and the estimated shear modulus $G_{effective}$ of 333 ksi (discussed in Section 10.2.2 of this report).

$$\begin{aligned} A \cdot G_{effective} &= 333\ ksi \cdot B \cdot t_d \\ &= 333\ ksi \cdot 56\ in. \cdot 0.030\ in. \\ &= 560\ kip \end{aligned} \qquad \textbf{(10-29)}$$

RSA using the mass and stiffness values summarized in Table 10-10 calculated spectral responses close to those measured. The analysis calculated a fundamental frequency of response, 9.3 Hz, within 25% of that observed, 12 Hz. The 5% damped spectral acceleration for the Test 5 transverse input motion at 9.3 Hz, 1.14*g*, is approximately equal to that measured during Seismic Test 5 of Specimen #2, 1.2*g*. Table 10-11 summarizes the calculated and the measured spectral responses.

**Table 10-10. DOF mass and stiffness values used for RSA (Specimen #2).**

| Degree of Freedom | Mass | Stiffness |
|---|---|---|
| $q_1$ - Shear Walls | 2150 lb (force) | 460,000 lb / in. |
| $q_2$ - Diaphragm | 2050 lb (force) | 19,000 lb / in. |

**Table 10-11. Measured and calculated spectral responses (Specimen #2, Test 5).**

| Model | Fundamental Frequency | Diaphragm Acceleration, *Sa* | Diaphragm Deflection, *Sd* |
|---|---|---|---|
| Measured | 12 Hz (0.083 sec) | 1.2*g* | 0.120 in. |
| 2-DOF RSA | 9.3 Hz (0.11 sec) | $S_a$ = 1.14*g* | 0.134 in. |
| Refined FEM | 10 Hz (0.10 sec) | 1.2*g* | 0.115 in. |
| Original FEM | 20 Hz (0.05 sec) | 0.60*g* | 0.012 in. |

In this case, the diaphragm reaction shear and the overall base shear (Table 10-12) calculated by RSA do not agree well with the shears calculated by the Refined FEM model.

**Table 10-12. Calculated seismic shears (Specimen #2, Test 5).**

| Model | Diaphragm Shear | Overall Base Shear |
|---|---|---|
| Refined FEM | 1200 lb | 1600 lb |
| 2-DOF | 2400 lb | 2700 lb |

### 10.3.4 Sensitivity of Results From Spectral Analysis

The accuracy of the spectral response depends on the accuracy with which the mass and stiffness associated with degrees of freedom $q_1$ and $q_1$ can be approximated. The sensitivity of the results to errors in these approximations is now discussed.

To arrive at general expressions for the spectral response of a 2-DOF system, it is useful to consider the ratios of the generalized stiffness and mass corresponding to the degrees of freedom $q_1$ and $q_1$:

$$\alpha \equiv \frac{K^*_2}{K^*_1} = \frac{k_{diaphragm}}{k_{walls}} \qquad \text{(10-30)}$$

$$\beta \equiv \frac{M^*_2}{M^*_1} = \frac{m_{diaphragm}}{m_{walls}}$$

The governing equation of motion for an undamped MDOF system is

$$\underline{\mathbf{M}}\,\ddot{u} + \underline{\mathbf{K}}\,u = \underline{\mathbf{0}} \qquad \textbf{(10-31)}$$

For the generalized 2-DOF system representing the half-scale specimens, the stiffness matrix is

$$\underline{\mathbf{K}} = \begin{bmatrix} \left(k_{walls} + k_{diaph}\right) & -k_{diaph} \\ -k_{diaph} & k_{diaph} \end{bmatrix} \qquad \textbf{(10-32)}$$

or

$$\underline{\mathbf{K}} = \begin{bmatrix} \left(1/\alpha + 1\right) & -1 \\ -1 & 1 \end{bmatrix} \cdot \alpha \cdot k_{walls} \qquad \textbf{(10-33)}$$

and the mass matrix is

$$\underline{\mathbf{M}} = \begin{bmatrix} m_{walls} & 0 \\ 0 & m_{diaph} \end{bmatrix} \qquad \textbf{(10-34)}$$

or

$$\underline{\mathbf{M}} = \begin{bmatrix} 1/\beta & 0 \\ 0 & 1 \end{bmatrix} \cdot \beta \cdot m_{walls} \qquad \textbf{(10-35)}$$

In Section 9, it is shown that the fundamental mode dominates the dynamic response of the buildings addressed in this report. For that reason, this analysis considers only that mode.

The fundamental frequency is:

$$\omega_1 = \gamma \sqrt{\frac{k_{walls}}{m_{walls}}} \qquad \textbf{(10-36)}$$

Where $\gamma$ can be considered a "frequency modification factor,"

$$\gamma = \sqrt{\frac{1}{2\beta}\left[\beta + \alpha\beta + \alpha + \left(\beta^2 + 2\alpha\beta^2 - 2\alpha\beta + \alpha^2\beta^2 + 2\alpha^2\beta + \alpha^2\right)^{1/2}\right]} \qquad \textbf{(10-37)}$$

The corresponding fundamental eigenvector of the 2-DOF system is

$$\Phi_1 = \begin{Bmatrix} \phi_{21} \\ \phi_{11} \end{Bmatrix} \tag{10-38}$$

After arbitrarily assigning the diaphragm DOF a modal amplitude, $\phi_{21}$ = 1.0, the modal amplitude for the shear-wall DOF, $\phi_{11}$ , is

$$\phi_{11} = \frac{\alpha - \gamma^2 \beta}{\alpha} \tag{10-39}$$

Substitution into the fundamental eigenvector gives

$$\Phi_1 = \begin{Bmatrix} 1.0 \\ \\ \dfrac{\alpha - \gamma^2 \beta}{\alpha} \end{Bmatrix} \tag{10-40}$$

The modal participation vector, *s*, for the fundamental mode of response, is defined as

$$s = \Gamma_1 \cdot \underline{\mathbf{M}} \cdot \Phi_1 \tag{10-41}$$

Where the modal excitation factor is,

$$\Gamma_1 = \frac{\sum_{j=1}^{2} (M_{j,j} \cdot \phi_{j,1})}{\Phi_1^{\,T} \cdot \underline{\mathbf{M}} \cdot \Phi_1} \tag{10-42}$$

The degree-of-freedom participation factors $s_1$ and $s_2$, associated with the walls and diaphragm degrees of freedom, are defined as

$$s_1 = s_{walls} = m_{walls} \cdot \phi_{11} \cdot \frac{\phi_{11} + \beta}{\phi_{11}^{\,2} + \beta} \tag{10-43}$$

$$s_2 = s_{diaphragm} = m_{walls} \cdot \beta \cdot \frac{\phi_{11} + \beta}{\phi_{11}^{\,2} + \beta} \tag{10-44}$$

The equivalent lateral inertial forces for a 2-DOF system, considering the fundamental mode of response, are:

$$f_{walls} = s_{walls} \cdot S_{a1} \quad \textbf{(10-45)}$$

$$f_{diaphragm} = s_{diaphragm} \cdot S_{a1} \quad \textbf{(10-46)}$$

Where $S_{a1}$ is the spectral acceleration ordinate at the fundamental frequency. The shears are therefore:

$$V_{diaphragm} = s_{diaphragm} \cdot S_{a1} \quad \textbf{(10-47)}$$

$$V_{walls} = s_{walls} \cdot S_{a1} + s_{diaphragm} \cdot S_{a1} \quad \textbf{(10-48)}$$

The sensitivity of these expressions over a range of DOF mass and stiffness ratios can now be evaluated. It is further instructive, however, to determine over what range those ratios should be considered. Flexible roof diaphragms are usually less stiff than the walls supporting them. Therefore, in practical terms, the diaphragm-to-wall stiffness ratio, $\alpha$, is less than unity. To see this, consider the ratio of the stiffness of the diaphragm to that of the walls.

$$\frac{k_{diaphragm}}{k_{walls}} \approx \frac{K^*_2}{K^*_{S1}} = \frac{\dfrac{A' G_{diaph} \pi^2}{2L}}{\dfrac{A' G_{walls} \pi^2}{8H}} \approx \frac{4H}{L} \frac{t_{diaph}}{t_{walls}} \frac{G_{diaph}}{G_{walls}} < 1 \quad \textbf{(10-49)}$$

The diaphragm-to-wall mass ratio, $\beta$, can vary over a larger range, however, as it depends on architectural as well as structural considerations. A practical lower limit for the mass ratio is taken, in this report, as 0.5 and the upper limit as 2.0. Thus, the behaviors of the modal participation factors, $s_1$ and $s_2$, and the frequency modification factor $\gamma$ (Equations 10-43, 10-44, and 10-37) are examined over the range of $0 < \alpha < 1.0$ and $0.5 < \beta < 2.0$. For simplicity, the participation factors are normalized by the mass associated with the wall degree of freedom, $m_{walls}$, in Figure 10.26, Figure 10.27, Figure 10.28, and Figure 10.29.

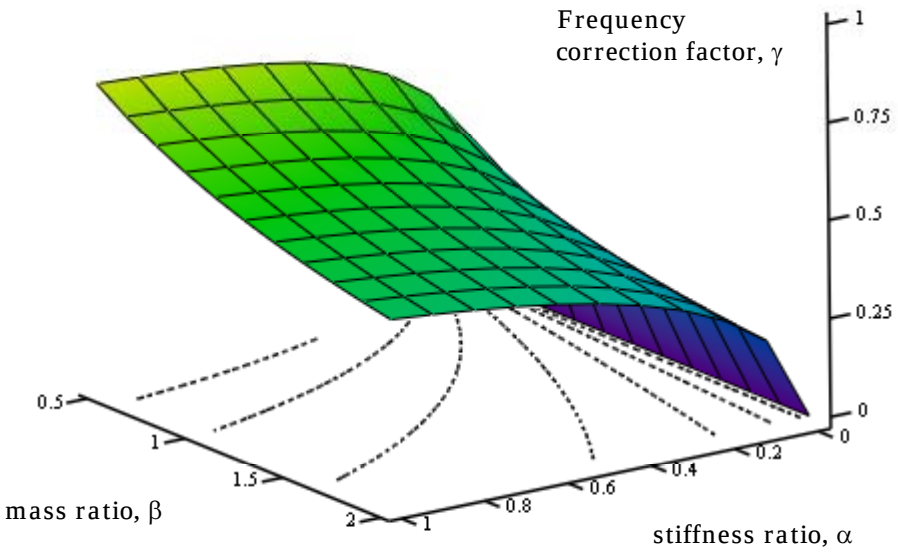


**Figure 10.26. Fundamental frequency modification factor; dashed lines are contours.**

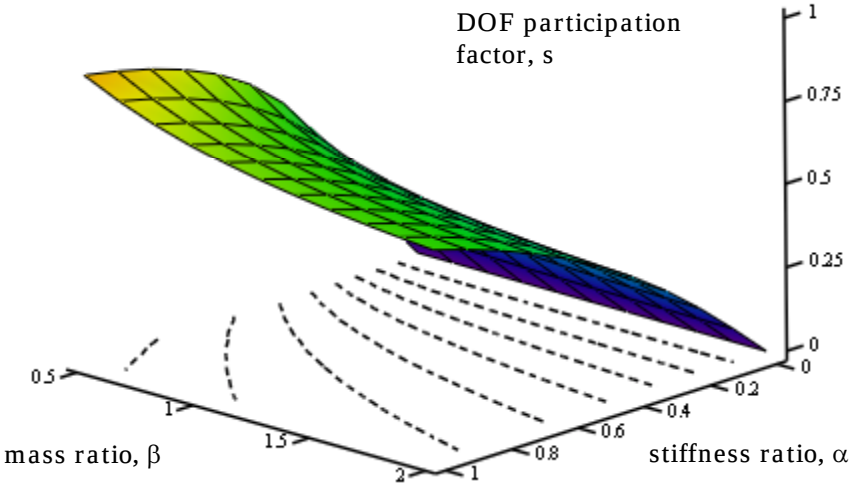


**Figure 10.27. Shear walls DOF participation factor normalized by shear-wall DOF mass; dashed lines are contours.**

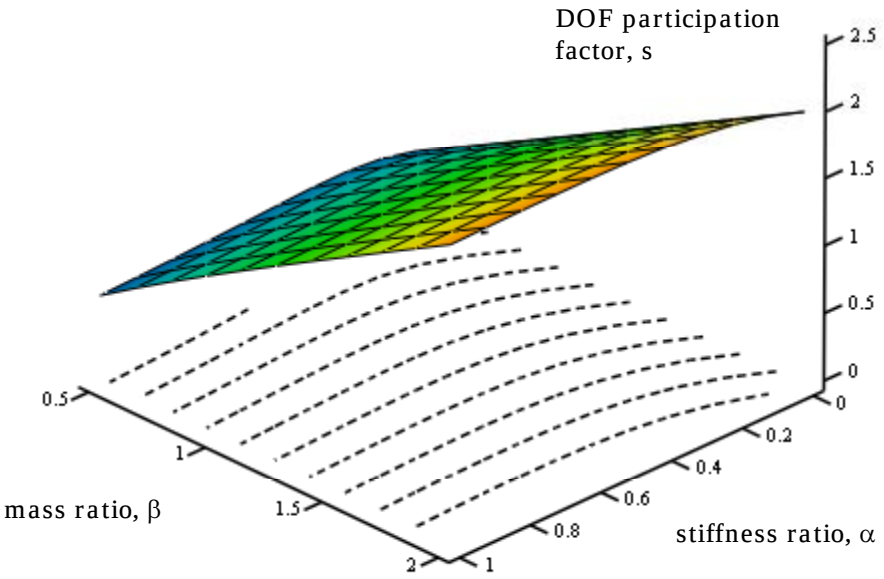


**Figure 10.28. Diaphragm DOF participation factor normalized by shear-wall DOF mass; dashed lines are contours.**

Figure 10.26, Figure 10.27, and Figure 10.28 illustrate that the expressions for the frequency correction factor, $\gamma$, and the degree-of-freedom participation factors, *s*, are smooth in the range of expected input values. Furthermore, the surfaces do not have strong or unexpected rates of change.

Figure 10.26, describing the frequency correction factor, $\gamma$ (Equation 10-37), depends on the DOF ratios, $\alpha$ and $\beta$. The stiffness of flexible diaphragms, and thus the diaphragm degree of freedom, cannot currently be well modeled. Consequently, the DOF stiffness ratio $\alpha$ is not accurate, the frequency correction factor is thus not accurate; therefore, the fundamental frequency of the system cannot be accurately estimated. Nevertheless, accurate knowledge of the fundamental frequency is not critical to the seismic design of these structures, for two reasons:

1. The frequency modification factor $\gamma$ (Equation 10-37) is less than unity within the limits defined above (Figure 10.26). Application of this factor could only decrease the calculated frequency. Smoothed design spectra, for example in Figure 10.1, generally decrease with frequencies greater than those defining the region of constant acceleration. Thus, neglecting the frequency modification factor in design is conservative.

2. Typically, fundamental frequencies of low-rise masonry buildings lie in the "constant acceleration" region of smoothed design spectra. This is reflected in the *Simplified Design* procedures outlined in IBC-2000 Section 1617.5.

Modifying the fundamental frequency of the structure using the frequency correction factor would not likely alter the design spectral acceleration and thus not the applied seismic design forces.

In response spectrum analysis, the pseudo-spectral displacements $S_d$ are inversely proportional to the square of the frequency. Therefore, a conservative (high) estimate of the fundamental frequency would not generate a conservative (low) estimate of the pseudo-spectral displacement, $S_d$. Future research should address this need for a quick and accurate method for the prediction of seismic spectral displacements of flexible diaphragms, excited in-plane.

Figure 10.27 depends primarily on the DOF stiffness ratio $\alpha$. The figure is not very sensitive to variation in DOF mass ratio, $\beta$. As mentioned, the DOF stiffness ratio $\alpha$ is not accurate. Therefore, the participation of the shear walls degree of freedom to the dynamic response of the system is also not accurate. Design and proportioning of these shear walls is generally governed by prescriptive reinforcement requirements or design for out-of-plane wind loads, and not by applied seismic design loads. Therefore, accurate knowledge of the participation of the shear wall degree of freedom is not critical to the seismic design of such structures.

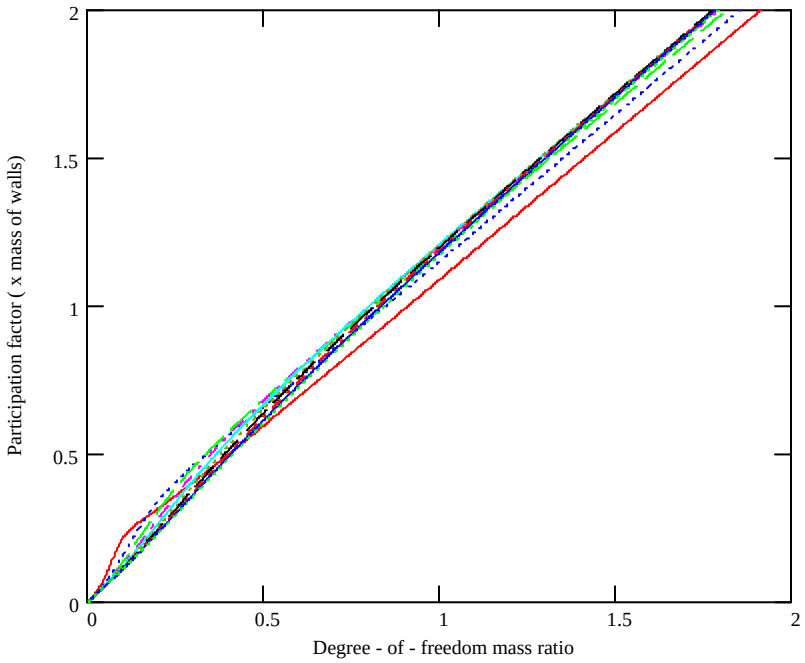


**Figure 10.29. Multiple slices through Figure 10.28 at $\alpha$ = 0.1, 0.2 . . . 1.0.**

Figure 10.28 and Figure 10.29 show that for any stiffness ratio, the DOF participation factor increases linearly with the mass ratio, $\beta$. In fact, Figure 10.29 shows that the slope of that relationship is close to unity, and the DOF participation factor is almost exactly equal to the DOF mass ratio, $\beta$. Thus,

$$\beta = \frac{m_{diaphragm}}{m_{walls}} \approx \frac{s_{diaphragm}}{m_{walls}} \quad \textbf{(10-50)}$$

or

$$s_{diaphragm} \approx m_{diaphragm} \quad \textbf{(10-51)}$$

Accurate approximation of the mass associated with the diaphragm is outlined in Section 10.3 of this report. Equation 10-51 implies that the structure behaves as a single-degree-of-freedom system. That single degree of freedom, however, corresponds with the in-plane transverse response of the diaphragm and the associated out-of-plane response of the longitudinal walls, and not the in-plane response of the shear walls, as is often assumed in design.

# 11 Implications of Scaling

In order to arrive at meaningful conclusions and recommendations regarding the behavior, analysis and design of low-rise masonry buildings with flexible roof diaphragms, the implications of geometric scaling need to be examined. In particular, those implications provide a bridge between observations regarding response of the half-scale specimens studied here and the expected behavior of full-scale prototype structures. The half-scale models embodied some limitations, which resulted from the scaling process. Those limitations are now discussed and evaluated using geometric scaling analysis.

It was shown in Section 5.2 of this report that the relationship between the natural circular frequency of a half-scale specimen and that of its prototype is:

$$\frac{\omega_{model}}{\omega_{prototype}} \propto \frac{1}{\alpha} \qquad \textbf{(11-1)}$$

The relationship between the stiffness of the specimen and that of the prototype is:

$$\frac{K_{model}}{K_{prototype}} \propto \frac{G_m A_m / L_m}{G_p A_p / L_p} = \frac{G_p A_p \alpha^2 / L_p \alpha}{G_p A_p / L_p} = \alpha \qquad \textbf{(11-2)}$$

where,

$G$ = shear modulus

$A$ = measure of in-plane area

$L$ = measure of length

The scaled input record had ordinates (acceleration values) identical to those of the prototype record. The time scale of the prototype input record was multiplied by the scaling factor, $\alpha$, to preserve the relationship between the natural frequencies of the specimen and the spectral peaks, *Sa*, of the input motion.

Thus,

$$\frac{Sa_{model}}{Sa_{prototype}} = 1 \tag{11-3}$$

The relationship between the pseudo-displacement, *Sd*, of the specimen and that of the prototype is therefore:

$$\frac{Sd_{model}}{Sd_{prototype}} \propto \frac{\frac{Sa_m}{\omega_m^2}}{\frac{Sa_p}{\omega^2{}_p}} = \alpha^2 \tag{11-4}$$

The relationship between the pseudo-displacement, *Sd*, the stiffness, *K*, and the effective lateral force, *F*, is:

$$F \propto K \cdot Sd \tag{11-5}$$

Thus,

$$\frac{F_{model}}{F_{prototype}} = \alpha^3 \tag{11-6}$$

The relationship between the average internal, in-plane shear stress in the walls of the specimen and those in the prototype is:

$$\frac{\tau_{model}}{\tau_{prototype}} \propto \frac{F_m / A'_m}{F_p / A'_p} = \frac{F_p \alpha^3 / A'_p \alpha^2}{F_p / A'_p} = \alpha \tag{11-7}$$

where $A'$ is the effective shear area of the transverse shear walls. Similarly, the relationship between the flexural stresses due to out-of-plane bending in the walls is:

$$\frac{\sigma_{model}}{\sigma_{prototype}} \propto \frac{F_m L_m t_m / I_m}{F_p L_p t_p / I_p} = \frac{F_p \alpha^3 L_p t_p \alpha^2 / I_p \alpha^4}{F_p L_p t_p / I_p} = \alpha \tag{11-8}$$

where,

$L$ = measure of length of the walls

$t$ = thickness of the walls

$I$ = out-of-plane moment of inertia of the walls

Finally, the relationship between the lateral drifts (due to shearing deformations) in the specimen and those in the prototype is:

$$\frac{\delta_{model}}{\delta_{prototype}} \propto \frac{\dfrac{F_m}{A'_m / L_m}}{\dfrac{F_p}{A'_p / L_p}} = \frac{\dfrac{F_p \alpha^3}{A'_p \alpha^2 / L_p \alpha}}{\dfrac{F_p}{A'_p / L_p}} = \alpha^2 \qquad \textbf{(11-9)}$$

The same relationship can be derived considering flexural deformations.

In this case, the geometric scaling factor $\alpha$ equals 1/2. Therefore, for a given ground motion in the appropriate time scale:

- the effective inertial forces on the half-scale specimen are one-eighth those that would exist in the prototype structure (Equation 11-5);
- the in-plane shear stresses in the transverse shear walls of the half-scale specimen are one-half those that would exist in the prototype structure (Equation 11-6);
- the flexural stresses from out-of-plane bending in the longitudinal walls of the half-scale specimen are one-half those that would exist in the prototype structure (Equation 11-7); and
- the drifts in the half-scale specimen are one-quarter those that would occur in the prototype structure (Equation 11-8).

This dimensional analysis proves that the prototype structures would have sustained higher levels of damage than the half-scale specimens under the same level of excitation. For a given ground motion in the appropriate time scale, stresses in the prototype structures would have been twice as large, and drifts

four times as large, as in the half-scale specimens. The additional damage would have likely been in the form of additional cracking along yield lines, and increased damage to the roof diaphragms.

Practical constraints prevented complete similitude between the half-scale specimens and the full-scale prototype structures. For instance, it was impractical to provide similitude between scale and prototype material properties. At small scales, a lack of similitude can result in distinct differences between scale and prototype responses. This study scaled by only one-half, however. In addition to the relatively large scale of the test specimens, observed behavioral characteristics, such as the tendency of the roof diaphragm to respond independently of the transverse shear walls, were quite pronounced and would significantly change only at very high levels of scaling. Thus, the lack of similitude between scale and prototype material properties did not significantly affect the results of the study, and conclusions regarding the response behavior of the half-scale specimens remain valid for the full-scale prototype structures.

# 12 Significance of Results

## 12.1 Behavior

The half-scale specimens studied here did not behave as systems with a single-degree-of-freedom associated with the in-plane response of the shear walls. The longitudinal walls responded predominantly out-of-plane, and confirmed the expected effects of in-plane diaphragm flexibility under transverse excitation. The half-scale specimens remained essentially elastic during the maximum expected earthquakes (PGA = 0.67*g* transverse, PGA = 0.50*g* longitudinal). Geometric scaling analysis proves that the full-scale structures would have sustained more damage.

## 12.2 Analytical Modeling Techniques

The half-scale specimens were analytically modeled using three different procedures:

1. linear-elastic FEM analysis using first assumed and then refined material and dimensional parameters;

2. equivalent two-degree-of-freedom idealizations of the half-scale specimens and response spectrum analyses of those idealizations; and

3. a typical seismic design analysis as outlined in the IBC-2000.

Each analytical method embodied both strengths and limitations. The FEM models accurately calculated the response of the half-scale specimens. Those models were robust, with respect to assumed diaphragm thickness and assumed equivalent viscous damping value, in their prediction of spectral responses. The FEM modeling corroborated the measured response and justified its use for the dynamic analyses of the types of structures addressed in this report. The modeling required a considerably larger amount of time for model development and analysis than that required by techniques typically used in design.

The second method, response spectrum analyses of the 2-DOF generalizations, calculated responses close to the measured responses. The RSA corroborated the results of the FEM models and thus justified its use for the dynamic analysis of these types of structures. The method required empirical approximation of the diaphragm stiffness, however. Discussion of the technique's sensitivity to changes in the degrees of freedom mass and stiffness values demonstrated that the buildings represented in this report could in fact be accurately modeled as single-degree-of-freedom systems if that degree of freedom was associated with the in-plane, transverse response of the diaphragm.

By comparison, the Simplified Analysis procedure outlined in the IBC-2000 did not provide sufficient guidance for the distribution of the overall design base shear to the diaphragm and the supporting walls or for the determination of in-plane diaphragm deflections.

## 12.3 *Evaluation* of Damage

### 12.3.1 Specimen #1 (lumber diaphragm)

The specimen was ultimately subjected to over 1.0*g* of longitudinal table acceleration and over 1.3*g* of transverse table acceleration. The masonry walls sustained damage in the form of yield lines and flexural bed-joint cracks. Cracks formed primarily during transverse excitation. The diaphragm sustained damage in the form of cracking of the sheathing lumber and pullout of nails during strong transverse excitation.

The specimen was moderately damaged. For example, it would be categorized at a Grade 2 to Grade 3 level of damage under the European Macroseismic Scale (EMS) (Tomazevic 1999, EMS-98). The walls sustained extensive but not destructive cracking, and the roof diaphragm sustained slight structural damage. More specific classification under the EMS would require non-structural component evaluation that this testing did not provide.

Although the FEMA 306 document, *Evaluation of Earthquake Damaged Concrete and Masonry Wall Buildings* (FEMA 1998), does not explicitly consider the out-of-plane behavior of reinforced masonry walls, that document does discuss the following related topics:

- out-of-plane flexural behavior of unreinforced masonry walls;
- out-of-plane flexural behavior of masonry infills; and

- potential out-of-plane damage to masonry walls from flexible diaphragms of inadequate in-plane strength, stiffness, or both.

The primary cracks in the longitudinal walls of the specimen developed during strong transverse excitation as a result of diaphragm flexibility and out-of-plane dynamic loads normal to the surface. It could be concluded that the test specimen was moderately damaged according to FEMA 306 criteria.

### 12.3.2 Specimen #2

The specimen was ultimately subjected to over 1.5*g* of longitudinal table acceleration and over 1.3*g* of transverse table acceleration. The masonry walls sustained damage in the form of yield lines and shear cracks. Cracks formed primarily during transverse excitation. The diaphragm sustained damage in the form of pullout of side-lap screws and brittle fracture of puddle welds. The puddle welds fractured primarily during longitudinal excitation.

Specimen #2 was moderately damaged according to the same criteria used in the damage evaluation of Specimen #1.

# 13 Summary, Conclusions and Recommendations

## 13.1 Summary

Researchers at the University of Texas at Austin and engineers and staff at the CERL successfully developed, constructed, and tested two one-half scale low-rise masonry buildings with flexible roof diaphragms. One specimen had a diagonally sheathed lumber diaphragm on lumber roof joists. The other specimen had a light-gauge, wide-rib, corrugated metal-deck diaphragm on open-web steel joists. The half-scale specimens emulated design and construction practices typical for the US Army's facilities in the central United States prior to 1960.

The CERL Tri-axial Earthquake and Shock Simulator subjected each half-scale specimen to a suite of carefully selected ground motions. Instrumentation of the specimens captured their dynamic response. Damage to the specimens during testing was detected using white-noise excitation and visual observation. Published criteria were used to evaluate the resulting damage states of the specimens.

Evaluation of the data collected during seismic testing of the specimens provided information regarding dynamic response, including;

- in-plane deformation of the roof diaphragm and the masonry walls;
- displacement response of the roof diaphragm;
- acceleration response of the masonry walls and the roof diaphragm; and
- rocking behavior of the transverse shear walls.

Analytical models of the specimens were developed and evaluated. Three-dimensional, linear elastic finite models of the half-scale specimens provided a comparison to the measured response. Generalized 2-DOF idealizations and response spectrum analysis of those idealizations provided a second comparison to the measured response and outlined a possible simplified design procedure for

these types of structures. The sensitivity of analytical results to variation in different assumptions was also assessed.

Comparison of responses from shaking-table testing and analytical predictions, evaluated in the context of geometric scaling, provided a coherent description of the seismic response of low-rise masonry structures with flexible roof diaphragms.

## 13.2 Conclusions

1. Shaking-table testing of half-scale specimens gave results that were useful in predicting full-scale prototype response.

2. The half-scale specimens were moderately damaged. Their masonry walls sustained damage in the form of yield lines, bed-joint cracks characteristic of rocking, and shear cracking. The lumber diaphragm of Specimen #1 was lightly damaged, sustaining nailing-point splitting and some splitting parallel to the grain. The metal deck diaphragm of Specimen #2 was moderately damaged, sustaining fracture of puddle weld and pullout of side-lap screws. The diaphragms deformed primarily in shear.

3. Seismic damage in walled structures with flexible, horizontal diaphragms cannot be completely characterized by inter-story drift ratios of the walls. It also depends on the diaphragm drift ratio, defined here and correlated to diaphragm and wall damage.

4. Geometric scaling analysis proved that stresses in the full-scale prototype structures would have been twice as high as those in the half-scale specimens. Likewise, drifts in the prototype structures would have been four times greater than those in the half-scale specimens. The prototype structure would have sustained more damage than the half-scale specimens for the same level of excitation.

5. In contrast to what is usually assumed in design, the half-scale specimens did not behave as systems with a single-degree-of-freedom associated with the in-plane response of the shear walls. The in-plane, transverse response of the roof diaphragms and the associated out-of-plane, transverse response of the longitudinal walls confirmed the expected effects of roof diaphragm flexibility. Clearly, the in-plane, transverse response of the diaphragm and the associated out-of-plane, transverse response of the masonry walls play important roles in the seismic response of buildings represented by the test

specimens. The typical design methodology outlined in the IBC-2000 does not provide sufficient guidance for the seismic design of these types of structures.

6. Linear-elastic finite element models are robust, with respect to assumed diaphragm thickness and assumed equivalent viscous damping value, in their prediction of dynamic response of the half-scale specimens. Linear-elastic modeling is justified for the analysis of low-rise masonry buildings with flexible roof diaphragms.

7. Linear-elastic modeling can be simplified to a generalized 2-DOF idealization. Response-spectrum analysis of such an idealization is accurate and justified for prediction of dynamic response of the half-scale specimens, and a full-scale prototype.

8. Low-rise rectangular masonry buildings can be designed for seismic motion as single-degree-of-freedom systems, if that degree of freedom is associated with the in-plane, transverse response of the diaphragm, rather than that of the transverse shear walls. Accurate knowledge of the mass associated with the roof diaphragm is critical for determination of seismic actions in these structures. Accurate knowledge of the roof diaphragm stiffness is critical for determination of seismic drifts.

## 13.3 Recommendations for Implementation

The out-of-plane, transverse response of the masonry walls and the in-plane, transverse response of the diaphragm should be addressed in the seismic design of low-rise masonry structures. Current design codes allow designers to perform dynamic multi-degree-of-freedom analysis in lieu of single-degree-of-freedom equivalent lateral force procedures (IBC-2000 Section 1617 and 1618). The prototype specimen would generally be designed as a single-degree-of-freedom system, using the degree of freedom representing the in-plane response of the shear walls. Guidance does not currently exist regarding the design of low-rise masonry buildings with flexible roof diaphragms as multi-degree-of-freedom systems.

For transverse response of low-rise masonry buildings with flexible roof diaphragms, the degree of freedom selected for single-degree-of-freedom modeling should represent the in-plane, transverse response of the diaphragm and the associated out-of-plane, transverse response of the longitudinal masonry walls.

Accurate knowledge of the diaphragm stiffness is not essential to design for strength, as this would not likely alter the design spectral accelerations. The designer should use conservative assumptions (higher diaphragm flexibility) when estimating the in-plane diaphragm stiffness. This estimate strongly affects the predicted diaphragm deflections. The designer should determine the mass associated with the diaphragm using a rational method.

Shear deformations should be included when calculating the response of roof diaphragms.

Care should be taken in the assignment of masonry material properties, such as the elastic modulus $E$, during the analytical modeling of these types of structures, because these parameters strongly affect the calculated response of the structure. In contrast, acceptable agreement between calculated and measured spectral responses can be achieved using typical design properties and dimensions for the diaphragm. If rational analysis cannot determine diaphragm properties, the designer should assume properties that err in the direction of higher diaphragm flexibility.

## 13.4 Recommendations for Future Research

The recommendations for implementation in this report are generally limited by knowledge of the in-plane stiffness of the diaphragm. Future research should address the need for an accurate prediction of that stiffness, of in-plane diaphragm deflection, and of the associated out-of-plane deflections of the masonry walls. In particular, research on wood diaphragms should address the need for an effective shear modulus of lumber diaphragms, should determine the effect of nailing patterns on in-plane stiffness, and should indicate whether or not the masonry walls contribute to the stiffness or strength of diaphragm chords, and if so, to what extent. The seismic reliability and performance of diaphragm components and connecting elements should also be investigated. These topics need to be studied with respect to a wide range of typical low-rise masonry structures. The vulnerabilities of these buildings need to be identified. Mitigation and rehabilitation techniques need to be developed. Finally, the information gained ultimately needs to be disseminated and implemented.

# Appendix A: As-Built Drawings of Half-Scale Masonry Walls

- Reinforcement in masonry walls
- Reinforcement splices at corners and intersections
- Wall-to-lift girder connection

AS-BUILT REINFORCED MASONRY WALLS FOR
SPECIMEN #1 AND SPECIMEN #2
NTS

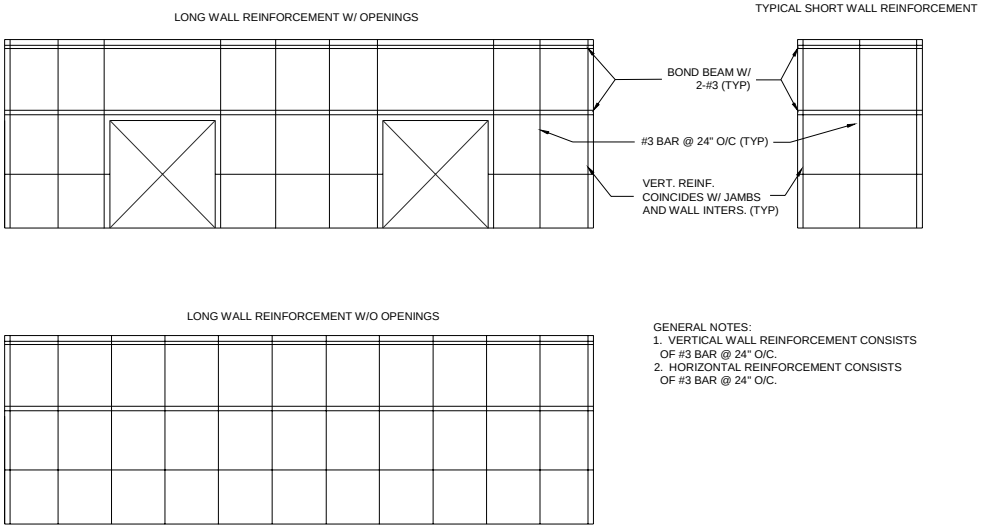

## REINFORCEMENT SPLICE AT CORNERS AND INTERSECTIONS

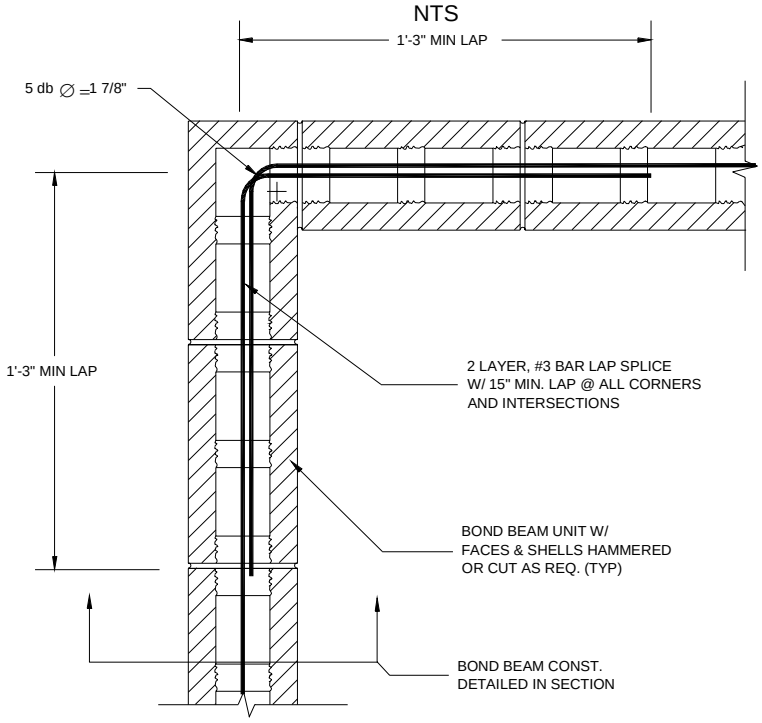


## WALL-TO-LIFT GIRDER CONNECTION

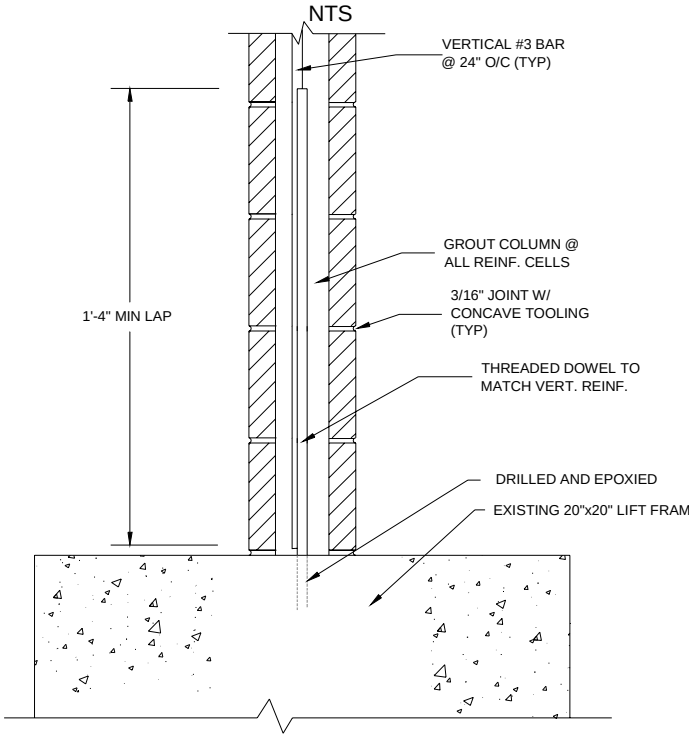

# Appendix B: As-Built Drawings of Half-Scale Specimen #1

- Roof diaphragm
- Rafter-to-wall connection
- Rafter-to-wall connection

AS-BUILT SPECIMEN #1 ROOF (LUMBER)

NTS

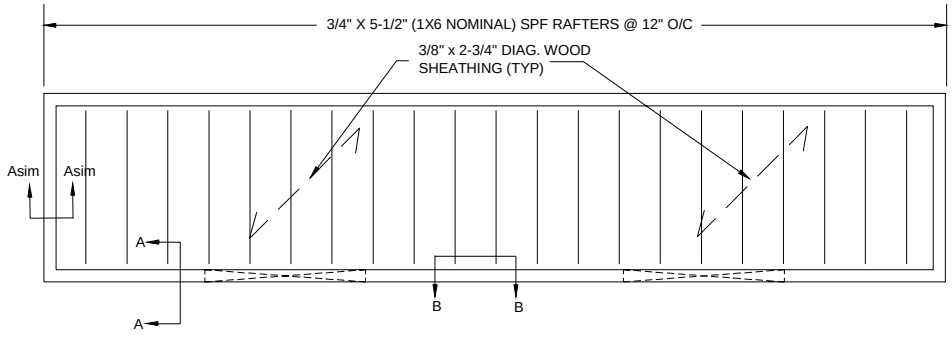


GENERAL NOTES:
1. ALL DIMENSIONAL LUMBER IS SPRUCE-PINE-FIR NO.1 OR NO.2 OR BETTER.
2. ALL LUMBER IS GENERALLY FREE OF DEFECTS AND IN A CONDITION SUITABLE FOR THE INTENDED USE.
3. ALL SPECIFIED FASTENERS ARE BE USED
4. SHEATHING IS IN A CONTROL-RANDOM LAYUP WITH A 12" MINIMUM STAGGER

## AS-BUILT TYPICAL SECTION A-A
## RAFTER-TO-WALL CONNECTION

NTS

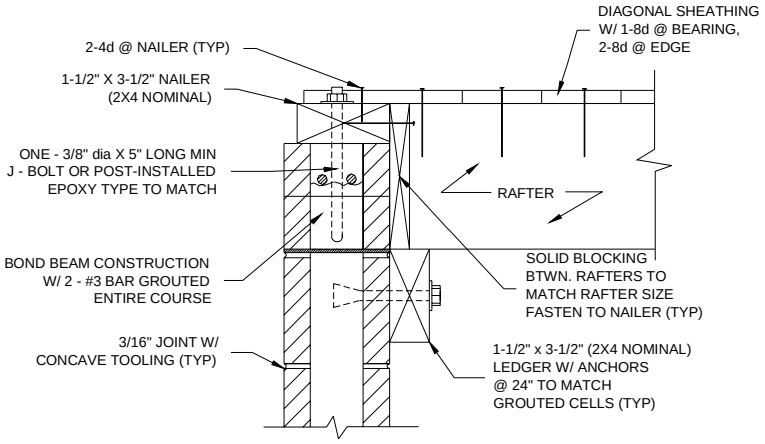


## AS-BUILT TYPICAL SECTION B-B
## RAFTER-TO-WALL CONNECTION

NTS

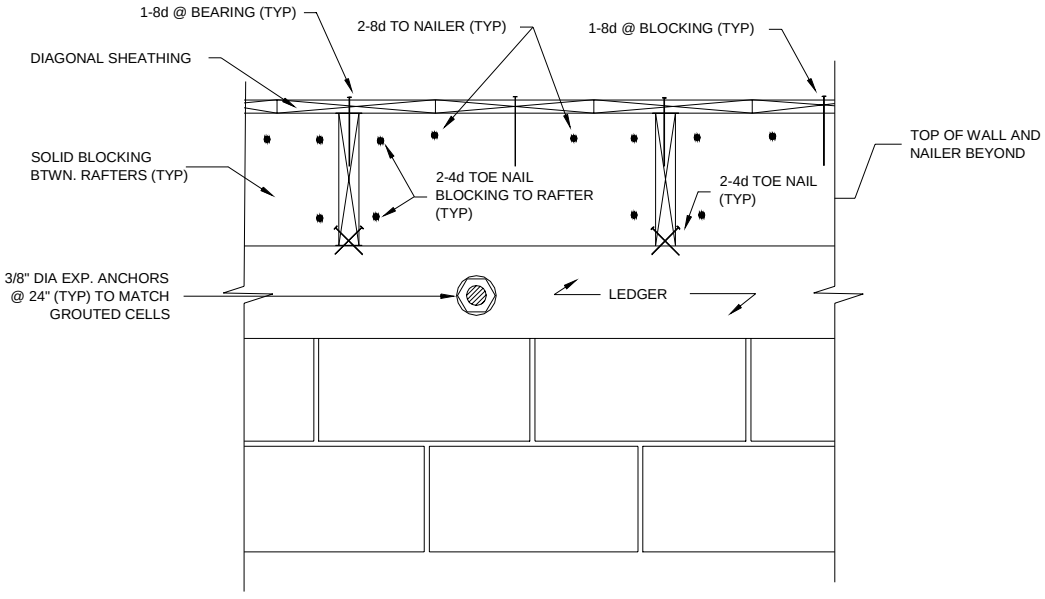

# Appendix C: As-Built Drawings of Half-Scale Specimen #2

- Roof diaphragm
- Horizontal bridging
- Joist-to-wall connection
- Joist-to-wall connection
- Horizontal bridging-to-wall connection

AS-BUILT SPECIMEN #2 ROOF (STEEL)
NTS

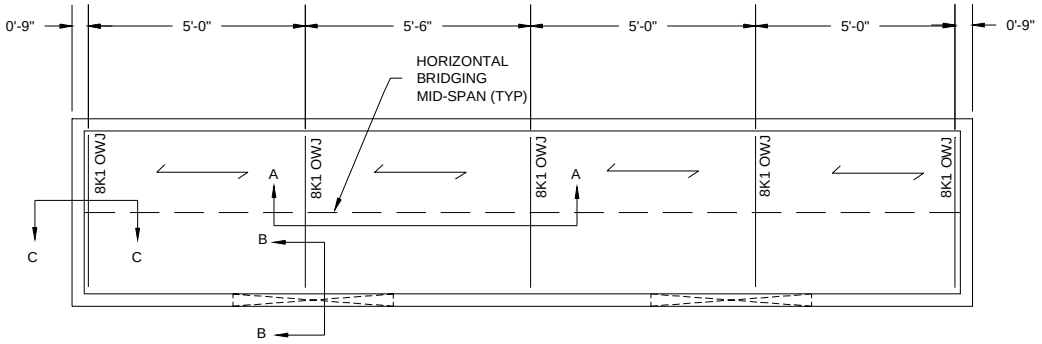


GENERAL NOTES:
1. ⟷ DENOTES SPAN OF 1-1/2" TYPE B METAL ROOF DECK AS MANUFACTURED BY VULCRAFT.
2. ROOF DECK IS FASTENED WITH AN EQUIVALENT 36/3 PUDDLE WELD PATTERN.
3. WELDING RODS ARE E60XX OR E70XX.
4. EACH SIDELAP HAS 1-10# TEK-SCREW PER SPAN.
5. STEEL BAR JOISTS ARE SIZE 8K1 AS MANUFACTURED BY VULCRAFT STEEL JOIST COMPANY.

AS-BUILT TYPICAL SECTION A-A
HORIZONTAL BRIDGING AT OWJ MID-SPAN

NTS

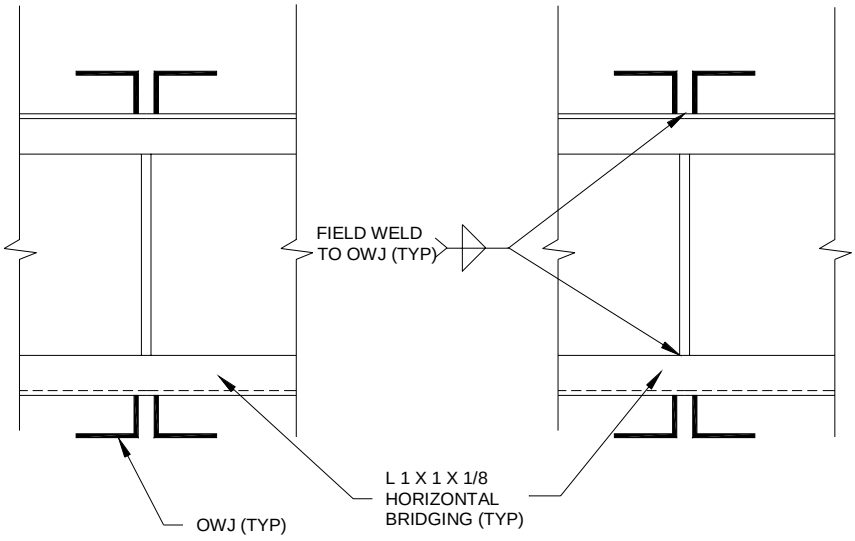


AS-BUILT TYPICAL SECTION B-B (TOP VIEW)
JOIST-TO-WALL CONNECTION

NTS

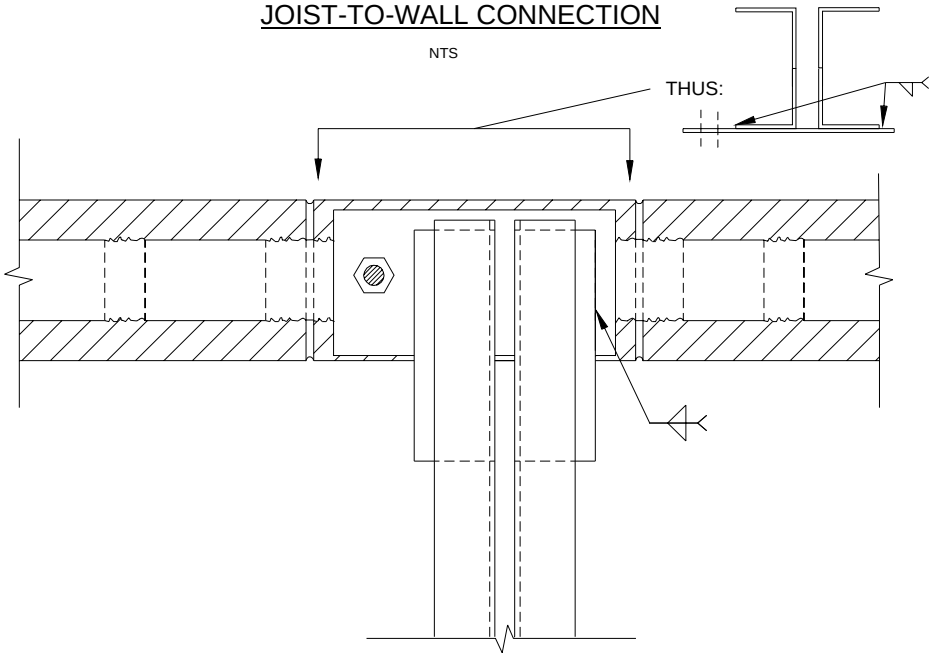

AS-BUILT TYPICAL SECTION B-B
JOIST-TO-WALL CONNECTION

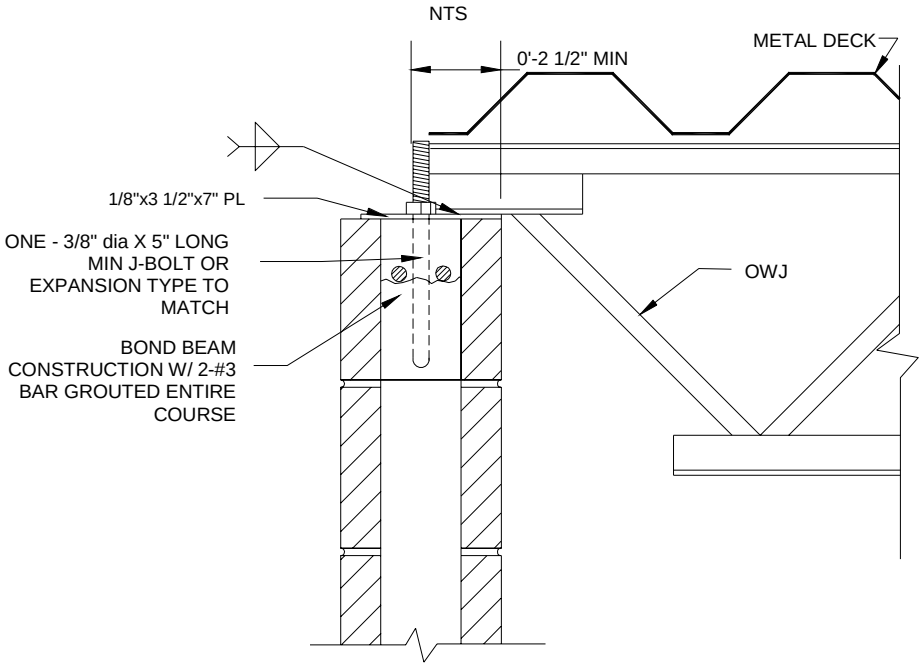


AS-BUILT TYPICAL SECTION C-C
HORIZONTAL BRIDGING TO CMU WALL

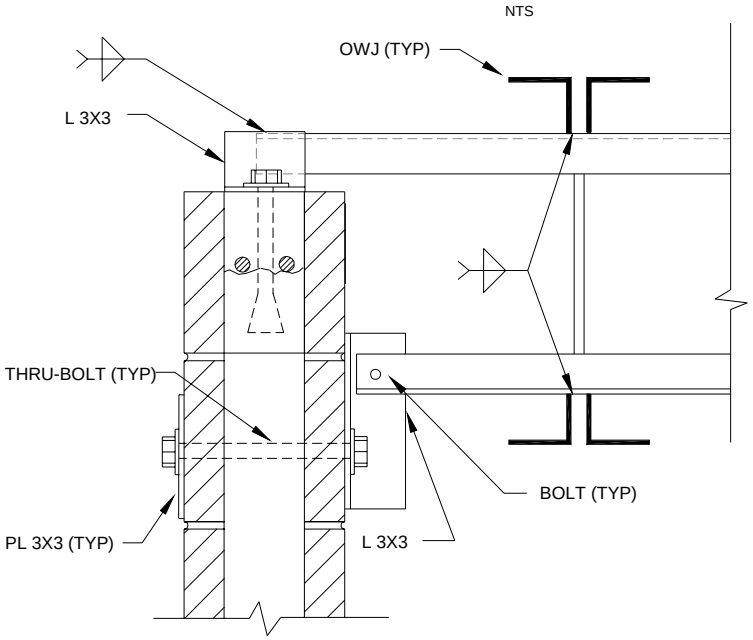

# References

ABK, A Joint Venture (1981), "Methodology for Mitigation of Seismic Hazards in Existing Unreinforced Masonry Buildings: Categorization of Buildings," *Topical Report ABK-TR-01,* El Segundo, CA.

ABK, A Joint Venture (1981), "Methodology for Mitigation of Seismic Hazards in Existing Unreinforced Masonry Buildings: Diaphragm Testing," *Topical Report ABK-TR-02*, El Segundo, CA.

ABK, A Joint Venture (1981), "Methodology for Mitigation of Seismic Hazards in Existing Unreinforced Masonry Buildings: Wall Testing, Out-of-plane," *Topical Report ABK-TR-03*, El Segundo, CA

Abrams, D., Paulson, T. (1991), "Modeling Earthquake Response of Concrete Masonry Building Structures," *ACI Structural Journal*, V. 88, No.4, 475-485

Applied Technology Council (1981), *Guidelines for the Design of Horizontal Wood Diaphragms,* Publication ATC-7, Berkeley, CA.

Blondet, M. and Mayes, R. L. (1991), "The Transverse Response of Clay Masonry Walls Subjected to Strong Motion Earthquakes – Volume 1: General Information," U.S.-Japan Coordinated Program for Masonry Building Research, *TCCMAR Report No. 3.2(b)-2*.

Bruneau, M. (1994), "State-of-the-Art Report on Seismic Performance of Unreinforced Masonry Buildings," *Journal of Structural Engineering*, V. 120, No. 1, 230-251.

Button, R. R., Mayes, R. L., "Out-of-plane Seismic Response of Reinforced Masonry Walls," *Journal of Structural Engineering*, V. 118, No. 9, 2495-2513.

Chopra, A. (1995), *Dynamics of Structures,* Prentice-Hall.

Clark, A. J. (1992), "Dynamic charactersitics of large multiple degree of freedom shaking tables," *Proceedings*, Tenth World Conference on Earthquake Engineering, Madrid, 2823-2828.

Costley, A. C., Abrams, D. P., Calvi, G. M. (1994), "Shaking Table Testing of an Unreinforced Brick Masonry Building," *Proceedings*, Fifth U.S. National Conference on Earthquake Engineering, 1994, 127-136.

Costley, A. C., Abrams, D. P. (1996), "Response of Building Systems with Rocking Piers and Flexible Diaphragms," *Proceedings*, Structures Congress of the American Society of Civil Engineers, 1996, 135-140.

Easley, J. T. (1977), "Strength and Stiffness of Corrugated Metal Shear Diaphragms," *Journal of Structural Engineering*, V. 103, No. ST1, 169-180.

European Seismological Commission (1998), *European Macroseismic Scale 1998*, Luxembourg.

Federal Emergency Management Agency (1998), *Evaluation of Earthquake Damaged Concrete and Masonry Wall Buildings*, Publication 306, Washington D.C.

Federal Emergency Management Agency (1997), *NEHRP Guidelines for the Seismic Rehabilitation of Buildings*, Publication 273, Washington D.C.

Federal Emergency Management Agency (1997), *NEHRP Commentary on the Guidelines for the Seismic Rehabilitation of Buildings*, Publication 274, Washington D.C.

Fonseca, F. S., Wood Sh. L., Hawkins, N.M. (1996), "Measured Response of Roof Diaphragms and Wall Panels in Tilt-up Systems Subjected to Cyclic Loading," *Earthquake Spectra*, V. 12, No. 4, 783-802.

Hamid, A., Abboud, B., Farah, M., Hatem, K., Harris, H. (1989), "Response of Reinforced Block Masonry Walls to Out-of-plane State Loads," U.S.-Japan Coordinated Program for Masonry Building Research, *TCCMAR Report No. 3.2(a)-1*.

International Code Council Inc. (2000), *International Building Code-2000*, United States of America.

Kariotis, J., El-Mustapha, A., Ewing, R. (1988), "Dynamic Response of Building Systems with Reinforced Masonry Shear Walls," *Proceedings*, Eighth International Brick and Block Masonry Conference, Trinity College, Dublin, Ireland, September 1988, V II, 740-751

Kariotis, J., El-Mustapha, A., Ewing, R. (1988), "A Nonlinear Dynamic Lumped Parameter Model for Reinforced Masonry Structures," *Proceedings*, Eighth International Brick and Block Masonry Conference, Trinity College, Dublin, Ireland, September 1988, V II, 728-739

Kariotis, J. (1995), "Seismic Response of Unreinforced Masonry Buildings with Flexible Diaphragms," *Proceedings*, Structures Congress of the American Society of Civil Engineers, 1995, 1817-1820

Kihn, H. H., El-Hakim, N., Fazio, P. (1979), "Refined Calculations for the Strength and Stiffness of Cold-Formed Steel Diaphragms," *Canadian Journal of Civil Engineering*, V. 6, No. 2, 268-275.

Leiva, G., Klingner, R. E., "Behavior and Design of Multi-Story Masonry Walls Under In-Plane Seismic Loading," *The Masonry Society Journal*, V. 13, No. 1, 15-24

SAP2000 Non-Linear V7.10 (1999), Computers and Structures, Inc., Berkeley, California.

Seible, F., Hegemier, A., Igarashi, A., Kingsley, G. (1994a), "Simulated Seismic-Load Tests on Full-Scale Five-Story Masonry Building," *Journal of Structural Engineering*, V. 120, No. 3, 903-924.

Seible, F., Priestley, N., Kingsley, G., Kurkchubashe, A. (1994b), "Seismic Response of Full-Scale Five-Story Reinforced-Masonry Building," *Journal of Structural Engineering*, V. 120, No. 3, 925-947.

Sudhir, J. K., Jennings, P. C. (1985), "Analytical Models of Low-Rise Buildings with Flexible Floor Diaphrgams," *Earthquake Engineering and Structural Dynamics*, V. 13, 225-241.

Tena-Colunga, A., Abrams, D. (1995), "Simplified 3-D Dynamic Analysis of Structures with Flexible Diaphragms," *Earthquake Engineering and Structural Dynamics*, V.24, 221-232.

Tena-Colunga, A., Abrams, D. (1996), "Seismic behavior of Structures with Flexible Diaphragms," *Journal of Structural Engineering*, V.122, No. 4, 439-445.

Tomazevic, M. (1999), *Earthquake Resistant Design of Masonry Buildings*, Imperial College Press.

Tremblay, R., Stiemer, S. (1996), "Seismic behavior of single-story steel structures with flexible roof diaphragm," *Canadian Journal of Civil Engineering*, V. 23, 49-62.

United Steel Deck Inc. (1999), *Design Manual and Catalog of Products*, South Plainfield, NJ.

Wen, Y.K. and Wu, C.L. (1999), "Generation of Ground Motions for Mid-America Cities," *Projects RR-1 and RR-2*, Mid-America Earthquake Center, University of Illinois at Urbana-Champaign.

Western Wood Products Association (1973), *Western Woods Use Book*, Portland, OR.

## CERL Distribution

Chief of Engineers
ATTN: CEHEC-IM-LH (2)

Engineer Research and Development Center (Libraries)
ATTN: ERDC, Vicksburg, MS
ATTN: Cold Regions Research, Hanover, NH
ATTN: Topographic Engineering Center, Alexandria, VA

Defense Tech Info Center 22304
ATTN: DTIC-O

6
6/00

# REPORT DOCUMENTATION PAGE

*Form Approved*
*OMB No. 0704-0188*



**1. REPORT DATE (DD-MM-YYYY)**
08-2001

**2. REPORT TYPE**
Final

**3. DATES COVERED (From - To)**

**4. TITLE AND SUBTITLE**
Seismic Response of Low-Rise Masonry Buildings With Flexible Roof Diaphragms

**5a. CONTRACT NUMBER**

**5b. GRANT NUMBER**

**5c. PROGRAM ELEMENT NUMBER**

**6. AUTHOR(S)**
Gregory L. Cohen, Richard E. Klingner, John R. Jr. Hayes, and Steven C. Sweeney

**5d. PROJECT NUMBER**
611102AT23

**5e. TASK NUMBER**

**5f. WORK UNIT NUMBER**

**7. PERFORMING ORGANIZATION NAME(S) AND ADDRESS(ES)**
Construction Engineering Research Laboratory (CERL)
PO Box 9005
Champaign, IL 61826-9005

**8. PERFORMING ORGANIZATION REPORT NUMBER**
ERDC/CERL SR-01-19

**9. SPONSORING / MONITORING AGENCY NAME(S) AND ADDRESS(ES)**
U.S. Army Corps of Engineers
441 G Street, NW.
Washington, DC 20314-1000

**10. SPONSOR/MONITOR'S ACRONYM(S)**

**11. SPONSOR/MONITOR'S REPORT NUMBER(S)**

**12. DISTRIBUTION / AVAILABILITY STATEMENT**
Approved for public release; distribution is unlimited.

**13. SUPPLEMENTARY NOTES**
Copies are available from the National Technical Information Service, 5285 Port Royal Road, Springfield, VA 22161.

**14. ABSTRACT**

This study compares the responses from shaking-table testing and analytical predictions evaluated in the context of geometric scaling, to provide a coherent description of the seismic response of low-rise masonry buildings with flexible roof diaphragms.

Two half-scale, low-rise reinforced masonry buildings with flexible roof diaphragms are subjected to carefully selected earthquake ground motion on the Tri-axial Earthquake and Shock Simulator at the Construction Engineering Research Laboratory. Damage to the half-scale specimens is assessed using published protocols. Geometric scaling analysis relates response and damage of the half-scale specimens to those of the full-scale prototype structures.

Linear elastic modeling is simplified to a generalized two-degrees-of-freedom idealization. Response-spectrum analysis of such an idealization is accurate and justified for prediction of dynamic response of the half-scale specimens and the corresponding full-scale prototype.

It is shown that low-rise masonry buildings with flexible roof diaphragms can be designed for seismic loads as single-degree-of-freedom systems, using the degree of freedom associated with the in-plane response of the diaphragm in the building's transverse direction, rather than the degree of freedom associated with the in-plane responses of the shear walls.

**15. SUBJECT TERMS**
seismic mitigation
masonry buildings
roof diaphragm
earthquake testing
low-rise masonry
earthquake engineering

| 16. SECURITY CLASSIFICATION OF: | | | 17. LIMITATION OF ABSTRACT | 18. NUMBER OF PAGES | 19a. NAME OF RESPONSIBLE PERSON |
|---|---|---|---|---|---|
| a. REPORT | b. ABSTRACT | c. THIS PAGE | | | Dr. John R. Jr. Hayes |
| Unclassified | Unclassified | Unclassified | SAR | 148 | 19b. TELEPHONE NUMBER (include area code) (217)373-7248 |